We thank the referee for his/her time to provide us with extensive and valuable input. Please find below our responses to the raised comments, questions and suggestions. In the following, raised **comments / suggestions are in red** and respective **responses in green**, while **alterations to the manuscript text are indicated in blue.**

General Comment

This manuscript presented a detailed analysis of a large data set of size-resolved particle composition measured by HR-AMS in Hong Kong. Both long-term trends and diurnal variations of the mass size distributions of submicron organic material, sulfate, and nitrate are discussed on the basis of previous understanding about the sources. Variations in the particle mixing state are also evaluated. This is perhaps the first study that looked at long-term AMS mass size distributions systematically, which potentially may serve as a good example of utilizing such data to derive better understanding of the sources and the atmospheric processing of submicron particles. The current manuscript has however not yet arrived there. My main suggestions are (1) to justify the possible bias of the deconvolution of the mass size distributions (Bian et al., 2014) maybe exclude some data; see my comment #1) and (2) to make a clear difference on which results are novel and which ones have already been published from previous analysis. Also, some figures contain too much information and hence are difficult to read. I therefore think a major revision or a resubmission is needed before this paper being accepted as a publication on ACP.

We provide a discussion with respect to (1) and (2) further below in the specific comment section. In terms of figure complexity, we understand that the provided information density per figure is high. We are thus providing a revised set of figures. The main data presented in this work have not been published before, but are based on further in-depth analysis of ambient datasets which have been discussed previously.

Specific Comments

Comment (1) As shown in Figure D1, Aitken-mode peak often occurred in the left tail of the Accumulation-mode peak. If the heights of the two peak differ a lot (for example, one as only a few percent of the other one), it is easy to overfit the small peak, which may cause large uncertainties in quantifying the small peak. It is unclear to me how such overfitting is controlled in this study. Are any of the data points in Figures 1, 2, and 5 subject to this possibility?

Response In the vast majority of analyzed size distributions the bimodal characteristics were very obvious, and unimodal fitting of such distributions would lead to large positive residuals in the lower size region, justifying the fitting of a second peak.

In extreme cases, as the reviewer notes, the difference in peak height (and peak area) between the two fitted modes can be large. When the ratio of Aitken to accumulation mode was very small (<10%), we evaluated both uni- and bimodal peak fits for which we depict one example such an extreme case below (Figure R1). In this case, from the day-to-day size distribution set (suburban HKUST site, fall, SO4), the peak area ratio of Aitken to accumulation mode was ~2%. The lognormal peak fittings are presented in subpanel (a) for the unimodal case and (b) for the bimodal case. Panels (c) and (d) show histograms of the residuals from both cases. Panel (e) shows the cumulative probability distribution for the residuals from both fittings and the calculated D value from the Kolmogorov-Smirnov Test at 95% CI. It is obvious that even in such an extreme case, the bimodal fitting resolve the raw distribution more accurately with a quasi-normal residual distribution and cumulative probability density function. In contrast, the unimodal fitting exhibits a considerably skewed residual distribution that is tail-heavy towards larger positive concentration values and centered towards negative residuals. We obtained similar results for all borderline cases in our measurements and thus generally opted for bimodal deconvolution. We are therefore confident that overfitting of the small peak was unlikely to be a major issue in this work, but we agree that this question is indeed relevant and we will include a more detailed discussion in the methodology sections of the main text and supplementary material for reference in the revised manuscript. The concerned discussion is appended at the bottom of this document.

With regard to the peak fit process itself, Igor's multipeak fitting tool uses the Levenberg-Marquardt algorithm to adjust the fit parameters with the goal to minimize the sum of squares of the deviations as an iterative process starting from the provided initial guesses. The standard deviations of the fit parameters provide an estimate of the variability of parameters between the final fit solution and the surrounding solution space with similar, but slightly larger residuals. We provide a discussion of these analyses in the revised manuscript and Supporting Material.

Alteration Revision and addition to Section B of the Supporting Material and associated Tables (C1-C3) and Figures (D2-D5). The relevant sections are appended at the bottom of this document.

Comment (2) I disagree that the transmission efficiency of the AMS lens unlikely affects the presented analysis (Line 122-126). Because the particle velocity calibration only spans for a certain range, extrapolation of fit may lead overestimation of the mass size distributions in small sizes. Slow vaporization and bounce may lead overestimation at D_{va} > 1 µm (Ref.: http://cires1.colorado.edu/jimenez-group/wiki/index.php / AMSUsrMtgs, Best Practices: IE and Velocity Calibrations - Ed Fortner & John Jayne). More importantly, the transmission efficiency for standard AMS lens drops at Dva> 400 nm or < 100 nm, and is below 20% for Dva > 1 µm or < 60 nm (Liu et al., 2007). The transmission therefore skews the size distributions. Zhang et al. (2005) showed that in Pittsburgh when the AMS suggests an accumulation mode at 500 nm, MOUDI shows a peak at 900 nm Dva. In this case, the fitting to AMS distributions might miss the main mode. Bian et al. (2014) showed that sulfate and nitrate etc. indeed occurred in mode size much greater than 500 nm Dva in Hong Kong. Given all the reasons, for urban area that has larger accumulation mode, I think the parameters (GSD, MMD, and integrated area) from fitting to the right peak (e.g., in Figure D1) cannot represent the actual accumulation-mode distributions. Ideally, the size distributions can be corrected for transmission efficiency (at least for the right side). But it is very difficult to obtain the transmission efficiency for a specific AMS with standard vaporizer. I suggest the authors to justify their accumulation-mode analysis by additional data (e.g., from SMPS or MOUDI) or improved algorithm. Otherwise, it may not be meaningful to discuss the accumulation-mode changes.

Response We agree with the reviewer that lens transmission is an important issue in AMS-related work in general and represents a key instrumental limitation, which affects the vast majority of AMS publications as lens transmission corrections are not commonly performed.

The main aim of our work however is to present an analysis method that can provide an additional dimension to standard AMS data analysis techniques, given that bi- or multimodal size distributions from AMS measurements have been reported frequently in the literature. In our study, we focus on discussing the trends of mode diameters and mode particle mass (peak area) to provide additional, complementing information to preceding studies that only utilized standard mass concentration based analyses.

Lens transmission efficiencies have been reported to vary between instruments (even at the same pressure level) and a standard lens as used in this study is expected to transmit efficiently (~100%) between 90nm and 700nm D_{va}, thereafter decreasing to ~0.3 at 1000nm (Williams et al., 2013). The largest observed mode diameters in the accumulation mode in our work at either sampling location were ~700nm (D_{va}). The referenced size distribution work (Bian et al., 2014) relies on MOUDI samples and showed mode diameters ~800-900nm of aerodynamic diameter D_a, which if we assume $D_a \sim D_p$ and a particle density of ~ 1.5 g/cm^3 is beyond the transmission capability of the AMS (with D_{va} ~ 1.4 µm) in the droplet mode range. We note that comparability of results from MOUDI studies and AMS is limited given the different sizing techniques, sampling times (minute resolution vs. daily samples) and more importantly aerosol pretreatment i.e. “as-is” for MOUDI vs. removal of water prior to AMS measurements, which can influence particle size in high humidity (>80%) conditions (Fang et al., 1991).

While we agree that additional particle sizing instrumentation for inter-instrumental comparison are useful, the measurements presented in this study were conducted with a limited set of available instruments and did unfortunately not encompass complementary particle size distribution measurements (by either electrostatic classification or MOUDI samplers).

We revised the statements in line 122-126 and further stress the aims and scope of our work as well as the definition of the Aitken and accumulation mode as representing the apparent Aitken- and accumulation-mode contributions to AMS-measurable particle mass (i.e. within the capabilities and limitations of AMS as an ambient analytical instrument). We still view that the presented work is useful to the growing AMS community to offer additional dimensions in the analysis of AMS size distribution data.

Alteration The transmission efficiency of the AMS aerodynamic lens is known to fall off beyond ~0.7 µm of vacuum-aerodynamic diameter (Liu et al., 2007;Takegawa et al., 2009;Zhang et al.,

2004;Bahreini et al., 2008;Williams et al., 2013) and may bias measured particle mass and mode diameters in the accumulation mode towards lower values if significant particle mass fractions fall in the size region of D_{va} > 0.7 µm. Resolved MMDs at either sampling location were typically within the efficient upper transmission limit in this work.
The discussion of size distributions in this work should be viewed in the context of the instrumental capabilities and limitations of aerosol mass spectrometry, i.e. resolved Aitken and accumulation modes in this work are understood to represent the apparent Aitken and accumulation modes within AMS measurable particle mass size distributions.

Comment Figures 1 and 2: The discussions in page 5-11 are difficult to follow by reading those figures. For example, diurnal profiles for four gaseous pollutants have no size dependence. Showing them twice with the two particle modes is very confusing. Similarly, the shaded diurnal profiles for total submicron mass of different species made the figures difficult to read. I suggest to move those into a separate figure.

Response Gas data are shown in duplicate (noted in the figure caption) to enable direct eye-guided comparison of concentration trends in both panels. We have revised the figures for more intuitive readability.

Alteration Figures 1 and 2 (now Figures 2 and 3 in the revised manuscript) have been replotted.

Comment The numbering of section 3.1, 3.2, and 3.2.1 seems wrong.

Response The numbering of sections in chapter 3 is erroneous. Part 3.2. is in fact 3.1.1., while 3.2. is 3.1.2. This also affects section numbers thereafter, and we provide a corrected chapter numbering in the revised manuscript.

Comment Line 157: “median values” - it is better to clarify in the captions of Figures 1 and 2 what are the medians.

Response We state more clearly in the text and figure captions that median refers to values from the bin-median size distribution in the revised manuscript.

Comment Line 161: What is “residual traffic”?

Response We employ the term “residual traffic” in analogy to “background” concentration levels, as traffic in the central inner-city districts remains continuous at night albeit at much lower vehicle number compared to the daytime, whereas in more remote areas or smaller cities traffic at night is typically intermittent. We will change the wording to avoid confusion.

Alteration […] as well as contributions from nighttime activity such as traffic, which remains continuous in the inner-city districts at night albeit at much lower vehicle numbers compared to the daytime.

Comment Line 168: The abbreviations only need to be defined when the full terms first appear. Same in figure captions.

Response We will remove duplicate definitions in the revised manuscript.

Comment Line 191: What is “residual organic particle mass”?

Response This term has been used in a context similar to the discussion of “residual traffic”, and refers to any background organic aerosol contributions as well as local contributions that are not immediately removed by settling or sweep-out. We agree that this may be confusing.

Alteration In the accumulation mode, organic particle mass during the night hours (00:00 – 06:00) was 2.5 times larger in spring (5.5 µg m^{-3}) than in summer (2.0 µg m^{-3}).

Comment Line 186 and Line 215: Figures do not appear in order.

Response In this manuscript, Figures have been arranged to enable the reader to compare the results from the two different sites. The manuscript text also follows this general structure. Given the size of the plots, some subfigures had to be grouped into separate plots and therefore may not appear strictly in numerical order in the manuscript text.

Comment Line 217-219: The smaller fraction of Aitken-mode to the total increase may be

caused by a greater accumulation mode contribution. In the summer, we expect to have more SOA in general (stronger emissions of the precursors and stronger oxidation), which also may lead increased organic submicron particle mass

Response We agree with the reviewer that SOA influence may be a viable explanation for the increased accumulation mass contribution, however, our measurement data do not support this.
Changes in SOA concentrations during the daylight hours were small in both seasons (Lee et al., 2015). We also note that accumulation mode particle mass increases were smaller in summer than spring, i.e. even with the likelihood of stronger oxidation conditions in summer the corresponding SOA formation did not seem to lead to significant enhancements in measured organic submicron particle mass.

Comment Line 244-247: The matching of ozone and sulfate is not enough to prove that the nighttime sulfate peak is contributed by heterogeneous SO2 oxidation by ozone. Are there any other evidence?

Response The limited amount of additional measurement data beyond gas-phase standard criteria pollutant data prevents a deeper analysis of this remarkable observation in this work.
We believe that the current wording in the manuscript clarifies that the observed trends are indications ("this points to…") and can serve as impetus for further future study.

Comment Line 273-274: While the median MMD seem showing little change, the mean and 25thn75th percentiles show significant diurnal variations (Figure D2). Why? Also, although in Line 103-105, there is a bit information about the diurnal distributions. Figure D2 would confuse readers a lot by the ranking of the values (meaning that medians were not located between 25th and 75th). It is important to clarify what the median, mean, and 25thn75th stand for? I mean not the median values of MMD values but the MMD from a reconstructed distribution, right?

Response The reviewer's interpretation of the different size distribution groups is correct. We have added an additional Figure 1 in the main text to illustrate the origin of these size distributions to better guide the reader in the discussions following later on. The Figure is appended at the bottom of this document.
In Figure D2, left lower panel for nitrate, there is indeed a notable diurnal variation in the mean set MMD. The 25^{th} and 75^{th} percentile distributions exhibit certain fluctuations, which are however minor and within a narrow range. We further take note of this observation in Lines 293-298, where the differences in distribution sets are discussed. We believe that this difference between the percentile (25^{th} PC, median, 75^{th}PC) sets and the mean set is an effect of averaging same-hour concentration values from different days to yield the diurnal average values. As different days may experience different concentration levels (longer-term fluctuations, e.g. transport, photochemically active periods etc.) and may be distributed disproportionately across certain hours of the day, this results in "skewed" average size distributions. As noted in the manuscript, we therefore chose to utilize median data in this study for the interpretation of diurnal variations.

Alteration Addition of Figure 1 to show the sequence of main data treatment and analysis steps.

Comment Overall the discussion in Section 3 only focused on what were seen from this study. Do the interpretations agree or disagree with what are known from other studies (other than AMS). For example, for mixing state, are the findings here consistent with the understanding from single particle analysis? The paper needs to show which results are novel and which ones have already been published from previous analysis in terms of understanding the sources and atmospheric processing of submicron particles.

Response Size distribution studies in Hong Kong are generally rare and are either not chemically resolved (SMPS, FMPS) or rely on MOUDI sampling.
Comparability is limited, given different sizing techniques (mobility vs. aerodynamic / vacuum-aerodynamic), sampling times (real-time or near-real time vs. 24h to 48h) and aerosol pre-treatment (removal of water for AMS measurements vs. "as-is" for MOUDI and SMPS typically). To our knowledge, single particle analysis from ambient measurements in Hong Kong analyzing particle mixing state have not been reported yet. We have added a section on particle size distribution measurements undertaken in Hong Kong in the revised manuscript.

With respect to novelty, as noted in the introduction, the main focus of this paper is to demonstrate a systematic method of utilizing AMS size distributions and to provide chemically resolved particle mass size distributions on finer temporal scales. Detailed chemically resolved diurnal size distribution variations and longer term daily size distribution measurements from ambient AMS sampling campaigns are scarce, as are detailed size distribution studies focusing on the Hong Kong and Pearl River Delta Region.

Alteration Addition of Chapter 3.3 in the main text. The relevant part is appended to the bottom of this document.

Comment Technical remarks: Line 107: Extra period after “the world”. Line 157: Add hyphen between “Aitken” and “mode” when used as adjective. Similarly for “accumulation mode particle concentrations” and so on.

Response We have taken these technical remarks into account in our manuscript revision.

Changes in sections of main manuscript and Supporting Material
Main manuscript

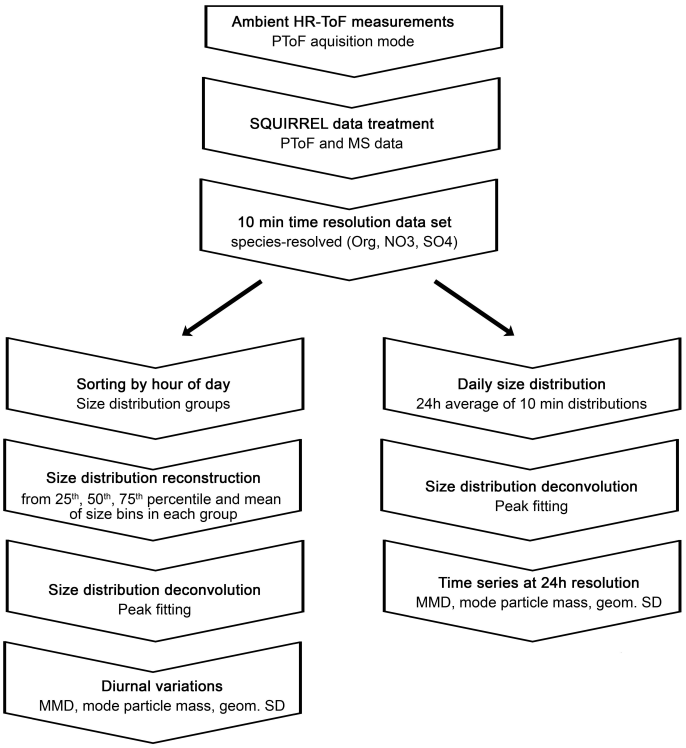

Figure 1. Flow chart of main data acquisition, data treatment and data analysis procedures

[…]

3.3 Comparison to previous studies

Particle size distribution studies in Hong Kong are generally scarce and have focused on either size segregated filter samples (MOUDI) for general ambient measurements or electrostatic classification in particle formation and particle growth studies (Guo et al., 2012;Cheung et al., 2015) . The latter studies focus on specific and narrow time periods and lack general discussions on ambient particle size distributions.

Two ambient studies were undertaken at the suburban coastal HKUST site using size-segregated samples from a ten-stage MOUDI sampler and offline chromatographic analysis. Inorganic constituents (NH4, NO3, SO4) in fine particles (i.e. D_p<1.8 µm) were shown to follow bimodal distributions with mode diameters in the range of 0.14-0.21 µm and 0.46-0.58 µm in samples collected in the winter season, while the main mode was observed in the coarse region (4-6 µm) for all three species (Zhuang et al., 1999). A subsequent year-long observational study also reported bimodal fine particle distributions with mode diameters of 0.1-0.3 µm and 0.7–0.9 µm and 1-2 additional modes in the coarse region (Bian et al., 2014), however, the main mode in the size distributions of sulfate, ammonium, potassium and oxalate was observed in the droplet mode (0.7 – 0.9 µm) in this study. Vehicle exhaust plumes sampled on-road from a Mobile Real-time Air Monitoring Platform (MAP) across Hong Kong's road network exhibited three distinct particle volume size distributions: a unimodal distribution with an accumulation mode at 0.2 µm and two bimodal distributions with a minor mode at 0.2 µm and the dominant mode at 0.5 or 0.7 µm (Yao et al., 2007).

The bimodality in the fine particle range across these studies is consistent with the AMS-based results in this work. Nominally, the accumulation mode diameters from filter based studies and the chase studies are larger than those from AMS measurements where maximum mode diameters occurred at D_{va} ~ 700nm, corresponding to D_a ~ 470 (assuming D_{va} ~ D_a * density; particle density ~ 1.5 g/cm^3). Direct comparability is however limited due to

fundamental differences in sizing techniques (MOUDI: atmospheric pressure; AMS: near-vacuum), sampling times (MOUDI: 24h samples, scattered time line; AMS: minute raw resolution averaged to hourly or daily, continuous time line), measurement uncertainties (MOUDI: sampling artifacts such as vapor adsorption and desorption; AMS: inlet lens transmission) and aerosol pretreatment (none for MOUDI with potential impacts on particle size in high humidity (>80%) conditions (Fang et al., 1991); AMS: removal of water prior to introduction to instrument).

Supporting Material

Lognormal peaks were fitted to each 24h and hour-of-day AMS mass size distribution respectively employing the *Multipeak Fit V2* algorithm in *Igor Pro (Wavemetrics)* using a simple vertical offset as the baseline and initial guesses on peak position, height, and width based on visual inspection of the raw size distribution. The multipeak fitting tool employs the Levenberg-Marquardt algorithm (Gill et al., 1981) as a non-linear least squares fit and iteratively adjusts the initial fit parameter guesses until a convergent solution with minimized residuals is achieved. In sporadic cases, the fitted solution led to excessive deviations from the initial guesses with greatly shifted peak locations and large fluctuations in peak width. In such cases, results from the peak fits of immediately adjacent size distributions (i.e. previous and next distributions in the sequence) were evaluated and used to adjust the fitting process by fixing either the location (*primary*) or the width of the peak (*secondary*) to the average value of the two adjacent fitted distributions.

For the diurnal size distributions, measurement data from time periods with large differences in species concentration levels were pooled together. The averaging of mass (or volume) based size distribution involves different uncertainties for each size bin due to the cubic relationship between particle mass (or volume) and particle diameter and the corresponding improvement in signal-to-noise ratio with increasing particle size. To establish reliable diurnal trends, we adopt an approach similar to the analysis of conventional species concentration diurnal trends by evaluating size distributions reconstructed from the average, median, 25^{th} and 75^{th} percentile of each size bin. Similar diurnal trends in the fitting parameters across these different size distributions would confirm that changes were indeed recurrent daily while divergent trends would indicate that irregular processes (e.g. episodic events) were more significant in determining size distribution characteristics. Since episodic pollution events and clean periods (e.g. prolonged precipitation) were not removed from the dataset, the quantitative analysis focuses on trends observed in the median dataset to minimize skewing effects of high and low concentration periods.

Uncertainties can arise from the peak fitting process itself. While the bimodality of the size distributions was obvious in most cases (i.e. a main mode with a shoulder towards smaller particle sizes, e.g. Figure D1), accumulation mode particle mass can occasionally dominate the mass size distribution and diminish the Aitken mode. To achieve confidence in the appropriateness of the bimodal fitting we evaluated both unimodal and bimodal peak fits whenever the Aitken to accumulation mode peak ratio was <10% and we depict a representative example below (Figure D2a. b). The distribution of the fit residuals (Figure D2c, d) was examined and cumulative probability distributions of the fit residuals compared by the Kolmogorov-Smirnov test (Figure D2e) to assess whether fit residuals were significantly different at 95% confidence level (CL). It is evident that the bimodal fit performs better at resolving the raw size distribution in the smaller size region and overall yields a more normal residual distribution. The Kolmogorov-Smirnov test confirms that the residual distributions are statistically different ($D>D_{critical}$ at 95% CL). We tested all borderline cases using the outlined procedure. In this study, bimodal fits yielded unanimously better results in all cases for both diurnal and day-to-day size distributions and all investigated species, i.e. the Aitken mode always remained clearly distinguishable from the accumulation mode.

While the peak fitting algorithm yields a unique individual solution with a set of parameters for which resulting residuals (*difference of fitted and original distribution*) are minimized, the surrounding solution space provides a potentially infinite number of similar solutions with slightly larger residuals. The standard deviations of the fit parameters can provide an estimate of the variability of the peak parameters between the final fit solution and the surrounding solution space. We evaluated the uncertainty in peak area (i.e. integrated mode particle mass) which represents the combined uncertainty of the peak position, width and height (which altogether directly determine the peak area) for all fitted size distributions in this work.

Figure D3 depicts the standard deviation of resolved peak area (i.e. integrated mode particle mass concentration) nominally and relative to the peak area for the diurnal size distributions of NO3 at the urban Mong Kok site in summer 2013 and Tables C1-C2 summarize the values of percent standard deviations for all species at both measurement sites respectively. The median datasets, which were used for quantitative discussion for the diurnal size distribution analysis, exhibited particle mass uncertainties of 14-48% in the Aitken mode and 1-12% in the accumulation mode at the suburban HKUST site, and 7-44% in the Aitken mode and 1-6% in the accumulation

mode at the urban MK site. Figure D4 depicts the 75th percentile-bin diurnal variation of NO3 (which displayed the largest uncertainties in Figure D3) with the corresponding peak area variability, and shows that the interpretation of the diurnal variation would remain largely unaffected from the incurred uncertainties.
For the day-to-day 24h size distributions a corresponding analysis was undertaken, with Figure D5 depicting the size distributions of NO3 at the HKUST site for all covered seasons exemplarily, and Table C3 summarizes the values of percent standard deviations for all species at both measurement sites respectively. Peak fit uncertainties typically increase with decreasing integrated peak area and can exceed the values of the peak area in the Aitken mode in a small number of cases (e.g. Figure D5c,e – ratios >1). Quantification of the Aitken mode may not be possible at high levels of confidence in these isolated cases. They were retained in the dataset due to their low frequency of occurrence and to enable a complete discussion over the full concentration range without biasing towards larger concentration (i.e. fitted peak areas) values.

Table C1. Percentiles of relative standard deviation (*rows; corresponding to the box-whiskers plot in Figure D3e,f*) in percent from lognormal peak fits (bimodal deconvolution) for the resolved Aitken mode (a) and accumulation mode (b) particle concentration for diurnal size distributions at the HKUST supersite (2011/12), *columns* describe the data set, i.e. reconstructed size distributions from the 25th percentile, median, 75th percentile and mean of the size bins
Sp=Spring, Su=Summer, Fa=Fall, Wi=Winter

(a)

Aitken mode		25th PC Distr.				Median Distr.				75th PC Distr.				Mean Distr.				Range
% SD		Sp	Su	Fa	Wi	Sp	Su	Fa	Wi	Sp	Su	Fa	Wi	Sp	Su	Fa	Wi	
NO3 (UST)	PC-90	67	76	39	85	76	44	54	55	80	75	56	39	36	77	44	42	36-85
	PC-75	52	42	28	57	66	32	39	40	61	59	44	29	22	38	35	34	22-66
	PC-50	**36**	**33**	**22**	**46**	**44**	**26**	**31**	**22**	**40**	**43**	**34**	**23**	**18**	**28**	**24**	**30**	**18-46**
	PC-25	29	25	16	28	26	14	24	18	25	29	22	17	14	19	20	25	14-29
	PC-10	21	20	15	24	19	12	19	15	17	19	17	10	13	13	15	21	10-24
SO4 (UST)	PC-90	38	38	42	74	19	36	39	43	22	40	40	42	19	36	37	81	19-81
	PC-75	35	33	38	55	18	28	33	32	18	30	35	64	17	30	30	66	17-66
	PC-50	**28**	**30**	**33**	**32**	**16**	**26**	**27**	**25**	**14**	**24**	**27**	**27**	**14**	**24**	**26**	**48**	**14-48**
	PC-25	21	25	26	24	13	21	22	21	11	18	24	22	12	21	23	40	11-40
	PC-10	17	23	24	19	11	20	20	13	10	14	20	19	10	19	22	35	10-35
Org (UST)	PC-90	52	23	41	44	42	28	32	27	47	48	45	53	46	29	24	32	23-53
	PC-75	41	18	26	28	30	22	27	22	26	39	35	44	36	23	21	25	18-44
	PC-50	**26**	**14**	**17**	**21**	**19**	**18**	**21**	**17**	**20**	**32**	**26**	**35**	**23**	**18**	**19**	**21**	**14-35**
	PC-25	16	11	13	18	17	16	19	15	18	28	20	29	18	14	16	17	11-29
	PC-10	9	9	10	11	14	9	15	12	15	20	17	21	17	11	14	16	9-21

(b)

Accum. mode		25th PC Distr.				Median Distr.				75th PC Distr.				Mean Distr.				Range
% SD		Sp	Su	Fa	Wi	Sp	Su	Fa	Wi	Sp	Su	Fa	Wi	Sp	Su	Fa	Wi	
NO3 (UST)	PC-90	8	5	8	4	7	5	6	3	4	9	6	3	3	4	5	1	1-9
	PC-75	6	4	7	3	3	4	5	2	4	7	5	2	2	3	5	1	1-7
	PC-50	**4**	**3**	**5**	**2**	**3**	**3**	**5**	**2**	**3**	**4**	**5**	**2**	**2**	**3**	**4**	**1**	**1-5**
	PC-25	3	3	4	2	2	3	4	1	3	3	4	2	2	2	4	1	1-4
	PC-10	2	2	4	1	2	2	4	1	2	2	3	1	2	2	3	1	1-4
SO4 (UST)	PC-90	2	3	3	5	2	2	2	3	3	2	3	4	2	2	2	2	2-5
	PC-75	2	2	2	2	2	2	2	2	2	2	2	3	1	2	2	2	1-3
	PC-50	**2**	**2**	**2**	**1**	**2**	**2**	**2**	**2**	**2**	**2**	**2**	**2**	**1**	**2**	**2**	**1**	**1-2**
	PC-25	2	2	2	1	1	2	2	1	1	2	2	2	1	2	2	1	1-2
	PC-10	1	2	1	1	1	2	2	1	1	1	2	1	1	2	2	1	1-2
Org (UST)	PC-90	29	12	16	9	18	8	9	5	10	6	7	3	18	7	5	5	3-29
	PC-75	18	9	11	7	10	5	5	3	6	4	5	2	11	5	4	3	2-18
	PC-50	**12**	**7**	**5**	**5**	**6**	**4**	**4**	**3**	**4**	**3**	**4**	**2**	**7**	**3**	**3**	**3**	**2-12**
	PC-25	7	4	3	3	5	3	3	2	3	2	3	2	5	2	2	2	2-7
	PC-10	4	4	1	2	4	2	2	1	2	2	2	1	2	1	2	2	1-4

Table C2. Percentiles of relative standard deviation (*rows; corresponding to the box-whiskers plot in Figure D3e,f*) in percent from lognormal peak fits (bimodal deconvolution) for the resolved Aitken mode (a) and accumulation mode (b) particle concentration for diurnal size distributions at the urban MK site (2013), *columns* describe the data set, i.e. reconstructed size distributions from the 25th percentile, median, 75th percentile and mean of the size bins *Sp=Spring, Su=Summer*

(a)

Aitken mode % SD		25th PC Distr. Sp	25th PC Distr. Su	Median Distr. Sp	Median Distr. Su	75th PC Distr. Sp	75th PC Distr. Su	Mean Distr. Sp	Mean Distr. Su	Range
NO3 (MK)	PC-90	38	46	40	34	40	41	22	26	22-46
	PC-75	27	34	26	28	34	35	20	16	16-35
	PC-50	**15**	**24**	**23**	**21**	**25**	**28**	**18**	**14**	**14-28**
	PC-25	9	20	19	17	18	22	15	12	9-22
	PC-10	6	19	16	14	15	20	13	11	6-20
SO4 (MK)	PC-90	63	46	35	38	24	31	23	21	21-63
	PC-75	50	36	30	36	21	28	21	20	20-50
	PC-50	**44**	**33**	**28**	**24**	**20**	**23**	**19**	**18**	**18-44**
	PC-25	37	27	24	21	17	20	15	17	15-37
	PC-10	33	25	21	19	15	18	15	16	15-33
Org (MK)	PC-90	22	12	22	19	30	21	15	14	12-30
	PC-75	16	10	12	12	18	11	12	8	8-18
	PC-50	**10**	**8**	**10**	**9**	**10**	**9**	**8**	**7**	**7-10**
	PC-25	8	7	8	7	7	8	6	6	6-8
	PC-10	7	6	7	6	6	6	5	5	5-7

(b)

Accum. mode % SD		25th PC Distr. Sp	25th PC Distr. Su	Median Distr. Sp	Median Distr. Su	75th PC Distr. Sp	75th PC Distr. Su	Mean Distr. Sp	Mean Distr. Su	Range
NO3 (MK)	PC-90	9	9	6	7	3	5	2	5	2-9
	PC-75	6	8	4	5	3	4	2	4	2-8
	PC-50	**4**	**6**	**3**	**4**	**2**	**3**	**2**	**3**	**2-6**
	PC-25	2	5	2	4	2	3	1	3	1-5
	PC-10	2	4	1	3	1	3	1	2	1-4
SO4 (MK)	PC-90	4	3	2	3	2	5	2	3	2-5
	PC-75	3	2	2	3	2	4	2	2	2-4
	PC-50	**3**	**2**	**2**	**2**	**1**	**4**	**2**	**2**	**1-4**
	PC-25	2	2	2	2	1	3	1	2	1-3
	PC-10	2	2	1	2	1	3	1	2	1-3
Org (MK)	PC-90	9	8	8	7	9	5	6	6	5-9
	PC-75	6	7	5	5	5	4	5	4	4-7
	PC-50	**5**	**5**	**4**	**4**	**3**	**4**	**3**	**4**	**3-5**
	PC-25	4	4	3	3	3	3	3	3	3-4
	PC-10	2	3	3	3	5	2	2	2	2-3

Table C3. Percentiles of percent standard deviation (*rows; corresponding to the box-whiskers plot in Figure D5e,f*) from lognormal peak fits (bimodal deconvolution) for the resolved Aitken mode and accumulation mode for 24h day-to-day size distributions at the suburban HKUST site (a) and the urban MK site (b) for all investigated species, *columns* describe the uncertainties in terms of quartiles of resolved peak area, where Q1 refers to the lowest 25% and Q4 the highest 25% of resolved peak area (see also Figure D4)

(a)

HKUST '11/12 % SD		NO3					SO4					Org				
		Q1	Q2	Q3	Q4	Range	Q1	Q2	Q3	Q4	Range	Q1	Q2	Q3	Q4	Range
Aitken mode	PC-90	95	64	50	27	27-95	97	78	49	30	30-97	62	37	28	26	26-62
	PC-75	58	47	37	24	24-58	91	57	36	20	20-91	41	24	21	22	21-41
	PC-50	**47**	**35**	**25**	**17**	**17-47**	**60**	**39**	**29**	**16**	**16-60**	**30**	**17**	**14**	**17**	**14-30**
	PC-25	30	25	20	13	13-30	32	26	21	13	13-32	25	14	10	12	10-25
	PC-10	20	16	15	8	8-20	24	18	13	11	11-24	16	11	6	7	6-16
Accum. mode	PC-90	31	9	7	4	4-31	4	3	3	3	3-4	18	11	9	7	7-18
	PC-75	13	6	5	3	3-13	3	3	3	2	2-3	9	7	6	5	5-9
	PC-50	**8**	**4**	**3**	**2**	**2-8**	**2**	**2**	**2**	**2**	**~2**	**6**	**4**	**5**	**3**	**3-6**
	PC-25	3	3	2	2	2-3	2	2	2	2	~2	4	3	3	2	2-4
	PC-10	1	2	2	1	1-2	2	2	2	1	1-2	3	2	2	2	2-3

(b)

MK '13 % SD		NO3					SO4					Org				
		Q1	Q2	Q3	Q4	Range	Q1	Q2	Q3	Q4	Range	Q1	Q2	Q3	Q4	Range
Aitken mode	PC-90	62	52	47	30	30-62	94	50	29	24	24-94	23	17	13	16	13-23
	PC-75	41	42	30	25	25-42	47	35	22	16	16-47	16	14	11	12	11-16
	PC-50	**28**	**34**	**21**	**18**	**18-34**	**33**	**24**	**17**	**12**	**12-33**	**11**	**10**	**6**	**8**	**6-11**
	PC-25	21	22	19	12	12-22	26	17	13	9	9-26	8	7	5	6	5-8
	PC-10	6	10	13	8	6-13	19	14	10	5	5-19	6	5	3	3	3-6
Accum. mode	PC-90	22	21	6	6	6-22	7	6	6	4	4-7	13	8	9	8	8-13
	PC-75	17	10	5	3	3-17	4	4	4	2	2-4	8	7	6	4	4-8
	PC-50	**10**	**6**	**4**	**2**	**2-10**	**3**	**2**	**2**	**1**	**1-3**	**6**	**5**	**4**	**2**	**2-6**
	PC-25	6	3	2	2	2-6	2	2	1	1	1-2	4	4	3	2	2-4
	PC-10	3	1	2	1	1-3	1	1	1	1	~1	2	3	2	1	1-3

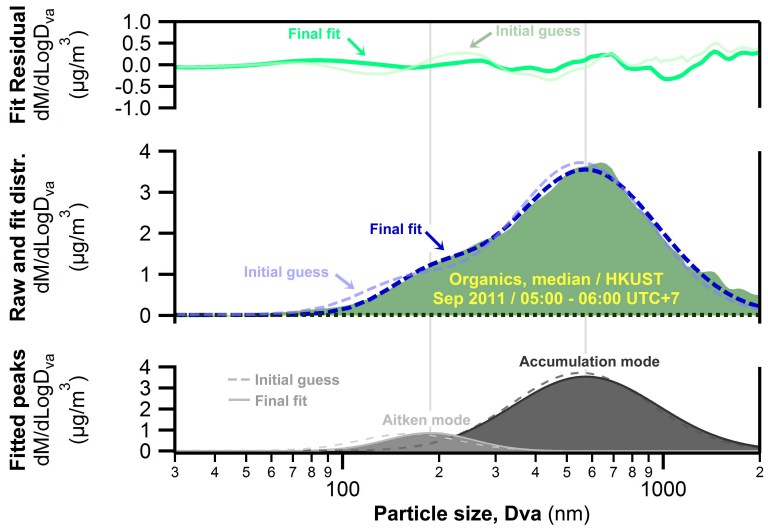

Figure D1. Example of a log-normal peak fit *(Multipeak Fit V2, Igor Pro, Wavemetrics, Levenberg-Marquardt algorithm)* of an AMS organics size distribution

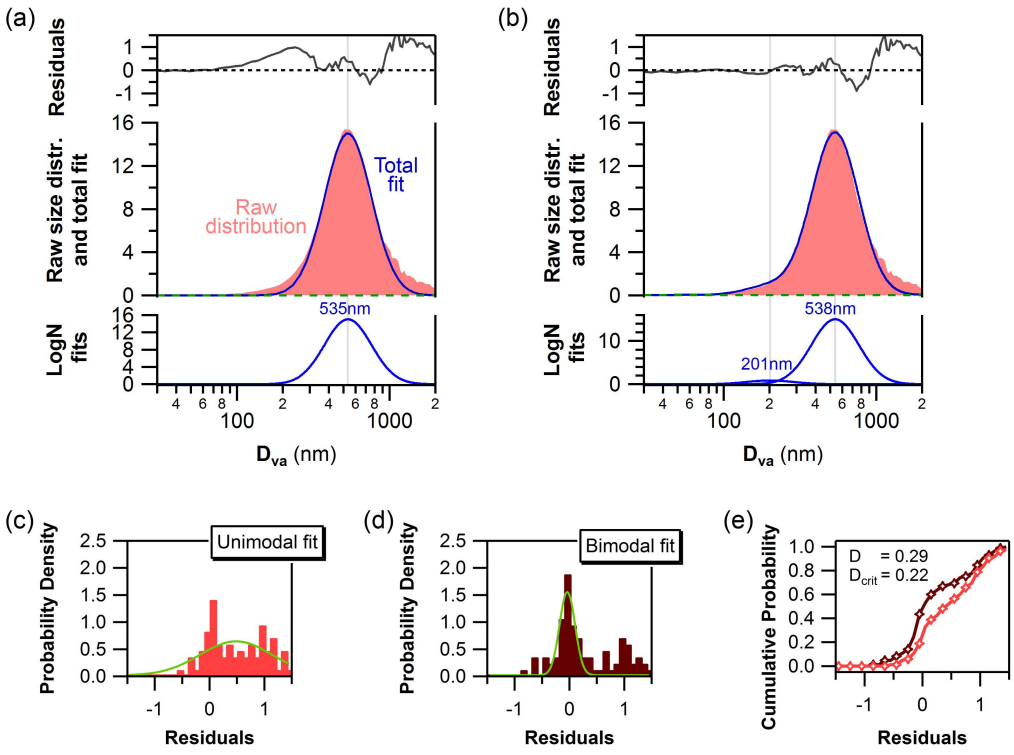

Figure D2. 24h average size distribution of sulfate (12/12/2011, suburban HKUST site) with (a) unimodal and (b) bimodal logN peak fitting applied; histograms of residuals from the unimodal (c) and bimodal (d) distributions with Gaussian fit (green); and cumulative probability density functions of uni- and bimodal fit residuals (e) with Kolmogorov-Smirnov D metric values at 95% confidence level

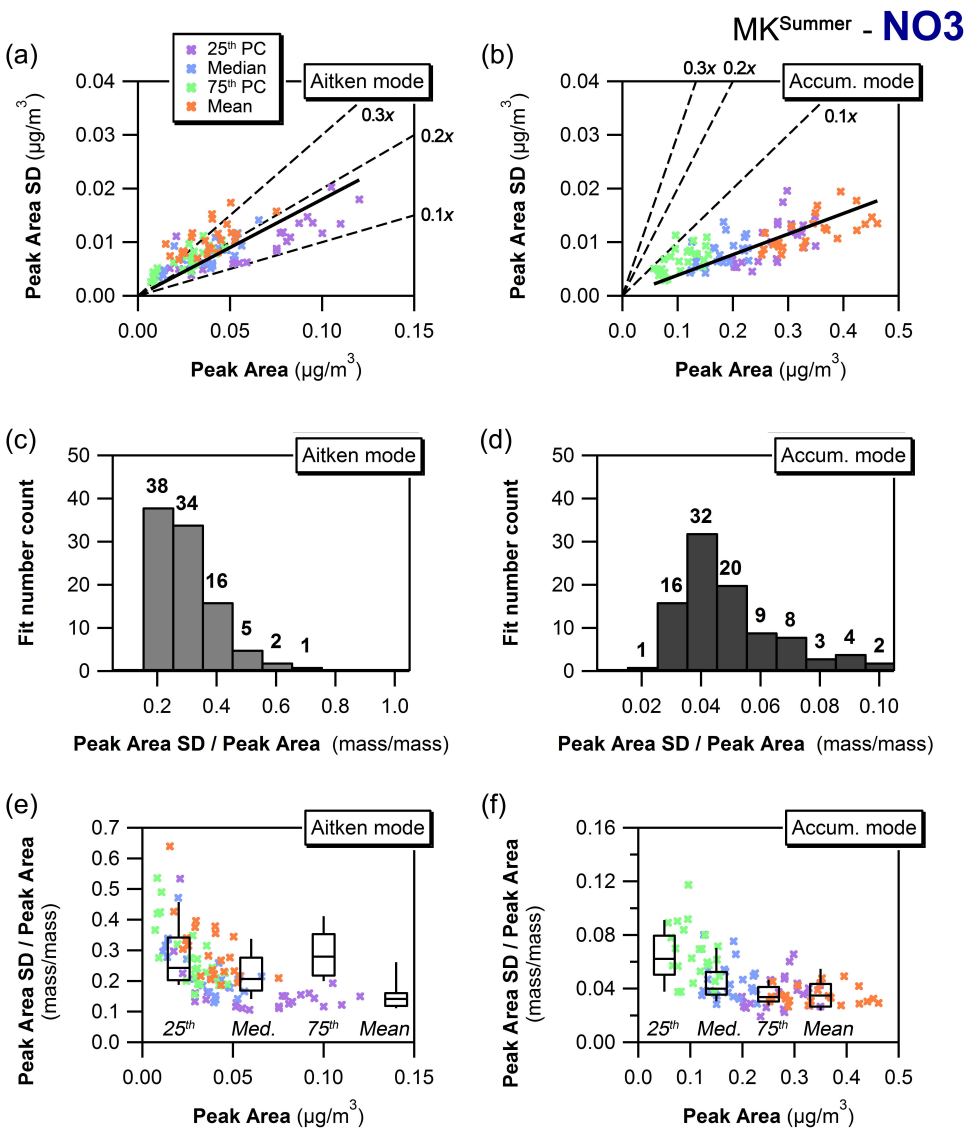

Figure D3. Standard deviation of peak area as a function of mode peak area (a,b), histogram of relative standard deviation i.e. the ratio of standard deviation to mode peak area (c,d) where the last bin also contains all values beyond the last bin range, and relative standard deviation as a function of mode peak area (e,f) for the fitted Aitken and accumulation mode with binned box-whiskers plot (25th to 75th PC box with horizontal median line and 10th to 90th PC whiskers where bins refer to quartiles of peak area from lowest Q1 to highest Q4); data for diurnal size distributions of NO3 at the urban Mong Kok site in summer 2013.

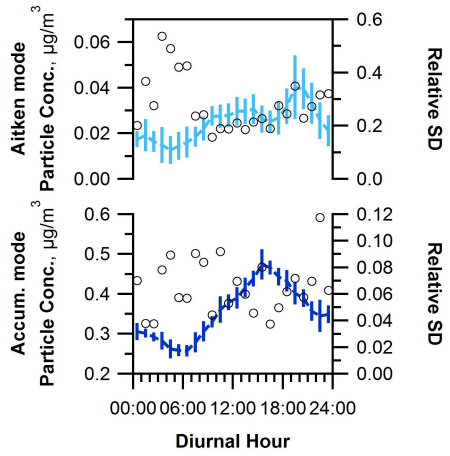

Figure D4. Plot of 75th percentile-bin diurnal variation with peak area fit variability and relative standard deviation (corresponding to green data and second to last box in Figure D3e,f)

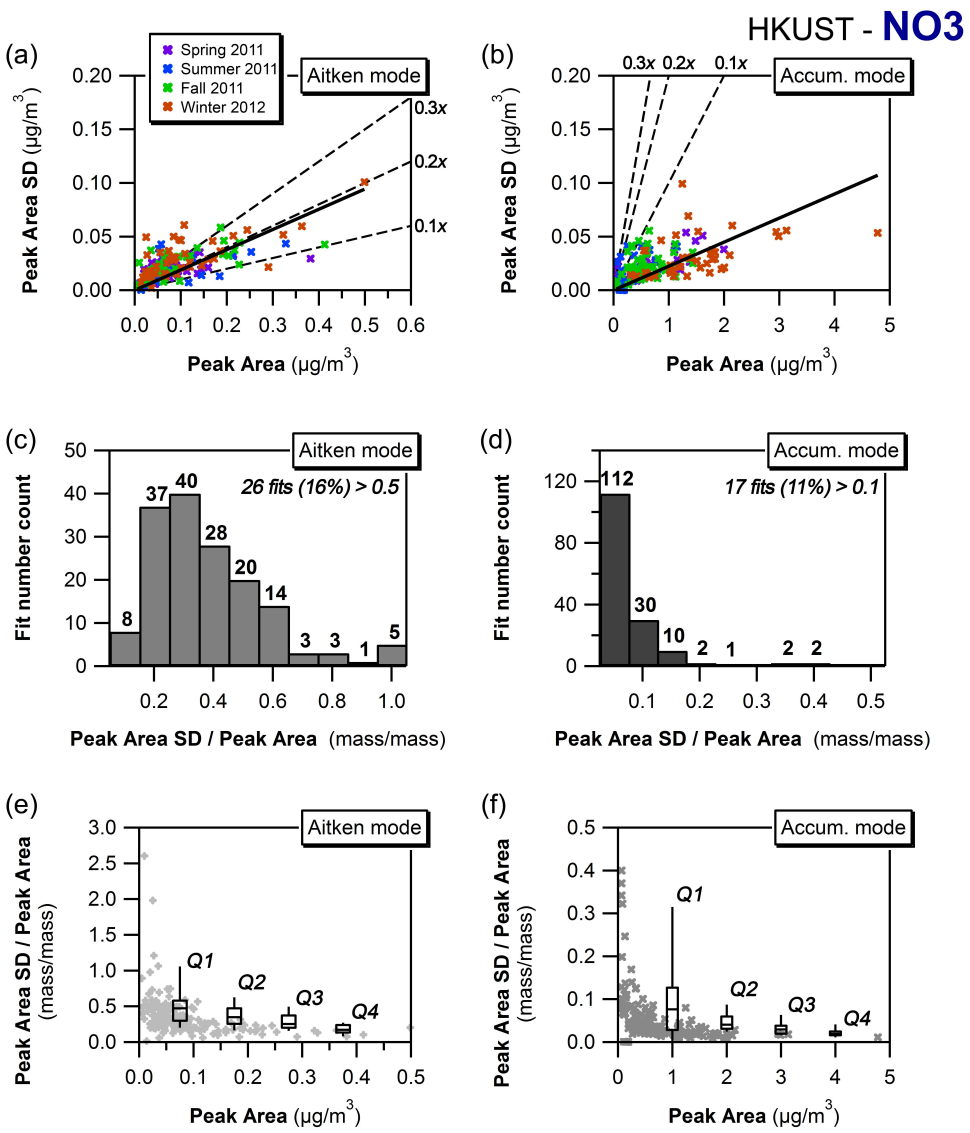

Figure D5. Standard deviation of peak area as a function of mode peak area (a,b), histogram of relative standard deviation i.e. the ratio of standard deviation to mode peak area (c,d) where the last bin also contains all values beyond the last bin range, and relative standard deviation as a function of mode peak area (e,f) for the fitted Aitken and accumulation mode with binned box-whiskers plot (25th to 75th PC box with horizontal median line and 10th to 90th PC whiskers where bins refer to quartiles of peak area from lowest Q1 to highest Q4); data for day-to-day size distributions of NO3 at the HKUST site including all seasons.

References

Bahreini, R., Dunlea, E. J., Matthew, B. M., Simons, C., Docherty, K. S., DeCarlo, P. F., Jimenez, J. L., Brock, C. A., and Middlebrook, A. M.: Design and Operation of a Pressure-Controlled Inlet for Airborne Sampling with an Aerodynamic Aerosol Lens, Aerosol Science and Technology, 42, 465-471, 10.1080/02786820802178514, 2008.

Bian, Q., Huang, X. H. H., and Yu, J. Z.: One-year observations of size distribution characteristics of major aerosol constituents at a coastal receptor site in Hong Kong – Part 1: Inorganic ions and oxalate, Atmos. Chem. Phys., 14, 9013-9027, 10.5194/acp-14-9013-2014, 2014.

Cheung, K., Ling, Z. H., Wang, D. W., Wang, Y., Guo, H., Lee, B., Li, Y. J., and Chan, C. K.: Characterization and source identification of sub-micron particles at the HKUST Supersite in Hong Kong, Science of The Total Environment, 527–528, 287-296, http://dx.doi.org/10.1016/j.scitotenv.2015.04.087, 2015.

Fang, C. P., McMurry, P. H., Marple, V. A., and Rubow, K. L.: Effect of Flow-induced Relative Humidity Changes on Size Cuts for Sulfuric Acid Droplets in the Microorifice Uniform Deposit Impactor (MOUDI), Aerosol Science and Technology, 14, 266-277, 10.1080/02786829108959489, 1991.

Gill, P. E., Murray, W., and Wright, M. H.: The Levenberg-Marquardt method, in: Practical optimization, Academic Press, London, 1981.

Guo, H., Wang, D. W., Cheung, K., Ling, Z. H., Chan, C. K., and Yao, X. H.: Observation of aerosol size distribution and new particle formation at a mountain site in subtropical Hong Kong, Atmos. Chem. Phys., 12, 9923-9939, 10.5194/acp-12-9923-2012, 2012.

Lee, B. P., Li, Y. J., Yu, J. Z., Louie, P. K. K., and Chan, C. K.: Characteristics of submicron particulate matter at the urban roadside in downtown Hong Kong—Overview of 4 months of continuous high-resolution aerosol mass spectrometer measurements, Journal of Geophysical Research: Atmospheres, 120, 7040-7058, 10.1002/2015JD023311, 2015.

Liu, P. S. K., Deng, R., Smith, K. A., Williams, L. R., Jayne, J. T., Canagaratna, M. R., Moore, K., Onasch, T. B., Worsnop, D. R., and Deshler, T.: Transmission efficiency of an aerodynamic focusing lens system: Comparison of model calculations and laboratory measurements for the Aerodyne Aerosol Mass Spectrometer, Aerosol Science and Technology, 41, 721-733, 10.1080/02786820701422278, 2007.

Takegawa, N., Miyakawa, T., Watanabe, M., Kondo, Y., Miyazaki, Y., Han, S., Zhao, Y., van Pinxteren, D., Bruggemann, E., Gnauk, T., Herrmann, H., Xiao, R., Deng, Z., Hu, M., Zhu, T., and Zhang, Y.: Performance of an Aerodyne Aerosol Mass Spectrometer (AMS) during Intensive Campaigns in China in the Summer of 2006, Aerosol Science and Technology, 43, 189-204, 10.1080/02786820802582251, 2009.

Williams, L. R., Gonzalez, L. A., Peck, J., Trimborn, D., McInnis, J., Farrar, M. R., Moore, K. D., Jayne, J. T., Robinson, W. A., Lewis, D. K., Onasch, T. B., Canagaratna, M. R., Trimborn, A., Timko, M. T., Magoon, G., Deng, R., Tang, D., de la Rosa Blanco, E., Prévôt, A. S. H., Smith, K. A., and Worsnop, D. R.: Characterization of an aerodynamic lens for transmitting particles greater than 1 micrometer in diameter into the Aerodyne aerosol mass spectrometer, Atmos. Meas. Tech., 6, 3271-3280, 10.5194/amt-6-3271-2013, 2013.

Yao, X., Lau, N. T., Chan, C. K., and Fang, M.: Size distributions and condensation growth of submicron particles in on-road vehicle plumes in Hong Kong, Atmospheric Environment, 41, 3328-3338, 10.1016/j.atmosenv.2006.12.044, 2007.

Zhang, Q., Stanier, C. O., Canagaratna, M. R., Jayne, J. T., Worsnop, D. R., Pandis, S. N., and Jimenez, J. L.: Insights into the chemistry of new particle formation and growth events in Pittsburgh based on aerosol mass spectrometry, Environmental Science & Technology, 38, 4797-4809, 10.1021/es035417u, 2004.

Zhuang, H., Chan, C. K., Fang, M., and Wexler, A. S.: Size distributions of particulate sulfate, nitrate, and ammonium at a coastal site in Hong Kong, Atmospheric Environment, 33, 843-853, 10.1016/s1352-2310(98)00305-7, 1999.

We thank the referee for his/her time to provide us with extensive and valuable input. Please find below our responses to the raised comments, questions and suggestions. In the following, raised **comments / suggestions are in red** and respective **responses in green**, while **alterations to the manuscript text are indicated in blue**.

General Comment

This manuscript reports a systematic study on the long term chemically-resolved size distribution data measured by a high-resolution AMS from an urban and a suburban location in Hong Kong. Measured size distributions of individual species were fitted using a bimodal lognormal model and the derived mode sizes and submode concentrations were analyzed for seasonal and diurnal variations. Based on these results, the authors discussed the influences of different sources on aerosol sizes, differences between urban and suburban aerosols, and variations in aerosol mixing states. The work reported in this ms is technically sound and interesting and the synthesis of long-term AMS size distribution data is a novel undertaking. However, the assumption that all aerosol size distributions are bimodal appears to be overly simplified and somewhat arbitrary. Urban particles, in particular, are contributed by various primary and secondary sources and particle from different sources tend to have different size distributions. Although I could see the benefit of simplifying the complexity by using a bimodal assumption, it would be helpful that the authors elaborate a bit more on the justification for this treatment and provide more details on how well the biomodal log-normal model perform in fitting the observation data. Maybe a more systematic evaluation of the quality of fit for the size distribution data is more appropriate than one example (Fig. D1). Also, I would like mention that more sophisticated methods, such as the 3-dimentional factor analysis reported in Ulbrich et al. (2012), maybe useful to explore the number of modes. I also notice that the naming of the size modes in this work is a bit confusing. Aitken mode refers to particles smaller than 100 nm in diameter. However, according to Fig. 1 and 2, the mode diameters for the so-called "Aitken mode" determined through bimodal log-normal fitting are all above 100 nm, some even reaching 200 nm. Additionally, the discussions on diurnal variations of aerosol size mode focus very much on the impacts of emissions sources and physical and chemical processes. However, changes of air masses due to wind shifts or upwind impacts could also be important and should be evaluated.

We will present a brief review of AMS-related size distribution work as well as more details for the considerations and procedures involved in the peak fitting in the revised manuscript and Supporting Material. While we agree that especially in more complex urban environments, multimodality in size distributions is likely we can only clearly distinguish two modes in the mass size distributions from our field measurements. The impacts from coarser particles (>PM_1) are usually visible as enhanced tails at the upper boundary of the mass size distributions, however, the influence of decreasing lens transmission and possible impacts of longer evaporation times of larger particles (Canagaratna et al., 2004) render further examination unfeasible. Otherwise, there were no clear indications of possible further submodes (e.g. shoulders, peaks, etc.) and fitting of additional modes did not appear warranted, leading to our approach of a bimodal deconvolution.

The naming conventions have been chosen as to capture the overall character of the modes. Bearing in mind that presented particle diameters are in terms of vacuum-aerodynamic diameter, which is related to the more commonly used mobility diameter by approximately a factor of particle density, the resolved mode diameters correspond to mobility diameters around 100-150nm, thus close to the Aitken mode.

We recognize that our Aitken particle mode is in the borderline region between Aitken and accumulation mode and we will clarify the definition more clearly in the introductory and methodology part in the revised manuscript.

For the day-to-day size distributions, we examined wind frequency data and data from backtrajectory analysis (see Figures D12-13 in the Supporting Material). The diurnal analysis is split by seasons and thus encompasses 1-2 months of measurement data. Surface wind patterns at both measurement sites were rather complex and subject to irregular processes (e.g. street canyon effects, land-sea-breeze, monsoon circulation). It is unlikely that air mass changes or wind shifts occurred at regular diurnal time scales at both measurement sites and are therefore not discussed in the context of the diurnal size distributions.

The smaller mode typically exhibited mode diameters in the range of 100-200 nm (d_{va}) and is thus in the transition region between Aitken and lower accumulation mode. For a clearer distinction from the larger mode which unambiguously belonged to the accumulation size range, we opt to refer to the small mode as *Aitken mode* in this work.

Associated further changes:

- Addition of Chapter 3.3 to the manuscript, discussing previous studies.
- Revision and addition to Section B of the Supporting Material.

The relevant changes are appended at the bottom of this document

Specific Comments

Comment The numbering of the sections does not seem logic. For example, according to content, 3.2.1 is parallel to 3.2.

Response The numbering of sections in chapter 3 is erroneous. Part 3.2. should in fact be 3.1.1., while 3.2. should be 3.1.2. This also affects section numbers thereafter, and we provide a corrected chapter numbering in the revised manuscript.

Comment Line 11 - 12: this sentence is difficult to understand, consider to revise.

Response We have revised the concerned sentence.

Alteration The size distributions displayed bimodal characteristics and were deconvoluted into submodes which were analyzed for diurnal trends and longer term day-to-day variations.

Comment Line 63, the AMS lens transmission is close to zero for particles smaller than 30-35 nm, so it is not precise to say the Aitken mode particles (10-100 nm) are covered by AMS.

Response We agree that the AMS inlet lens is not capable of capturing particles in the smallest Aitken mode range which is relevant in terms of particle number concentration. Particle volume and thus particle mass is however dominated by large particles in each mode, and thus the AMS would still be able to capture most of the Aitken mode (from a particle mass perspective), which is mentioned in Line 63 ("particle mass").

Comment Line 65 states that the AMS particle size data from ambient measurements are rarely investigated in depth. This is not true. A number of studies, including a few from more than 10 years ago, analyzed the size-resolved composition data from AMS quite extensively and utilized the information to elucidate aerosol sources, new particle formation and growth mechanisms, and other atmospheric processes. Several references (not the complete list) are provided at the end of this comment in the reference section. In addition, Ulbrich et al. (2014) reported a comprehensive study on the size-resolved mass spectral data from an ambient study using 3-D factorization models. Considering that this manuscript focuses on AMS size distribution data, I'd like to recommend that the authors provide a background review on previous works in the introduction. Additionally,I notice that citations are sometime missing when findings from the authors' own research group are mentioned. This could cause confusion when the results from this work alone are sufficient to support the claim. A thorough check for in-text citations is recommended.

Response We seek to clarify the sentence concerned (Line 65). We aim to stress that AMS particle size distribution on finer time scales are in fact rarely investigated. The majority of studies examined overall average size distributions i.e. covering the whole sampling campaign, specific episodic event or limited time periods of interest.

We will rephrase this sentence and incorporate a short section reviewing these studies as recommended by the reviewer.

Alteration Thus far most studies employing ambient size distribution data from aerosol mass spectrometer measurements investigated longer time period averages, i.e. campaign averages (Salcedo et al., 2006;Sun et al., 2009;Aiken et al., 2009;Huang et al., 2010;Takegawa et al., 2009;Saarikoski et al., 2012;Li et al., 2015) or specific time periods of interest (Elser et al., 2016;Lee et al., 2013). Mohr et al. separated organic particle mass size distributions by periods of dominant influence of different PMF-resolved organic aerosol factors to study the properties of mass size distributions in relation to organic aerosol composition (Mohr et al., 2012). The 3D-factorization technique is an extension of traditional AMS PMF analysis on organic aerosol allowing estimates on the size distributions of organic aerosol factors, however under the assumption that factor size distributions remain invariant over the measurement period (Ulbrich et al., 2012).

The temporal evolution of species-specific size distributions, are mostly discussed qualitatively (Drewnick et al., 2005) and only few studies have evaluated temporal trends in mass size distributions in greater detail. Particle nucleation and subsequent growth events were investigated in Pittsburgh using size data from an AMS and two SMPS as well as various gaseous pollutant instruments and meteorological information. The AMS mass size distributions were evaluated quantitatively using the time series of binned particle

concentrations generated from the grouping of raw data into wider size bins to represent different stages in the particle growth process. (Zhang et al., 2004). The same method was employed to evaluate contributions of ultrafine mode and accumulation mode particles to total organic particle mass (Zhang et al., 2005) by summation of size bins in the range of 30-100 nm and 100-1000nm. The authors also explored diurnal changes in size distributions of particle species by averaging over 3h periods in the morning (6–9 am) and afternoon (1–4 pm). Sun et al. present a qualitative discussion of diurnal variations in the mass size distributions of the m/z 44, m/z 57 and derived $C_4H_9^+$ ion signals from measurements at an urban site in New York (Sun et al., 2011). Similarly, Setyan et al. examined diurnal changes in the mass size distributions of organics and sulfate qualitatively and used binned concentrations (40–120, 120–200, and 200–800) nm in their quantitative analysis to study the evolution of particle chemistry in new particle formation and growth events (Setyan et al., 2012).

Comment Line 91, what's the RH at the exit of the dryer?
Response The relative humidity at the diffusion drier outlet was consistently in a range of 20-30% and tested periodically in both campaigns.

Comment Line 130 - 132, the sentence "Utilizing ..." is vague, consider to revise
Response We have revised the sentence.
Alteration AMS mass-based size distributions can be utilized more systematically and complementary to standard AMS data analysis techniques by deconvoluting multimodal distributions into their constituting submodes and evaluating their variation and contribution to overall species concentration variations on a diurnal time scale.

Comment Line 160, "sweep-out" by what, rain?
Response "Sweep out" refers to removal by circulation (e.g. surface wind, traffic induced turbulence), which is particularly important for urban street canyons where periodic changes in circulation (heating, traffic patterns) exist. Washout by rain is another possibility, but is more dependent on specific meteorological conditions, i.e. occurs on irregular basis.

Comment Line 161, what's residual traffic?
Response We employ the term "residual traffic" in similarity to "background" concentration levels, as traffic in the central inner-city districts remains continuous albeit at much lower vehicle number compared to the daytime, whereas in more remote areas or smaller cities traffic at night is typically intermittent. We will change the wording to avoid confusion.
[…] as well as contributions from nighttime activity such as traffic, which remains continuous in the inner-city districts at night albeit at much lower vehicle numbers compared to the daytime.

Comment Line 167 – 169, clarify what the decreases correspond to.
Response We have modified the sentence for clarification.
Alteration Significant changes were evident in the particle size metric (MMD) during the same time period, where a consistent decrease by 20-30% from about 170 nm (spring) or 160 nm (summer) to 130-140 nm (spring) or 120 nm (summer) was evident with the concurrent increase in road traffic.

Comment Line 170- 173, are there SMPS measurements to support the increase of particle number concentrations?
Response The measurements presented in this study were conducted with a limited set of available instruments and did unfortunately not encompass complementary particle size distribution measurements (by either electrostatic classification or MOUDI samplers).

Comment Line 172, where does the cutoff size of 50 nm come from?
Response We here refer to the limitations in AMS lens transmission (see references in Lines 123-124) at the lower size end. The current wording may be confusing and we will revise the sentence to clarify.

Alteration […] from elemental carbon particles and smaller Aitken mode and nucleation mode particles below the range of efficient particle transmission of the AMS inlet lens.

Comment Line 174 – 190, how important was COA in Aitken mode around noon time? What about contributions from secondary aerosol formation and other primary sources such as HOA? Summertime SOA and SIA formation tend to be higher and can influence particles in all size modes. I am not sure change of cooking behavior was the only reason for the different diurnal shapes between spring and summer.

Response As discussed in the captioned section, changes in organic aerosol (as resolved by PMF) during the meal hours were almost exclusively due to changes in COA. Total HOA concentrations beyond the morning rush hour (6:00 – 9:00) remained stable throughout the day and only fell off in the late night hours. Changes in SOA concentrations during the daylight hours were small in both seasons (Lee et al., 2015) and concentration-wise much smaller than daytime COA concentrations. Significant influences from SOA and HOA are thus not likely. Similarly, changes in cooking behavior were not evident, but as mentioned in the captioned section, we consider advection/transport due to differences in wind patterns in spring and summer more likely to be responsible for the observed trend.

Comment Line 189 – 190, this sentence is somewhat confusing

Response We have revised this sentence for clarification.

Alteration Cooking emissions did not lead to conspicuous changes in the size-related distribution metrics, i.e. there were no obvious trends in particle diameters (MMDs) or distribution widths (GSDs) during the meal time periods.

Comment Line 213-215, this sentence is confusing. Please clarify.

Response This sentence is in support of the previous statement and underlines that meteorological parameters differed substantially between the two seasons. We note that the mentioning of the data source (temperature measurements were taken directly at the roadside station – solar irradiation data were only available from the farther away HKUST site) is not directly relevant to the discussion and may confuse the reader at this point. As the origin of the data is clearly mentioned in the caption of the related Figure, we will omit the information in-text in the revised manuscript.

Alteration Ambient temperatures and solar irradiation differed substantially with 7oC higher average temperatures and three times higher integrated daily solar irradiation in summer compared to spring (Figure D6e,f in the Supporting Material).

Comment Line 215-216, what does “nucleation of gas-phase emissions” mean?

Response The wording is erroneous and has been corrected.

Alteration Lower overall ambient temperatures enhance condensation of gas-phase emissions and particle nucleation and shift the gas-to-particle partitioning equilibrium of semi-volatile constituents […]

Comment Line 222-223, “reduce nucleation: : : of more volatile exhaust component on fresher, smaller particles: : :”? Did nucleation ever occur with the volatile component in the atmosphere?

Response “Reduce” refers to both particle nucleation and, separately, the condensation of volatile exhaust components. We revise this sentence for clarification.

The section in question discusses traffic-exhaust related components from the measurements at the urban roadside location. The site was impacted strongly by vehicle emissions and thus was affected by both nucleation and gas-to-particle conversion from components originating from vehicle exhaust. Both processes are inversely related to temperature. Vehicle exhaust upon discharge from the tailpipe into the ambient atmosphere is rapidly diluted and cooled leading to both gas-to-particle conversion of (semi-)volatile species, homogenous and heterogeneous nucleation and condensation or adsorption on pre-existing particles (Kittelson et al., 2006a;Kittelson et al., 2006b) in the immediate vicinity of the exhaust pipe. The extent of these processes would depend on various parameters including engine type, engine load, species distribution, as well as ambient conditions, e.g. temperature as discussed here.

Alteration […] consistent with the expected stronger impact of reduced particle nucleation and reduced condensation of semi-volatile exhaust components on fresher, smaller particles in the warmer season.

Comment Line 244-247, this discussion seems somewhat speculative. Are there data to support the nighttime heterogeneous oxidation of SO2 by O3 in Hongkong during spring time? Has this issue been investigated in previous publication(s)? Did wind direction or air mass origin play a role in the observed size mode change?

Response Neither wind direction nor air mass origin had any diurnal features that would explain this regularly recurring (i.e. diurnal) observation.
It must be noted that this effect is likely due to the roadside character of the measurement site, leading to ozone peaking during the nighttime (as noted in the manuscript due to NOx titration during the day), and was thus not evident at the suburban measurement site. We are not aware of any detailed investigations into the diurnal concentration characteristics of inorganic components at roadside measurement sites in Hong Kong. The limited amount of additional measurement data beyond gas-phase standard criteria pollutant data unfortunately prevents a deeper analysis in this work.

Comment Line 437, "particles containing different species were similar in size" is confusing.
Response We have revised the sentence for clarification.
Alteration Close nominal agreement (i.e. diameter ratios close to 1) infer that different species were distributed similarly across the particle size range which thus most likely represents a largely internally mixed particle population, while the spread of data (correlation coefficient) indicates the temporal homogeneity or divergence of resolved mode diameters.

Comment Line 449, small particles are not just processed by condensational growth and coagulation. In the presence of high humidity, they can also go through aqueous-phase processing.
Response We have revised the statement to include the possibility of aqueous-phase processing.
Alteration External mixing is more prevalent for freshly formed smaller particles which have typically undergone less atmospheric processing, such as condensational growth, coagulation or aqueous-phase reactions.

Comment Fig. D6, can wind data be provided as well?
Response Wind patterns at both measurement sites are strongly influenced by irregular processes (street canyon effects, land-sea-breeze, monsoon winds) which typically change from day-to-day. Including diurnal wind data in Figure D6 may thus not be meaningful.

Changes in sections of main manuscript and Supporting Material
Main manuscript

3.3 Comparison to previous studies

Particle size distribution studies in Hong Kong are generally scarce and have focused on either size segregated filter samples (MOUDI) for general ambient measurements or electrostatic classification in particle formation and particle growth studies (Guo et al., 2012;Cheung et al., 2015) . The latter studies focus on specific and narrow time periods and lack general discussions on ambient particle size distributions.

Two ambient studies were undertaken at the suburban coastal HKUST site using size-segregated samples from a ten-stage MOUDI sampler and offline chromatographic analysis. Inorganic constituents (NH4, NO3, SO4) in fine particles (i.e. D_p<1.8 µm) were shown to follow bimodal distributions with mode diameters in the range of 0.14-0.21 µm and 0.46-0.58 µm in samples collected in the winter season, while the main mode was observed in the coarse region (4-6 µm) for all three species (Zhuang et al., 1999). A subsequent year-long observational study also reported bimodal fine particle distributions with mode diameters of 0.1-0.3 µm and 0.7–0.9 µm and 1-2 additional modes in the coarse region (Bian et al., 2014), however, the main mode in the size distributions of sulfate, ammonium, potassium and oxalate was observed in the droplet mode (0.7 – 0.9 µm) in this study. Vehicle exhaust plumes sampled on-road from a Mobile Real-time Air Monitoring Platform (MAP) across Hong Kong's road network exhibited three distinct particle volume size distributions: a unimodal distribution with an accumulation mode at 0.2 µm and two bimodal distributions with a minor mode at 0.2 µm and the dominant mode at 0.5 or 0.7 µm (Yao et al., 2007).

The bimodality in the fine particle range across these studies is consistent with the AMS-based results in this work. Nominally, the accumulation mode diameters from filter based studies and the chase studies are larger than those from AMS measurements where maximum mode diameters occurred at d_{va} ~ 700nm, corresponding to d_a ~ 470 (assuming d_{va} ~ d_a * density; particle density ~ 1.5 g/cm^3). Direct comparability is however limited due to fundamental differences in sizing techniques (MOUDI: atmospheric pressure; AMS: near-vacuum), sampling times (MOUDI: 24h samples, scattered time line; AMS: minute raw resolution averaged to hourly or daily, continuous time line), measurement uncertainties (MOUDI: sampling artifacts such as vapor adsorption and desorption; AMS: inlet lens transmission) and aerosol pretreatment (none for MOUDI with potential impacts on particle size in high humidity (>80%) conditions (Fang et al., 1991); AMS: removal of water prior to introduction to instrument).

Supporting Material

Lognormal peaks were fitted to each 24h and hour-of-day AMS mass size distribution respectively employing the *Multipeak Fit V2* algorithm in *Igor Pro (Wavemetrics)* using a simple vertical offset as the baseline and initial guesses on peak position, height, and width based on visual inspection of the raw size distribution. The multipeak fitting tool employs the Levenberg-Marquardt algorithm (Gill et al., 1981) as a non-linear least squares fit and iteratively adjusts the initial fit parameter guesses until a convergent solution with minimized residuals is achieved. In sporadic cases, the fitted solution led to excessive deviations from the initial guesses with greatly shifted peak locations and large fluctuations in peak width. In such cases, results from the peak fits of immediately adjacent size distributions (i.e. previous and next distributions in the sequence) were evaluated and used to adjust the fitting process by fixing either the location (*primary*) or the width of the peak (*secondary*) to the average value of the two adjacent fitted distributions.

For the diurnal size distributions, measurement data from time periods with large differences in species concentration levels were pooled together. The averaging of mass (or volume) based size distribution involves different uncertainties for each size bin due to the cubic relationship between particle mass (or volume) and particle diameter and the corresponding improvement in signal-to-noise ratio with increasing particle size. To establish reliable diurnal trends we adopt an approach similar to the analysis of conventional species concentration diurnal trends by evaluating size distributions reconstructed from the average, median, 25th and 75th percentile of each size bin. Similar diurnal trends in the fitting parameters across these different size distributions would confirm that changes were indeed recurrent daily while divergent trends would indicate that irregular processes (e.g. episodic events) were more significant in determining size distribution characteristics. Since episodic pollution events and clean periods (e.g. prolonged precipitation) were not removed from the dataset, the quantitative analysis focuses on trends observed in the median dataset to minimize skewing effects of high and low concentration periods.

Uncertainties can arise from the peak fitting process itself. While the bimodality of the size distributions was obvious in most cases (i.e. a main mode with a shoulder towards smaller particle sizes, e.g. Figure D1), accumulation mode particle mass can occasionally dominate the mass size distribution and diminish the Aitken

mode. To achieve confidence in the appropriateness of the bimodal fitting we evaluated both unimodal and bimodal peak fits whenever the Aitken to accumulation mode peak ratio was <10% and we depict a representative example below (Figure D2a. b). The distribution of the fit residuals (Figure D2c, d) was examined and cumulative probability distributions of the fit residuals compared by the Kolmogorov-Smirnov test (Figure D2e) to assess whether fit residuals were significantly different at 95% confidence level (CL). It is evident that the bimodal fit performs better at resolving the raw size distribution in the smaller size region and overall yields a more normal residual distribution. The Kolmogorov-Smirnov test confirms that the residual distributions are statistically different ($D>D_{critical}$ at 95% CL). We tested all borderline cases using the outlined procedure. In this study, bimodal fits yielded unanimously better results in all cases for both diurnal and day-to-day size distributions and all investigated species, i.e. the Aitken mode always remained clearly distinguishable from the accumulation mode.

While the peak fitting algorithm yields a unique individual solution with a set of parameters for which resulting residuals (*difference of fitted and original distribution*) are minimized, the surrounding solution space provides a potentially infinite number of similar solutions with slightly larger residuals. The standard deviations of the fit parameters can provide an estimate of the variability of the peak parameters between the final fit solution and the surrounding solution space. We evaluated the uncertainty in peak area (i.e. integrated mode particle mass) which represents the combined uncertainty of the peak position, width and height (which altogether directly determine the peak area) for all fitted size distributions in this work.

Figure D3 depicts the standard deviation of resolved peak area (i.e. integrated mode particle mass concentration) nominally and relative to the peak area for the diurnal size distributions of NO3 at the urban Mong Kok site in summer 2013 and Tables C1-C2 summarize the values of percent standard deviations for all species at both measurement sites respectively. The median datasets, which were used for quantitative discussion for the diurnal size distribution analysis, exhibited particle mass uncertainties of 14-48% in the Aitken mode and 1-12% in the accumulation mode at the suburban HKUST site, and 7-44% in the Aitken mode and 1-6% in the accumulation mode at the urban MK site. Figure D4 depicts the 75^{th} percentile-bin diurnal variation of NO3 (which displayed the largest uncertainties in Figure D3) with the corresponding peak area variability, and shows that the interpretation of the diurnal variation would remain largely unaffected from the incurred uncertainties.

For the day-to-day 24h size distributions a corresponding analysis was undertaken, with Figure D5 depicting the size distributions of NO3 at the HKUST site for all covered seasons exemplarily, and Table C3 summarizes the values of percent standard deviations for all species at both measurement sites respectively. Peak fit uncertainties typically increase with decreasing integrated peak area and can exceed the values of the peak area in the Aitken mode in a small number of cases (e.g. Figure D5c,e – ratios >1). Quantification of the Aitken mode may not be possible at high levels of confidence in these isolated cases. They were retained in the dataset due to their low frequency of occurrence and to enable a complete discussion over the full concentration range without biasing towards larger concentration (i.e. fitted peak areas) values.

Table C1. Percentiles of relative standard deviation (*rows; corresponding to the box-whiskers plot in Figure D3e,f*) in percent from lognormal peak fits (bimodal deconvolution) for the resolved Aitken mode (a) and accumulation mode (b) particle concentration for diurnal size distributions at the HKUST supersite (2011/12), *columns* describe the data set, i.e. reconstructed size distributions from the 25th percentile, median, 75th percentile and mean of the size bins
Sp=Spring, Su=Summer, Fa=Fall, Wi=Winter

(a)

Aitken mode		25th PC Distr.				Median Distr.				75th PC Distr.				Mean Distr.				Range
% SD		Sp	Su	Fa	Wi	Sp	Su	Fa	Wi	Sp	Su	Fa	Wi	Sp	Su	Fa	Wi	
NO3 (UST)	PC-90	67	76	39	85	76	44	54	55	80	75	56	39	36	77	44	42	36-85
	PC-75	52	42	28	57	66	32	39	40	61	59	44	29	22	38	35	34	22-66
	PC-50	**36**	**33**	**22**	**46**	**44**	**26**	**31**	**22**	**40**	**43**	**34**	**23**	**18**	**28**	**24**	**30**	**18-46**
	PC-25	29	25	16	28	26	14	24	18	25	29	22	17	14	19	20	25	14-29
	PC-10	21	20	15	24	19	12	19	15	17	19	17	10	13	13	15	21	10-24
SO4 (UST)	PC-90	38	38	42	74	19	36	39	43	22	40	40	42	19	36	37	81	19-81
	PC-75	35	33	38	55	18	28	33	32	18	30	35	64	17	30	30	66	17-66
	PC-50	**28**	**30**	**33**	**32**	**16**	**26**	**27**	**25**	**14**	**24**	**27**	**27**	**14**	**24**	**26**	**48**	**14-48**
	PC-25	21	25	26	24	13	21	22	21	11	18	24	22	12	21	23	40	11-40
	PC-10	17	23	24	19	11	20	20	13	10	14	20	19	10	19	22	35	10-35
Org (UST)	PC-90	52	23	41	44	42	28	32	27	47	48	45	53	46	29	24	32	23-53
	PC-75	41	18	26	28	30	22	27	22	26	39	35	44	36	23	21	25	18-44
	PC-50	**26**	**14**	**17**	**21**	**19**	**18**	**21**	**17**	**20**	**32**	**26**	**35**	**23**	**18**	**19**	**21**	**14-35**
	PC-25	16	11	13	18	17	16	19	15	18	28	20	29	18	14	16	17	11-29
	PC-10	9	9	10	11	14	9	15	12	15	20	17	21	17	11	14	16	9-21

(b)

Accum. mode		25th PC Distr.				Median Distr.				75th PC Distr.				Mean Distr.				Range
% SD		Sp	Su	Fa	Wi	Sp	Su	Fa	Wi	Sp	Su	Fa	Wi	Sp	Su	Fa	Wi	
NO3 (UST)	PC-90	8	5	8	4	7	5	6	3	4	9	6	3	3	4	5	1	1-9
	PC-75	6	4	7	3	3	4	5	2	4	7	5	2	2	3	5	1	1-7
	PC-50	**4**	**3**	**5**	**2**	**3**	**3**	**5**	**2**	**3**	**4**	**5**	**2**	**2**	**3**	**4**	**1**	**1-5**
	PC-25	3	3	4	2	2	3	4	1	3	3	4	2	2	2	4	1	1-4
	PC-10	2	2	4	1	2	2	4	1	2	2	3	1	2	2	3	1	1-4
SO4 (UST)	PC-90	2	3	3	5	2	2	2	3	3	2	3	4	2	2	2	2	2-5
	PC-75	2	2	2	2	2	2	2	2	2	2	2	3	1	2	2	2	1-3
	PC-50	**2**	**2**	**2**	**1**	**2**	**2**	**2**	**2**	**2**	**2**	**2**	**2**	**1**	**2**	**2**	**1**	**1-2**
	PC-25	2	2	2	1	1	2	2	1	1	2	2	2	1	2	2	1	1-2
	PC-10	1	2	1	1	1	2	2	1	1	1	2	1	1	2	2	1	1-2
Org (UST)	PC-90	29	12	16	9	18	8	9	5	10	6	7	3	18	7	5	5	3-29
	PC-75	18	9	11	7	10	5	5	3	6	4	5	2	11	5	4	3	2-18
	PC-50	**12**	**7**	**5**	**5**	**6**	**4**	**4**	**3**	**4**	**3**	**4**	**2**	**7**	**3**	**3**	**3**	**2-12**
	PC-25	7	4	3	3	5	3	3	2	3	2	3	2	5	2	2	2	2-7
	PC-10	4	4	1	2	4	2	2	1	2	2	2	1	2	1	2	2	1-4

Table C2. Percentiles of relative standard deviation (*rows; corresponding to the box-whiskers plot in Figure D3e,f*) in percent from lognormal peak fits (bimodal deconvolution) for the resolved Aitken mode (a) and accumulation mode (b) particle concentration for diurnal size distributions at the urban MK site (2013), *columns* describe the data set, i.e. reconstructed size distributions from the 25th percentile, median, 75th percentile and mean of the size bins *Sp=Spring, Su=Summer*

(a)

Aitken mode % SD		25th PC Distr.		Median Distr.		75th PC Distr.		Mean Distr.		Range
		Sp	Su	Sp	Su	Sp	Su	Sp	Su	
NO3 (MK)	PC-90	38	46	40	34	40	41	22	26	22-46
	PC-75	27	34	26	28	34	35	20	16	16-35
	PC-50	**15**	**24**	**23**	**21**	**25**	**28**	**18**	**14**	**14-28**
	PC-25	9	20	19	17	18	22	15	12	9-22
	PC-10	6	19	16	14	15	20	13	11	6-20
SO4 (MK)	PC-90	63	46	35	38	24	31	23	21	21-63
	PC-75	50	36	30	36	21	28	21	20	20-50
	PC-50	**44**	**33**	**28**	**24**	**20**	**23**	**19**	**18**	**18-44**
	PC-25	37	27	24	21	17	20	15	17	15-37
	PC-10	33	25	21	19	15	18	15	16	15-33
Org (MK)	PC-90	22	12	22	19	30	21	15	14	12-30
	PC-75	16	10	12	12	18	11	12	8	8-18
	PC-50	**10**	**8**	**10**	**9**	**10**	**9**	**8**	**7**	**7-10**
	PC-25	8	7	8	7	7	8	6	6	6-8
	PC-10	7	6	7	6	6	6	5	5	5-7

(b)

Accum. mode % SD		25th PC Distr.		Median Distr.		75th PC Distr.		Mean Distr.		Range
		Sp	Su	Sp	Su	Sp	Su	Sp	Su	
NO3 (MK)	PC-90	9	9	6	7	3	5	2	5	2-9
	PC-75	6	8	4	5	3	4	2	4	2-8
	PC-50	**4**	**6**	**3**	**4**	**2**	**3**	**2**	**3**	**2-6**
	PC-25	2	5	2	4	2	3	1	3	1-5
	PC-10	2	4	1	3	1	3	1	2	1-4
SO4 (MK)	PC-90	4	3	2	3	2	5	2	3	2-5
	PC-75	3	2	2	3	2	4	2	2	2-4
	PC-50	**3**	**2**	**2**	**2**	**1**	**4**	**2**	**2**	**1-4**
	PC-25	2	2	2	2	1	3	1	2	1-3
	PC-10	2	2	1	2	1	3	1	2	1-3
Org (MK)	PC-90	9	8	8	7	9	5	6	6	5-9
	PC-75	6	7	5	5	5	4	5	4	4-7
	PC-50	**5**	**5**	**4**	**4**	**3**	**4**	**3**	**4**	**3-5**
	PC-25	4	4	3	3	3	3	3	3	3-4
	PC-10	2	3	3	3	5	2	2	2	2-3

Table C3. Percentiles of percent standard deviation (*rows; corresponding to the box-whiskers plot in Figure D5e,f*) from lognormal peak fits (bimodal deconvolution) for the resolved Aitken mode and accumulation mode for 24h day-to-day size distributions at the suburban HKUST site (a) and the urban MK site (b) for all investigated species, *columns* describe the uncertainties in terms of quartiles of resolved peak area, where Q1 refers to the lowest 25% and Q4 the highest 25% of resolved peak area (see also Figure D4)

(a)

HKUST '11/12 % SD		NO3					SO4					Org				
		Q1	Q2	Q3	Q4	Range	Q1	Q2	Q3	Q4	Range	Q1	Q2	Q3	Q4	Range
Aitken mode	PC-90	95	64	50	27	27-95	97	78	49	30	30-97	62	37	28	26	26-62
	PC-75	58	47	37	24	24-58	91	57	36	20	20-91	41	24	21	22	21-41
	PC-50	**47**	**35**	**25**	**17**	**17-47**	**60**	**39**	**29**	**16**	**16-60**	**30**	**17**	**14**	**17**	**14-30**
	PC-25	30	25	20	13	13-30	32	26	21	13	13-32	25	14	10	12	10-25
	PC-10	20	16	15	8	8-20	24	18	13	11	11-24	16	11	6	7	6-16
Accum. mode	PC-90	31	9	7	4	4-31	4	3	3	3	3-4	18	11	9	7	7-18
	PC-75	13	6	5	3	3-13	3	3	3	2	2-3	9	7	6	5	5-9
	PC-50	**8**	**4**	**3**	**2**	**2-8**	**2**	**2**	**2**	**2**	**~2**	**6**	**4**	**5**	**3**	**3-6**
	PC-25	3	3	2	2	2-3	2	2	2	2	~2	4	3	3	2	2-4
	PC-10	1	2	2	1	1-2	2	2	2	1	1-2	3	2	2	2	2-3

(b)

MK '13 % SD		NO3					SO4					Org				
		Q1	Q2	Q3	Q4	Range	Q1	Q2	Q3	Q4	Range	Q1	Q2	Q3	Q4	Range
Aitken mode	PC-90	62	52	47	30	30-62	94	50	29	24	24-94	23	17	13	16	13-23
	PC-75	41	42	30	25	25-42	47	35	22	16	16-47	16	14	11	12	11-16
	PC-50	**28**	**34**	**21**	**18**	**18-34**	**33**	**24**	**17**	**12**	**12-33**	**11**	**10**	**6**	**8**	**6-11**
	PC-25	21	22	19	12	12-22	26	17	13	9	9-26	8	7	5	6	5-8
	PC-10	6	10	13	8	6-13	19	14	10	5	5-19	6	5	3	3	3-6
Accum. mode	PC-90	22	21	6	6	6-22	7	6	6	4	4-7	13	8	9	8	8-13
	PC-75	17	10	5	3	3-17	4	4	4	2	2-4	8	7	6	4	4-8
	PC-50	**10**	**6**	**4**	**2**	**2-10**	**3**	**2**	**2**	**1**	**1-3**	**6**	**5**	**4**	**2**	**2-6**
	PC-25	6	3	2	2	2-6	2	2	1	1	1-2	4	4	3	2	2-4
	PC-10	3	1	2	1	1-3	1	1	1	1	~1	2	3	2	1	1-3

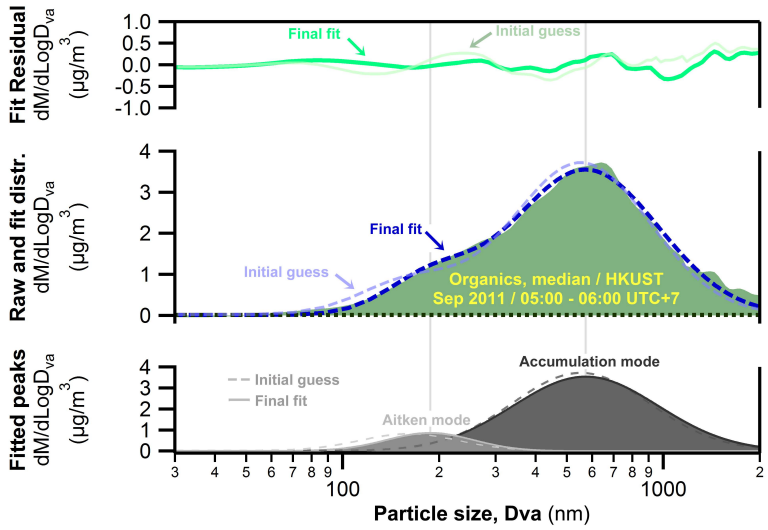

Figure D1. Example of a log-normal peak fit *(Multipeak Fit V2, Igor Pro, Wavemetrics, Levenberg-Marquardt algorithm)* of an AMS organics size distribution

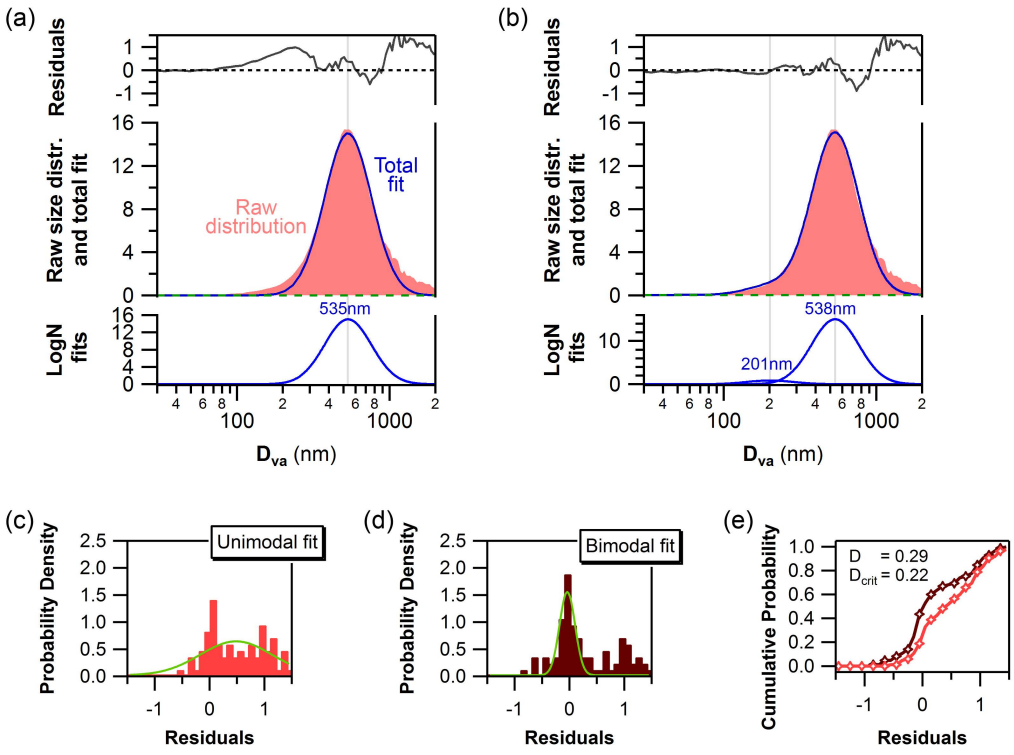

Figure D2. 24h average size distribution of sulfate (12/12/2011, suburban HKUST site) with (a) unimodal and (b) bimodal logN peak fitting applied; histograms of residuals from the unimodal (c) and bimodal (d) distributions with Gaussian fit (green); and cumulative probability density functions of uni- and bimodal fit residuals (e) with Kolmogorov-Smirnov D metric values at 95% confidence level

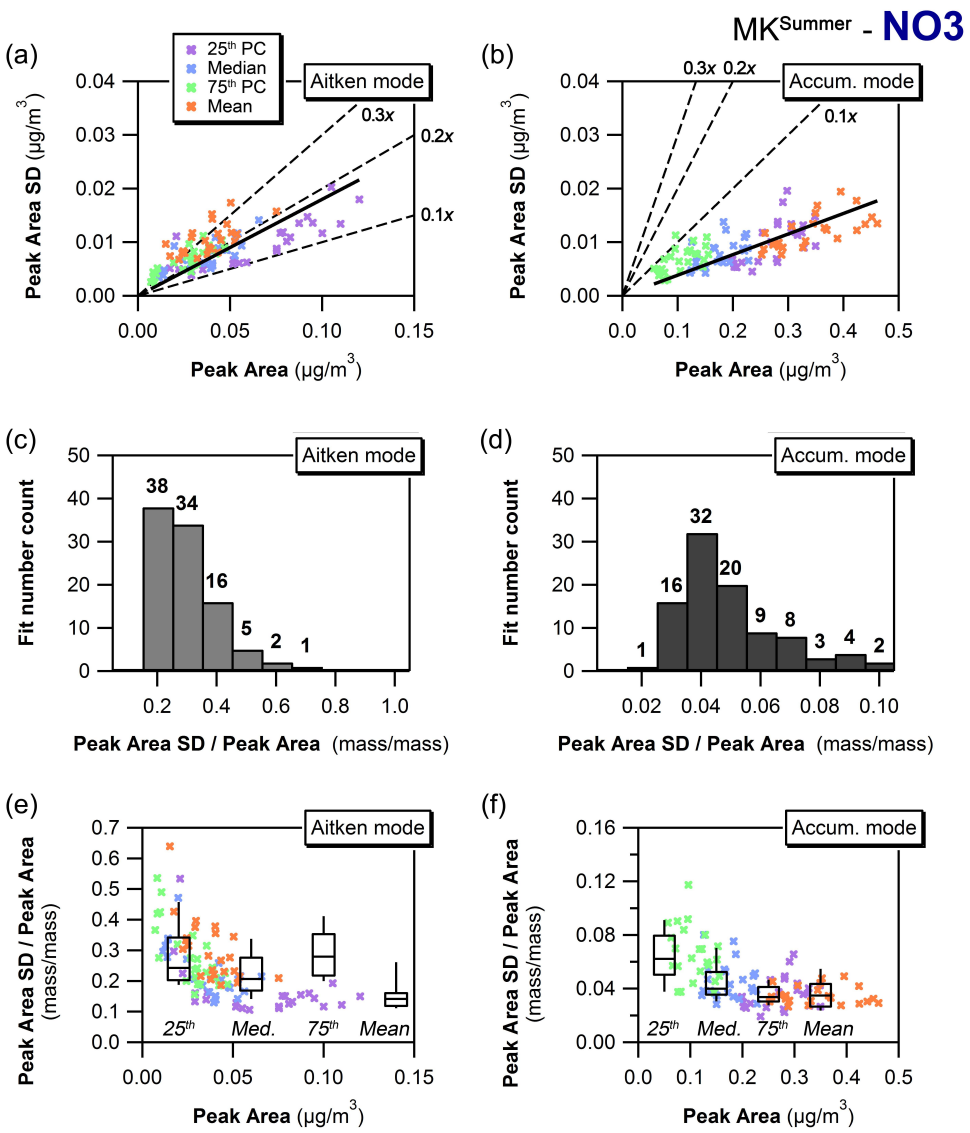

Figure D3. Standard deviation of peak area as a function of mode peak area (a,b), histogram of relative standard deviation i.e. the ratio of standard deviation to mode peak area (c,d) where the last bin also contains all values beyond the last bin range, and relative standard deviation as a function of mode peak area (e,f) for the fitted Aitken and accumulation mode with binned box-whiskers plot (25^{th} to 75^{th} PC box with horizontal median line and 10^{th} to 90^{th} PC whiskers where bins refer to quartiles of peak area from lowest Q1 to highest Q4); data for diurnal size distributions of NO3 at the urban Mong Kok site in summer 2013.

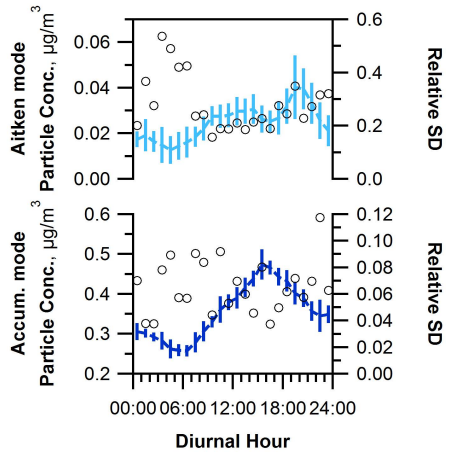

Figure D4. Plot of 75th percentile-bin diurnal variation with peak area fit variability and relative standard deviation (corresponding to green data and second to last box in Figure D3e,f)

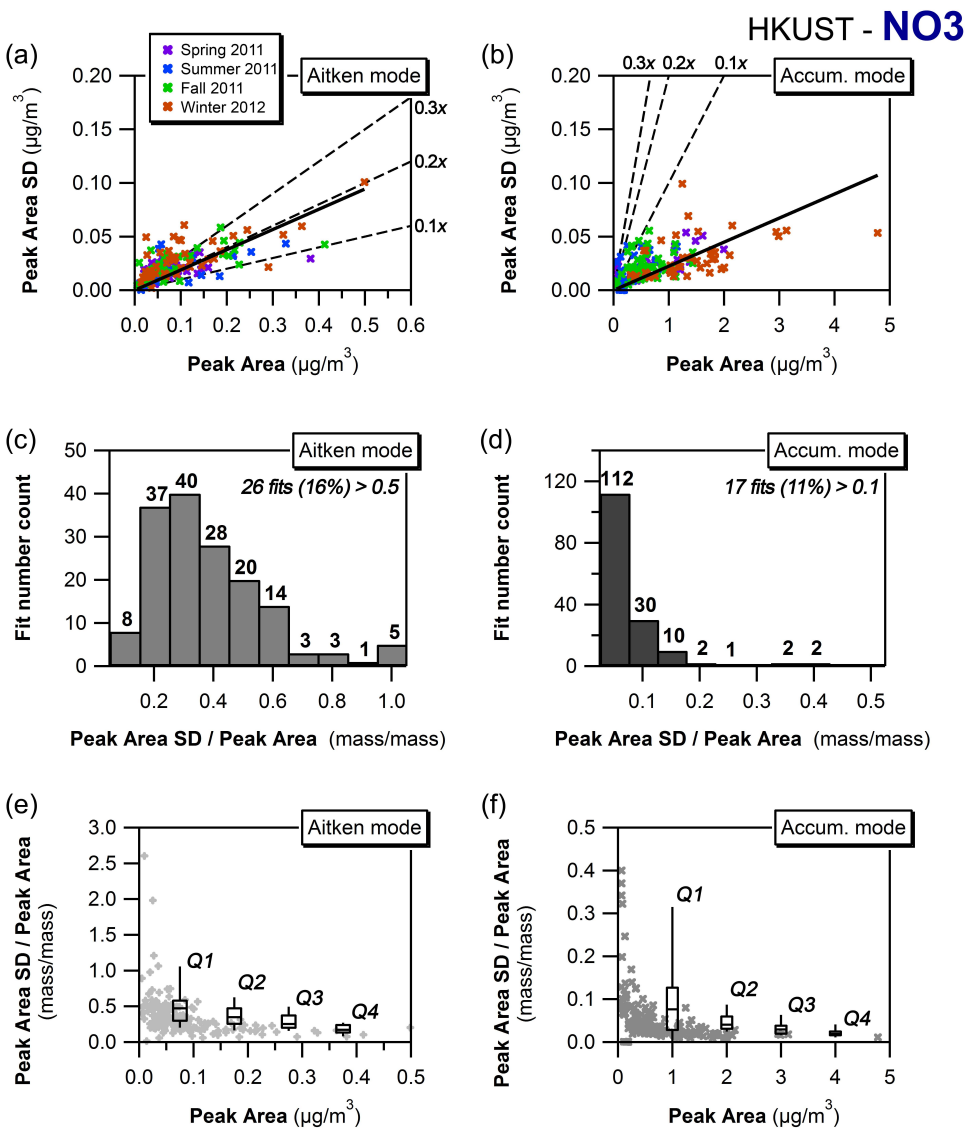

Figure D5. Standard deviation of peak area as a function of mode peak area (a,b), histogram of relative standard deviation i.e. the ratio of standard deviation to mode peak area (c,d) where the last bin also contains all values beyond the last bin range, and relative standard deviation as a function of mode peak area (e,f) for the fitted Aitken and accumulation mode with binned box-whiskers plot (25th to 75th PC box with horizontal median line and 10th to 90th PC whiskers where bins refer to quartiles of peak area from lowest Q1 to highest Q4); data for day-to-day size distributions of NO3 at the HKUST site including all seasons.

References

Aiken, A. C., Salcedo, D., Cubison, M. J., Huffman, J. A., DeCarlo, P. F., Ulbrich, I. M., Docherty, K. S., Sueper, D., Kimmel, J. R., Worsnop, D. R., Trimborn, A., Northway, M., Stone, E. A., Schauer, J. J., Volkamer, R. M., Fortner, E., de Foy, B., Wang, J., Laskin, A., Shutthanandan, V., Zheng, J., Zhang, R., Gaffney, J., Marley, N. A., Paredes-Miranda, G., Arnott, W. P., Molina, L. T., Sosa, G., and Jimenez, J. L.: Mexico City aerosol analysis during MILAGRO using high resolution aerosol mass spectrometry at the urban supersite (T0) - Part 1: Fine particle composition and organic source apportionment, Atmospheric Chemistry and Physics, 9, 6633-6653, 2009.

Bian, Q., Huang, X. H. H., and Yu, J. Z.: One-year observations of size distribution characteristics of major aerosol constituents at a coastal receptor site in Hong Kong – Part 1: Inorganic ions and oxalate, Atmos. Chem. Phys., 14, 9013-9027, 10.5194/acp-14-9013-2014, 2014.

Canagaratna, M. R., Jayne, J. T., Ghertner, D. A., Herndon, S., Shi, Q., Jimenez, J. L., Silva, P. J., Williams, P., Lanni, T., Drewnick, F., Demerjian, K. L., Kolb, C. E., and Worsnop, D. R.: Chase studies of particulate emissions from in-use New York City vehicles, Aerosol Science and Technology, 38, 555-573, 10.1080/02786820490465504, 2004.

Cheung, K., Ling, Z. H., Wang, D. W., Wang, Y., Guo, H., Lee, B., Li, Y. J., and Chan, C. K.: Characterization and source identification of sub-micron particles at the HKUST Supersite in Hong Kong, Science of The Total Environment, 527–528, 287-296, http://dx.doi.org/10.1016/j.scitotenv.2015.04.087, 2015.

Drewnick, F., Hings, S. S., DeCarlo, P., Jayne, J. T., Gonin, M., Fuhrer, K., Weimer, S., Jimenez, J. L., Demerjian, K. L., Borrmann, S., and Worsnop, D. R.: A new time-of-flight aerosol mass spectrometer (TOF-AMS) - Instrument description and first field deployment, Aerosol Science and Technology, 39, 637-658, 10.1080/02786820500182040, 2005.

Elser, M., Huang, R. J., Wolf, R., Slowik, J. G., Wang, Q., Canonaco, F., Li, G., Bozzetti, C., Daellenbach, K. R., Huang, Y., Zhang, R., Li, Z., Cao, J., Baltensperger, U., El-Haddad, I., and Prévôt, A. S. H.: New insights into PM2.5 chemical composition and sources in two major cities in China during extreme haze events using aerosol mass spectrometry, Atmos. Chem. Phys., 16, 3207-3225, 10.5194/acp-16-3207-2016, 2016.

Gill, P. E., Murray, W., and Wright, M. H.: The Levenberg-Marquardt method, in: Practical optimization, Academic Press, London, 1981.

Guo, H., Wang, D. W., Cheung, K., Ling, Z. H., Chan, C. K., and Yao, X. H.: Observation of aerosol size distribution and new particle formation at a mountain site in subtropical Hong Kong, Atmos. Chem. Phys., 12, 9923-9939, 10.5194/acp-12-9923-2012, 2012.

Huang, X. F., He, L. Y., Hu, M., Canagaratna, M. R., Sun, Y., Zhang, Q., Zhu, T., Xue, L., Zeng, L. W., Liu, X. G., Zhang, Y. H., Jayne, J. T., Ng, N. L., and Worsnop, D. R.: Highly time-resolved chemical characterization of atmospheric submicron particles during 2008 Beijing Olympic Games using an Aerodyne High-Resolution Aerosol Mass Spectrometer, Atmospheric Chemistry and Physics, 10, 8933-8945, 10.5194/acp-10-8933-2010, 2010.

Kittelson, D. B., Watts, W. F., and Johnson, J. P.: On-road and laboratory evaluation of combustion aerosols—Part1: Summary of diesel engine results, Journal of Aerosol Science, 37, 913-930, http://dx.doi.org/10.1016/j.jaerosci.2005.08.005, 2006a.

Kittelson, D. B., Watts, W. F., Johnson, J. P., Schauer, J. J., and Lawson, D. R.: On-road and laboratory evaluation of combustion aerosols—Part 2, Journal of Aerosol Science, 37, 931-949, http://dx.doi.org/10.1016/j.jaerosci.2005.08.008, 2006b.

Lee, B. P., Li, Y. J., Yu, J. Z., Louie, P. K. K., and Chan, C. K.: Physical and chemical characterization of ambient aerosol by HR-ToF-AMS at a suburban site in Hong Kong during springtime 2011, Journal of Geophysical Research: Atmospheres, 118, 8625-8639, 10.1002/jgrd.50658, 2013.

Lee, B. P., Li, Y. J., Yu, J. Z., Louie, P. K. K., and Chan, C. K.: Characteristics of submicron particulate matter at the urban roadside in downtown Hong Kong—Overview of 4 months of continuous high-resolution aerosol mass spectrometer measurements, Journal of Geophysical Research: Atmospheres, 120, 7040-7058, 10.1002/2015JD023311, 2015.

Li, Y. J., Lee, B. P., Su, L., Fung, J. C. H., and Chan, C. K.: Seasonal characteristics of fine particulate matter (PM) based on high resolution time-of-flight aerosol mass spectrometric (HR-ToF-AMS) measurements at the HKUST Supersite in Hong Kong, Atmos. Chem. Phys., 15, 37-53, doi:10.5194/acp-15-37-2015, 2015.

Mohr, C., DeCarlo, P. F., Heringa, M. F., Chirico, R., Slowik, J. G., Richter, R., Reche, C., Alastuey, A., Querol, X., Seco, R., Peñuelas, J., Jiménez, J. L., Crippa, M., Zimmermann, R., Baltensperger, U., and Prévôt, A. S. H.:

Identification and quantification of organic aerosol from cooking and other sources in Barcelona using aerosol mass spectrometer data, Atmos. Chem. Phys., 12, 1649-1665, 10.5194/acp-12-1649-2012, 2012.

Saarikoski, S., Carbone, S., Decesari, S., Giulianelli, L., Angelini, F., Canagaratna, M., Ng, N. L., Trimborn, A., Facchini, M. C., Fuzzi, S., Hillamo, R., and Worsnop, D.: Chemical characterization of springtime submicrometer aerosol in Po Valley, Italy, Atmos. Chem. Phys., 12, 8401-8421, 10.5194/acp-12-8401-2012, 2012.

Salcedo, D., Onasch, T. B., Dzepina, K., Canagaratna, M. R., Zhang, Q., Huffman, J. A., DeCarlo, P. F., Jayne, J. T., Mortimer, P., Worsnop, D. R., Kolb, C. E., Johnson, K. S., Zuberi, B., Marr, L. C., Volkamer, R., Molina, L. T., Molina, M. J., Cardenas, B., Bernabe, R. M., Marquez, C., Gaffney, J. S., Marley, N. A., Laskin, A., Shutthanandan, V., Xie, Y., Brune, W., Lesher, R., Shirley, T., and Jimenez, J. L.: Characterization of ambient aerosols in Mexico City during the MCMA-2003 campaign with Aerosol Mass Spectrometry: results from the CENICA Supersite, Atmospheric Chemistry and Physics, 6, 925-946, 2006.

Setyan, A., Zhang, Q., Merkel, M., Knighton, W. B., Sun, Y., Song, C., Shilling, J. E., Onasch, T. B., Herndon, S. C., Worsnop, D. R., Fast, J. D., Zaveri, R. A., Berg, L. K., Wiedensohler, A., Flowers, B. A., Dubey, M. K., and Subramanian, R.: Characterization of submicron particles influenced by mixed biogenic and anthropogenic emissions using high-resolution aerosol mass spectrometry: results from CARES, Atmos. Chem. Phys., 12, 8131-8156, 10.5194/acp-12-8131-2012, 2012.

Sun, Y., Zhang, Q., Macdonald, A. M., Hayden, K., Li, S. M., Liggio, J., Liu, P. S. K., Anlauf, K. G., Leaitch, W. R., Steffen, A., Cubison, M., Worsnop, D. R., van Donkelaar, A., and Martin, R. V.: Size-resolved aerosol chemistry on Whistler Mountain, Canada with a high-resolution aerosol mass spectrometer during INTEX-B, Atmos. Chem. Phys., 9, 3095-3111, 10.5194/acp-9-3095-2009, 2009.

Sun, Y. L., Zhang, Q., Schwab, J. J., Demerjian, K. L., Chen, W. N., Bae, M. S., Hung, H. M., Hogrefe, O., Frank, B., Rattigan, O. V., and Lin, Y. C.: Characterization of the sources and processes of organic and inorganic aerosols in New York city with a high-resolution time-of-flight aerosol mass spectrometer, Atmospheric Chemistry and Physics, 11, 1581-1602, 10.5194/acp-11-1581-2011, 2011.

Takegawa, N., Miyakawa, T., Watanabe, M., Kondo, Y., Miyazaki, Y., Han, S., Zhao, Y., van Pinxteren, D., Bruggemann, E., Gnauk, T., Herrmann, H., Xiao, R., Deng, Z., Hu, M., Zhu, T., and Zhang, Y.: Performance of an Aerodyne Aerosol Mass Spectrometer (AMS) during Intensive Campaigns in China in the Summer of 2006, Aerosol Science and Technology, 43, 189-204, 10.1080/02786820802582251, 2009.

Ulbrich, I. M., Canagaratna, M. R., Cubison, M. J., Zhang, Q., Ng, N. L., Aiken, A. C., and Jimenez, J. L.: Three-dimensional factorization of size-resolved organic aerosol mass spectra from Mexico City, Atmos. Meas. Tech., 5, 195-224, 10.5194/amt-5-195-2012, 2012.

Yao, X., Lau, N. T., Chan, C. K., and Fang, M.: Size distributions and condensation growth of submicron particles in on-road vehicle plumes in Hong Kong, Atmospheric Environment, 41, 3328-3338, 10.1016/j.atmosenv.2006.12.044, 2007.

Zhang, Q., Stanier, C. O., Canagaratna, M. R., Jayne, J. T., Worsnop, D. R., Pandis, S. N., and Jimenez, J. L.: Insights into the chemistry of new particle formation and growth events in Pittsburgh based on aerosol mass spectrometry, Environmental Science & Technology, 38, 4797-4809, 10.1021/es035417u, 2004.

Zhang, Q., Canagaratna, M. R., Jayne, J. T., Worsnop, D. R., and Jimenez, J. L.: Time- and size-resolved chemical composition of submicron particles in Pittsburgh: Implications for aerosol sources and processes, Journal of Geophysical Research-Atmospheres, 110, D07s09 Artn d07s09, 2005.

Zhuang, H., Chan, C. K., Fang, M., and Wexler, A. S.: Size distributions of particulate sulfate, nitrate, and ammonium at a coastal site in Hong Kong, Atmospheric Environment, 33, 843-853, 10.1016/s1352-2310(98)00305-7, 1999.

Diurnal and day-to-day characteristics of ambient particle mass size distributions from HR-ToF-AMS measurements at an urban site and a suburban site in Hong Kong

Berto P. Lee[1], Hao Wang[2], and Chak K. Chan[1,2*]

[1]School of Energy and Environment, City University of Hong Kong, Hong Kong, China

[2]Division of Environment, Hong Kong University of Science and Technology, Hong Kong, China

Correspondence to: Chak K. Chan (chak.k.chan@cityu.edu.hk)

Abstract. Mass concentration based particle size distributions measured by a high-resolution aerosol mass spectrometer were systematically analyzed to assess long and short-term temporal characteristics of ambient particle size distributions sampled at a typical urban environment close to emission sources and a suburban coastal site representing a regional and local pollution receptor location in Hong Kong. Measured distributions were bimodal and deconvoluted into submodes which were analyzed for day-to-day variations and diurnal variations.

Traffic and cooking emissions at the urban site contributed substantially to particle mass in both modes, while notable decreases in mass median diameters were limited to the morning rush hour. Inorganic particle components displayed varying diurnal behavior, including nocturnal nitrate formation and daytime photochemical formation evident in both modes. Suburban particle size distributions exhibited notable seasonal disparities with differing influence of local formation, particularly in spring and summer, and transport which dominated in the fall season leading to notably higher sulfate and organic accumulation mode particle concentrations. Variations in particle mixing state were evaluated by comparison of inter-species mass median diameter trends at both measurement sites. Internal mixing was prevalent in the accumulation mode in spring at the urban site, while greater frequency of time periods with external mixing of particle populations comprising different fractions of organic constituents was observed in summer. At the suburban site, sulfate and nitrate in the accumulation mode more frequently exhibited differing particle size distributions in all seasons signifying a greater extent of external mixing.

At the urban site, periods of greater submicron inorganic mass concentrations were more likely to be caused by increases in both Aitken and accumulation mode particle mass in summer, while at the suburban receptor location organic and nitrate Aitken mode particle mass contributed more regularly to higher total submicron species mass concentrations in most seasons (spring, summer and winter).

1. Introduction

Apart from mass and chemical composition, the size distribution of fine particles represents a vital physical property with important implications for human health and environmental effects of ambient aerosols (Seinfeld and Pandis, 2006). Particle size relates directly to the aerodynamic properties which govern the penetration and deposition of particles in the airways and lungs (Davidson et al., 2005) as well as the scattering and absorption of light which affect the radiative properties and hence ambient visibility (Ahlquist and Charlson, 1967;Bohren and Huffman, 1983;Charlson et al., 1991;Schwartz, 1996;Seinfeld and Pandis, 2006). Hygroscopic growth in response to changes in ambient humidity can alter particle light scattering properties (Seinfeld and Pandis, 2006;Köhler, 1936) and activation of condensation nuclei particles into cloud droplets depend on atmospheric conditions, chemical composition, mixing state as well as the size and morphology of particles (Abbatt et al., 2005;Kerminen et al., 2012;Meng et al., 2014;Westervelt et al., 2013).

Studies into the size distribution of ambient particulate matter in Hong Kong have been largely based on size-segregated filter samples (Yao et al., 2007b;Zheng et al., 2008;Zhuang et al., 1999;Huang et al., 2014;Bian et al., 2014) and measurements by electrostatic classifier instruments (Cheung et al., 2015;Yao et al., 2007a) and were hence either limited in size resolution (offline filter samples) or chemical resolution (total particle count by classification). Most measurements in Hong Kong were conducted in suburban environments. Inorganic ammonium and sulfate were mainly found in fine mode particles in condensation and droplet mode size ranges, while nitrate had strong coarse mode contributions (Zhuang et al., 1999). Seasonal differences were evident in solvent-extractable organics and trace metals which were mainly found in $PM_{0.5}$ particles in the wet season and winter whereas in fall a shift to larger particles (0.5–2.5 μm fraction) in fall indicated a possibly stronger influence of aged particle components in the transition period of the Asian monsoon (Zheng et al., 2008). Size distributions acquired by a fast mobility particle sizer at the suburban HKUST supersite were investigated more recently to study the formation and accumulation of ultrafine particles under different air flow regimes. Particle number concentration enhancements during the day were attributed to secondary formation, while evening and nighttime peaks were thought to be related to transport of aged aerosols from upwind locations. Nucleation mode particle peaks were often observed in fall and related to regional pollution influence (Cheung et al., 2015). New particle formation events at the same site occurred as single and two-stage growth processes with organics and sulfuric acid contributing mainly to first stage growth in the daytime while nighttime second stage growth was attributed to ammonium nitrate and organics. Particle size growth into the diameter range of cloud condensation nuclei (CCN) was typically only achieved with the second growth stage (Man et al., 2015).

Investigations into particle size distributions in urban areas of Hong Kong are even scarcer. Yao et al. (Yao et al., 2007a) studied the properties and behavior of particles in vehicle plumes and reported a competing process between ambient background particles and fresh soot particles in the condensation of gaseous precursors and a dependency on temperature with bimodal volume size distributions observed at lower ambient temperatures and unimodal distributions in the lower accumulation size range at higher ambient temperatures.

The Aerodyne aerosol mass spectrometer (Canagaratna et al., 2007) is widely used to determine the chemical composition of major organic and inorganic components of non-refractory submicron particulate matter ($NR\text{-}PM_1$). In contrast to most traditional aerosol sizing instruments, the AMS is capable of resolving main chemical constituents

within size distributions through analysis of particle flight times and particle ensemble mass spectra (Canagaratna et al., 2007;Jayne et al., 2000;Jimenez et al., 2003;Rupakheti et al., 2005) and thus yields valuable additional information on differences in composition of submicron particles with the gross of particle mass in the Aitken mode range (D_p ~ 10-100nm) and the accumulation mode range (D_p ~ 100-1000nm) covered by the AMS. Thus far most studies employing ambient size distribution data from aerosol mass spectrometer measurements investigated longer time period averages, i.e. campaign averages (Salcedo et al., 2006;Sun et al., 2009;Aiken et al., 2009;Huang et al., 2010;Takegawa et al., 2009;Saarikoski et al., 2012;Li et al., 2015) or specific time periods of interest (Elser et al., 2016;Lee et al., 2013). Mohr et al. separated organic particle mass size distributions by periods of dominant influence of different PMF-resolved organic aerosol factors to study the properties of mass size distributions in relation to organic aerosol composition (Mohr et al., 2012). The 3D-factorization technique is an extension of traditional AMS PMF analysis on organic aerosol allowing to obtain estimates on the size distributions of organic aerosol factors, however under the assumption that factor size distributions remain invariant over the measurement period (Ulbrich et al., 2012).

The temporal evolution of species-specific size distributions, are mostly discussed qualitatively (Drewnick et al., 2005) and only few studies have evaluated temporal trends in mass size distributions in greater detail. Particle nucleation and subsequent growth events were investigated in Pittsburgh using size data from an AMS and two SMPS as well as various gaseous pollutant instruments and meteorological information. The AMS mass size distributions were evaluated quantitatively using the time series of binned particle concentrations generated from the grouping of raw data into wider size bins to represent different stages in the particle growth process. (Zhang et al., 2004). The same method was employed to evaluate contributions of ultrafine mode and accumulation mode particles to total organic particle mass (Zhang et al., 2005) by summation of size bins in the range of 30-100 nm and 100-1000nm. The authors also explored diurnal changes in size distributions of particle species by averaging over 3h periods in the morning (6–9 am) and afternoon (1–4 pm). Sun et al. present a qualitative discussion of diurnal variations in the mass size distributions of the m/z 44, m/z 57 and derived $C_4H_9^+$ ion signals from measurements at an urban site in New York (Sun et al., 2011). Similarly, Setyan et al. examined diurnal changes in the mass size distributions of organics and sulfate qualitatively and used binned concentrations (40–120, 120–200, and 200–800) nm in their quantitative analysis to study the evolution of particle chemistry in new particle formation and growth events (Setyan et al., 2012).

In this work, we introduce a systematic approach of analyzing AMS mass-based particle size distributions on finer time scales and thus utilize two key instrumental advantages, i.e. species segregation and high time resolution, to obtain a more detailed understanding of the variabilities in ambient particle mass size distributions and to provide an additional dimension to standard AMS data analysis techniques. In this context, we present a detailed discussion of particle size data from HR-ToF-AMS measurements during two field campaigns in Hong Kong in both urban and suburban environments. We aim to evaluate characteristic recurrent changes in size distribution as well as longer term trends in different seasons by analyzing day-to-day variations and diurnal variations of size distributions of submicron organics, sulfate, and nitrate particle mass. The two contrasting sites represent a typical urban source environment (inner-city, roadside station) close to primary emission sources and a suburban location (coastal, HKUST supersite)

which is largely a downwind receptor of varying amounts of local urban, regional and long-range transported pollutants (Li et al., 2015;Huang et al., 2014).

2. Methodology

2.1. Field campaigns

Sampling of ambient submicron non-refractory particulate matter (NR-PM_1) was carried out using an Aerodyne HR-ToF-AMS at the HKUST air quality supersite covering four seasons between May 2011 and February 2012 (spring: 2011-05, summer: 2011-09, fall: 2011-11&12, winter: 2012-02). The HKUST supersite is located on the campus of the Hong Kong University of Science and Technology (22°20'N, 114°16'E), on the east coast of Hong Kong in a suburban area with few primary emission sources in the immediate vicinity. Sampled air was drawn from the rooftop of a pump house building at an approximate height of 25m above ground level. For detailed descriptions of the experimental setup, operating conditions, data treatment, and overall species composition we refer the reader to previous publications (Lee et al., 2013;Li et al., 2015;Li et al., 2013). A further sampling campaign took place between spring 2013 (2013-03 to 2013-05) and summer 2013 (2013-05 to 2013-07) at an inner-city urban location in the densely populated and built-up Kowloon peninsula. Measurements were conducted next to the roadside air quality monitoring station (AQMS) operated by the Environmental Protection Department (EPD) of the HKSAR Government in the Mong Kok (MK) district on a pedestrian crossing at a major road junction. Sampled air was drawn from a height of 3m above ground level. A comprehensive analysis of trends in species concentration and composition identified in this urban campaign has been presented previously (Lee et al., 2015). In both campaigns, particles were sampled through a $PM_{2.5}$ cyclone at a flow rate of 16.67 L/min into a sampling port from which 0.08 L/min was drawn by the AMS and the remainder drawn by co-sampling instruments and an auxiliary pump. Sample air for the AMS passed through a 1m long diffusion dryer (BMI, San Francisco CA, USA) filled with silica gel to remove bulk gas- and particle-phase water. Additional data from various collocated instruments including meteorological data (wind, temperature, relative humidity, solar irradiation), volatile organic compounds (VOCs) and standard trace gases such as NO_x, SO_2, and O_3 were available and details on employed instrument models and sampling methodologies are discussed in aforementioned studies (Lee et al., 2013, 2015;Li et al., 2015;Li et al., 2013).

2.2. Data acquisition and treatment

In both campaigns, mass concentration based size distributions in terms of vacuum-aerodynamic particle diameter ($dM/d\log D_{va}$) were established by joint acquisition of particle time-of-flight (PToF) measurements and unit mass resolution mass spectra (V-mode) with alternation between modes every 20s for 30 cycles amounting to 5 min of total sampling time. High-resolution mass spectra were acquired for the following 5 min, and thus the overall raw data time resolution for each mode was equal to 10 min. The total particle mass measured in the PToF mode was normalized to the V-mode mass concentration of the same time step. Daily size distributions were generated by averaging over 24h

periods (from 0:00 to 23:59). Hourly diurnal size distributions were reconstructed by grouping size distributions within the same hour of the day and establishing representative size distributions based on average, median, 25th and 75th percentile concentration values of each size bin (*referred to as size distribution sets hereinafter*).

At both sampling sites, the seasonally averaged AMS size distributions were bimodal (Lee et al., 2013, 2015;Li et al., 2015) with similar distributions having been observed in other AMS field studies in various parts of the world. (Zhang et al., 2014;Sun et al., 2011;Huang et al., 2011;Aiken et al., 2009;Zhang et al., 2005;Crippa et al., 2013;Docherty et al., 2011;Mohr et al., 2012). Multimodality of size distributions is typical for environments where different sources or formation processes of particles play a role and accordingly such distributions can also be represented as sums of discrete lognormal distributions of the respective constituting submodes (John, 2011).

The measured bimodal size distributions in this work were deconvoluted by fitting two log-normal distributed modes, including one closer to the Aitken size range (*mode diameter ~100nm*) and one in the accumulation size range (*mode diameter ~500nm*) employing the Levenberg-Marquardt algorithm (Gill et al., 1981) as a non-linear least squares fit, to evaluate differences in trends and formation or transformation processes in the two size regimes. An example of a size distribution fit and associated parameters is depicted in Figure D1 in the Supporting Material. Additional fit residual analyses were carried out in cases where the Aitken mode only accounted for small parts of (<10%) of the total particle mass and uncertainties in integrated mode particle mass from the peak fitting were examined for all size distributions. Details are presented in Section B of the Supporting Material. The smaller mode typically exhibited mode diameters in the range of 100-200 nm (D_{va}) and is thus in the transition region between Aitken and lower accumulation mode. For a clearer distinction from the larger mode which unambiguously belonged to the accumulation size range, we opt to refer to the small mode as *Aitken mode* in this work. Mode diameter (*i.e.* mass median diameter, MMD), curve width (*i.e.* geometric standard deviation, GSD) and curve area (*equivalent to particle mass concentration within the mode*) are sufficient parameters to completely describe a lognormal distribution and these key variables are used in the following analysis on trends in the fitted species-specific size distributions of organics, nitrate, and sulfate from both HR-AMS sampling campaigns in Hong Kong. Particle diameters are discussed in terms of vacuum-aerodynamic diameter, with detailed discussions on properties and relationships to other size metrics available elsewhere (DeCarlo et al., 2004;Slowik et al., 2004). Further details on procedures of PToF data acquisition and size distribution averaging can be found in the Supporting Material in Section A and B respectively. The sequence of main data treatment and analysis steps is shown in Figure 1.

The transmission efficiency of the AMS aerodynamic lens is known to fall off beyond ~0.7 µm of vacuum-aerodynamic diameter (Liu et al., 2007;Takegawa et al., 2009;Zhang et al., 2004;Bahreini et al., 2008;Williams et al., 2013) and may bias measured particle mass and mode diameters in the accumulation mode towards lower values if significant particle mass fractions fall in the size region of D_{va} > 0.7 µm. In this work, resolved MMDs at either sampling location were well within the efficient upper transmission limit for the vast majority of data.

The discussion of size distributions in this work should be viewed in the context of the instrumental capabilities and limitations of aerosol mass spectrometry, i.e. resolved Aitken and accumulation modes in this work are the apparent Aitken and accumulation modes within AMS measurable particle mass size distributions.

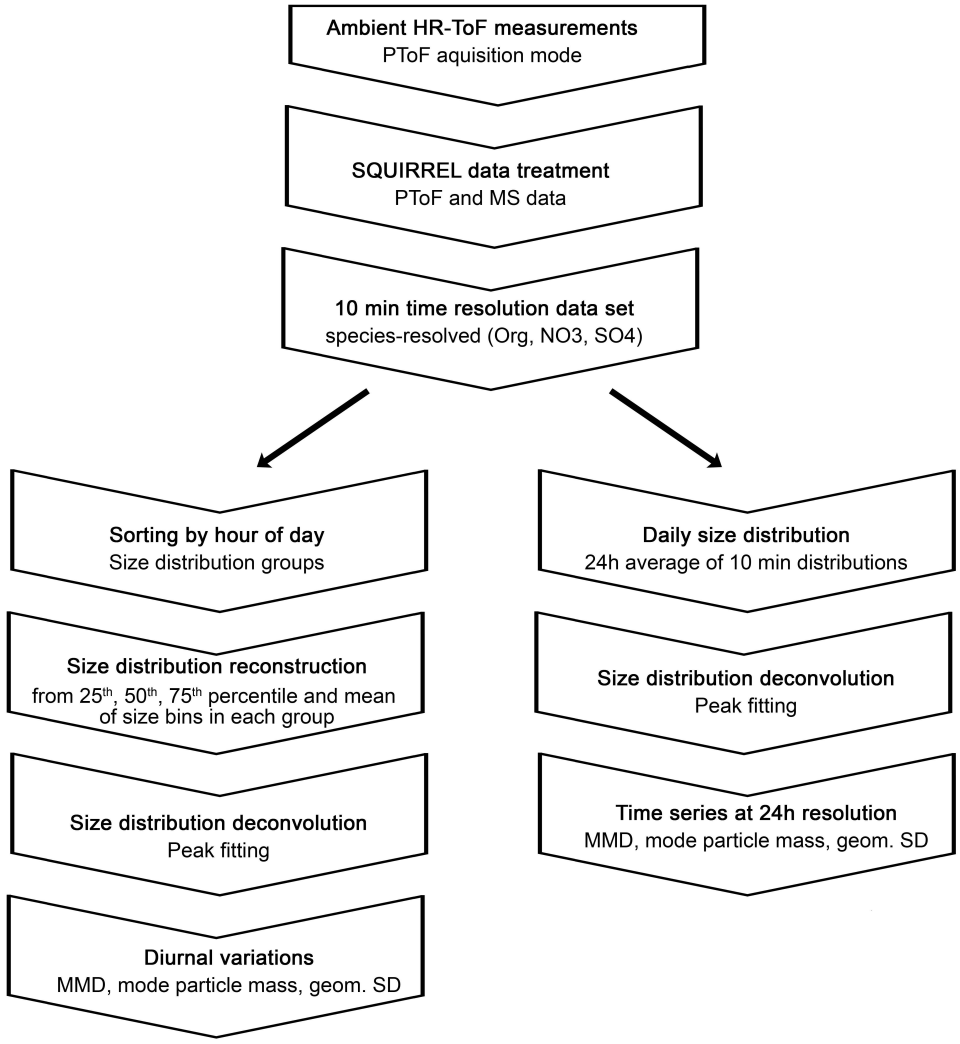

Figure 1. Flow chart of main data acquisition, data treatment and data analysis procedures

3. Results and Discussion

3.1. Diurnal size distribution characteristics

Diurnal species variations are predominantly discussed in terms of total mass concentration up to the size cut of the sampling inlet or the instrumental capability, e.g. total species concentrations in NR-PM_1 for AMS-based studies. AMS mass-based size distributions can be utilized more systematically and complementary to standard AMS data analysis techniques by deconvoluting multimodal distributions into their constituting submodes and evaluating their variation and contribution to overall species concentration variations on a diurnal time scale. As previously mentioned, we examined size distributions reconstructed from the average, median, 25th and 75th percentile of hourly grouped size distributions, analogous to commonly reported AMS species diurnal variations, with quantitative analysis focusing on concentrations from the median dataset.

3.1.1. Urban roadside NR-PM$_1$

The urban roadside measurements took place between March and July 2013 covering two seasons (Spring 2013: *March to mid-May 2013;* Summer 2013: *mid-May to July 2013*) at a location dominated by the influence of primary emission sources. Organics were the major particulate species in NR-PM$_1$ of which two-thirds were attributable to traffic and cooking sources. Anthropogenic gas-phase species, including various VOCs, NO_x, CO, and SO_2 were continuously abundant as well (Lee et al., 2015;Sun et al., 2016). Particle size distributions at the urban site exhibited discernible diurnal trends, with Figure 2 depicting the variations in (mass median) diameters of the lognormal fitted Aitken and accumulation modes, corresponding integrated peak areas representing the total mass accounted for by particles in each mode, the geometric standard deviation signifying the spread across particle sizes as well as the total submicron mass (NR-PM$_1$) diurnal variation for organics, sulfate, and nitrate based on AMS V-mode data. Individual trends are discussed species-wise in the following.

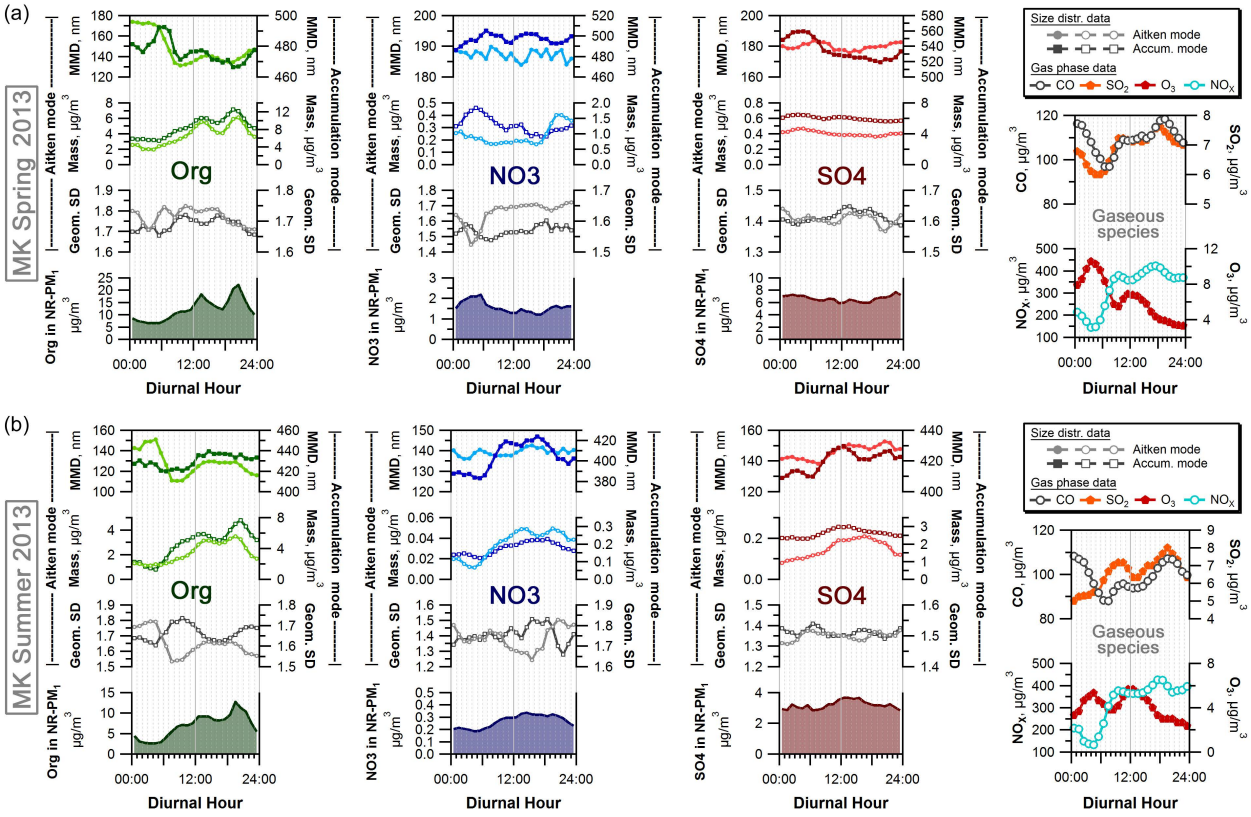

Figure 2. Diurnal variations of mode diameter (MMD), integrated mode mass concentration and width of the Aitken mode (*lighter color*) and accumulation mode (*darker color*) from bimodal peak fits of the bin-median reconstructed size distributions at the urban Mong Kok site and V-mode AMS species concentrations (*line with shaded background*) for organics, nitrate and sulfate (*left to right*) in (a) Spring 2013 and (b) Summer 2013; The right-most panel depicts the diurnal variations of relevant gas-phase pollutants (O_3, CO, NO_x, SO_2) measured at the adjacent Mong Kok Air Quality Monitoring Site (MK AQMS)

Organics

The diurnal variation of total Aitken and accumulation mode particle mass both largely followed the same trend as total submicron organic mass (lower panels in Figure 2 a, b) affirming that urban sources of organic particulate matter contributed substantially to PM mass across the covered size region. Mass concentrations in both modes were smallest during the night (*0:00 to 6:00*) and highest during lunch and dinner (*12:00 to 14:00, 19:00 to 21:00*), when the influence of organic aerosol from cooking (COA - cooking organic aerosol) and from traffic (HOA – hydrocarbon-like organic aerosol) were dominant (Lee et al., 2015). Trends in integrated mode particle mass and MMDs were similar across all size distribution sets (Figure D6 in the Supporting Material), confirming that they occurred persistently throughout the measurement period and making diurnal timescale processes the dominant factor in determining size characteristics of organic-containing particles at this urban roadside location.

Minimum Aitken mode particle mass concentrations (*median values*) amounted to 2.3 µg/m^3 in spring and 1.2 µg/m^3 in summer, accounting for 28-38% of total submicron particulate mass, and were typically reached between 03:00 and 04:00. These concentrations represent the estimated urban background mass of Aitken mode particles carried over from the daytime and not removed by gravitational settling, coagulation or sweep-out as well as contributions from nighttime activity such as traffic, which remains continuous in the inner-city districts at night albeit at much lower vehicle numbers compared to the daytime.

Organic concentrations increased notably between 6:00 and 9:00 during the morning rush hour with traffic-related constituents (*HOA – hydrocarbon-like organic aerosol*) accounting for the largest part (60% in spring, 40% in summer) of this increase. In the Aitken mode, particle mass concentrations rose by 1.6 µg/m^3 (spring) and 0.8 µg/m^3 (summer) in the same time period. Assuming direct proportionality between the contribution of HOA to total submicron organic mass increase and the increase of particle mass in each submode, 0.9 µg/m^3 (spring) and 0.3 µg/m^3 (summer) of particle mass were estimated as traffic-related organic components in the Aitken mode. Significant changes were evident in the particle size metric (MMD) during the same time period, where a consistent decrease by 20-30% from about 170 nm (spring) or 160 nm (summer) to 130-140 nm (spring) or 120 nm (summer) was evident with the concurrent increase in road traffic. This combined shift to smaller particle size and increase in total particle mass denotes a strong increase in the total number concentrations of particles in the Aitken mode range by at least a factor of 4-5 (assuming spherical particles and constant particle density) with significant additional contributions expected from elemental carbon particles and smaller Aitken mode and nucleation mode particles below the range of efficient particle transmission of the AMS inlet lens (Williams et al., 2013).

Beyond 10:00, changes in submicron organic mass concentrations were dominated by variations in cooking-related organic aerosol (COA) components. During the main meal times (12:00 – 14:00 and 19:00 – 21:00) changes in organic submicron mass were almost entirely (>80%) caused by COA in both seasons (Table C4 in the Supporting Material) and daily maximum Aitken mode particle mass concentrations typically occur during these hours (5.5 – 6.2 µg/m^3 in spring, 3.1 – 3.5 µg/m^3 in summer) with higher concentrations during the dinner period. Analogous to HOA, considering proportionality between COA fractional contribution and submode particle mass increase, primary cooking emissions accounted for 1.7 - 1.8 µg/m^3 of organic particle mass in the Aitken mode. Dinner in summer represents a notable exception, where the estimated cooking-related increase only amounted to 0.5 µg/m^3. This is

mainly due to specific local meteorological and geographical features owing to a greater frequency of easterly surface winds in the warmer season and the geographical distribution of cooking sources predominantly to the east of the sampling site (Sun et al., 2016;Lee et al., 2015), which led to considerably elevated Aitken mode mass concentration throughout the day including the late afternoon period and a correspondingly smaller additional increase during the dinner time. The aforementioned effect is particularly evident in the diurnal trend of the Aitken mode particle mass fraction among total organic submicron mass (Figure 4b) which displayed a broad bell-shape during the day in summer with nominal increases of 9-10%, whereas in spring the variation follows a double peak behavior with nominal increases of 4-5% during the meal times which emphasize the more intermittent behavior of cooking-related particle contributions in spring. Cooking emissions did not lead to conspicuous changes in the size-related distribution metrics, i.e. there were no obvious trends in particle diameters (MMDs) or distribution widths (GSDs) during the meal time periods (Figure 2a, b - *black lines in lower panels*).

In the accumulation mode, organic particle mass during the night hours (00:00 – 06:00) was 2.5 times larger in spring (5.5 µg/m^3) than in summer (2.0 µg/m^3). The mass concentration increase during the morning rush hour was larger in summer (ΔM=3.9 µg/m^3) than in spring (ΔM=3.0 µg/m^3), which was mainly caused by daytime increases of SOA components in summer (Lee et al., 2015), and consequently led to a lower fractional rush hour increase of traffic related organic constituents. Estimated particle mass contributions of traffic emissions in the accumulation mode amounted to 1.8 µg/m^3 in spring and 1.6 µg/m^3 in summer. In terms of particle size, the onset of the rush hour had little conspicuous effects on the accumulation mode without clear trends in MMDs in both seasons. In summer the shift to smaller MMDs was accompanied by a notable narrowing of the Aitken mode, whereas in spring Aitken mode distribution widths remained largely stable throughout the day (Figure 2a, b - *lower panels*).

Maximum accumulation mode particle concentrations during the meal hours reached 10.5 – 12.3 µg/m^3 in spring and 6.0 – 7.4 µg/m^3 in summer. Analogous to the Aitken mode, estimated cooking-related particle contributions in the accumulation mode amounted to 2.0 µg/m^3 (spring) and 1.0 µg/m^3 (summer) during lunch, and to 2.7 µg/m^3 (spring) and 2.4 µg/m^3 (summer) during dinner. Also, distribution widths (GSD) in the accumulation mode were not notably affected by cooking emissions. Seasonal differences were apparent in the mass median diameters of the accumulation mode. In spring, mode diameters remained largely constant (+/- 10nm) apart from a subtle peak during the morning rush hour, indicative of minor condensational growth of traffic-related primary organics or rapidly formed secondary species. In summer, a consistent increase in particle size by 20nm (~5%) during the daytime points to particle growth through secondary formation as a governing factor.

Aitken mode particles contributed larger fractions to the total increase in organic submicron particle mass during the rush hour and mealtimes in spring (33-56%) than in summer (16-38%). These differences were presumably due to seasonal meteorology and associated effects on the formation, accumulation, and dispersion of particles from primary emission sources, as source strengths and characteristics of road traffic and commercial cooking are unlikely to vary with seasons in the inner-city urban areas of Hong Kong. Ambient temperatures and solar irradiation differed substantially with 7^{o}C higher average temperatures and three times higher integrated daily solar irradiation in summer compared to spring (Figure D10e,f in the Supporting Material). Lower overall ambient temperatures enhance condensation of gas-phase emissions and particle nucleation and shift the gas-to-particle partitioning equilibrium of

semi-volatile constituents towards the particle-phase. We expect these volatility effects to be a main contributing factor, as sampling took place in direct vicinity of the emission source, i.e. next to the road and thus potential impacts of physical effects such as enhanced near-ground mixing and dispersion through thermally induced convection in summer are expected to be of minor influence. Considering the previously discussed estimated traffic contributions during the rush hour, the seasonal difference in mass concentration was much more pronounced in the Aitken mode (-67%, 0.6 µg/m^3) than the accumulation mode (-12%, 0.2 µg/m^3), consistent with the expected stronger impact of reduced particle nucleation and reduced condensation of semi-volatile exhaust components on fresher, smaller particles in the warmer season.

Comparing different size distribution sets (Figure D6 in the Supporting Material), the average concentration set in summer yielded notably larger resolved mass median diameters in both modes and greater Aitken mode mass compared to the median, 25th, and 75th percentile concentration sets. This indicates a strong influence of extreme values (i.e. time periods with both larger particle size and larger particle mass concentrations) and thus greater variability in size distributions in the warmer season caused by specific high and low concentration events such as photochemical episodes and precipitation, evident in the greater relative span of organic mass concentrations in summer (See Table C5 in the Supporting Material: ratio of 10th and 90th percentile to median concentration in NR-PM_1). In spring, such events masked the diurnal processes to a lesser extent and with consequently greater consistency across different size distribution sets.

Sulfate

Although variations of total submicron sulfate mass concentrations with time of day were generally subtle, distinct trends were notable in MMDs and integrated mode mass concentrations in both Aitken and accumulation mode. Generally, Aitken mode MMDs were 20% larger in spring (180nm) than in summer (150nm). While in spring fluctuations in Aitken mode MMDs were small throughout the day within a narrow range of +/- 10nm and without apparent regular features, the summertime diurnal variation exhibited a well-defined broad daytime peak with a shift to ~15nm larger particle diameters. A matching trend was evident in the accumulation mode where MMDs increased by ~20nm in summer. Conversely, in spring, a conspicuous nighttime peak in accumulation mode MMDs was observed in the low traffic period between 01:00 and 07:00 which tracked closely with the diurnal variation of O_3 which peaked in the same period with the reduction of the NO_x titration effects at low nighttime traffic volumes. While particulate sulfate production during the day can be achieved through both homogeneous gas-phase oxidation of SO_2 by the OH radical as well as heterogeneous oxidation of SO_2 by dissolved H_2O_2 or O_3 (Seinfeld and Pandis, 2006), nighttime production is limited to the non-photochemical heterogeneous pathway. The apparent increase in accumulation mode particle size was also associated with an increase of integrated submode particle mass by ~0.7 µg/m^3 and thus points to heterogeneous SO_2 oxidation by residual ozone in the cooler and more humid spring season as a local source of particulate sulfate. In the warmer and drier summer season, no corresponding trend was apparent in either accumulation mode MMD or integrated mode concentration. The small magnitude of additionally produced sulfate (< 1 µg/m^3) in spring renders the nighttime production a minor source of particulate sulfate however and affirms that the bulk of the accumulation mode sulfate burden at the urban roadside still originated from regional scale

processes in both seasons. In summer, both modes exhibited notable increases in particle mass concentration levels during the daylight hours by ~80% in the Aitken mode and by ~35% in the accumulation mode compared to their respective nighttime "baseline" concentrations. Integrated over the whole day, the additional sulfate burden above this baseline amounted to 0.4 µg/m^3 and 6 µg/m^3 and thereby accounted for 34% and 11% of the total daily Aitken and accumulation mode particle mass respectively. This represents a rough estimation of possible local photochemical contributions to the Aitken and accumulation size mode in summer at the urban roadside, excluding possible physical effects, e.g. vertical mixing and advection or dilution laterally through the street canyon. Enhancements in particle mass by photochemical contributions were more pronounced in the Aitken mode, with the median fraction of Aitken mode particle mass among total AMS-measured particle mass (Figure 4) increasing substantially from its nighttime minimum at 4% to a maximum of 7% in the late afternoon in summer, while in spring the fraction remained almost constant at 6% throughout the day.

Considering different size distribution sets (Figure D6 in the Supporting Material), the 75th percentile size distributions and the average size distributions displayed notable increases in Aitken mode particle mass during the nighttime by 20-50% in spring. There was no corresponding trend in the accumulation mode, where changes in integrated mass concentration remained consistently <10%. The skewing of the average and higher percentile data indicates the influence of time periods with significantly elevated nighttime concentrations, likely related to events and atmospheric conditions conducive to the extensive formation of Aitken mode sulfate particles. The accumulation mode showed no notable changes in the average and 75th percentile data during the same time period, thus precluding physical processes such as transport or lowering of the planetary boundary layer as likely influential factors for these observations.

Nitrate

Particulate nitrate mass concentrations in the Aitken and accumulation mode exhibited similar diurnal variations in spring with lower daytime concentrations due to evaporation and higher nighttime concentrations where secondary formation and gas-to-particle partitioning prevailed. Analogous to sulfate, the Aitken mode MMDs for nitrate showed little change (<5%) throughout the day in both seasons. Aitken mode mass concentrations, however, exhibited a twofold increase over the dinner hours accounting for approximately 0.9 µg/m^3 (~16%) of additional particle nitrate mass per day. This may be due to the much higher abundance of small particles from cooking emissions providing additional surface area to facilitate gas-to-particle partitioning of nitrate. Increased signal intensities of oxygenated organic nitrogen ions (see Figure D11 in the Supporting Material) have also been observed during dinner suggesting that organic nitrate or other oxygenated nitrogen-containing organic species that produce nitrate fragments (Farmer et al., 2010) may too have contributed to this observed concentration peak. Accumulation mode nitrate mass increased by almost one-third in the low traffic period (01:00 – 07:00) compared to earlier night concentration levels (22:00 – 00:00) accompanied by a slight increase in MMD by ~10nm in spring. This signifies notable nighttime nitrate production through possibly nitric acid formation by ozone chemistry via the nitrate radical route under influence of organic components or formation of N_2O_5 and subsequent hydrolysis during the night. Local nighttime nitrate production effectively contributed ~3 µg/m^3 (~10%) to the total daily accumulation mode nitrate burden in spring.

Summertime nitrate production in Hong Kong has been mainly attributed to photochemical activity based on previous measurements of inorganic gas- and particle-phase nitrogen species at the suburban HKUST site (Griffith et al., 2015). Particulate nitrate mass concentrations at the urban Mong Kok site likewise exhibited clear daytime peaks, similar to sulfate albeit at smaller magnitude with total integrated increases of ~0.3 $\mu g/m^3$ and ~0.8 $\mu g/m^3$ particulate nitrate per day in the Aitken and accumulation mode respectively. In the Aitken mode, particle mass remained elevated in the early night hours (~19:00 – 22:00), which was likely due to the previously mentioned cooking-related nitrate enhancement analogous to spring. The distribution of total submicron nitrate shifted slightly in favor of the Aitken mode in summer with ~18% of total submicron nitrate found in the Aitken mode compared to ~14% in spring.

Comparing different size distribution sets (Figure D6 in the Supporting Material), the average size distributions displayed notable disparity compared to the remaining sets in both seasons. In summer, integrated particle mass concentrations and MMDs from the average set exhibited consistently larger values than those from the 25^{th} percentile, 75^{th} percentile, and median sets indicating significant influence of time periods with high nitrate concentrations and larger nitrate-containing particles. In spring, the average data exhibited a decrease in MMD in the Aitken mode from night to day, implying prolonged periods of significantly smaller daytime Aitken mode particles.

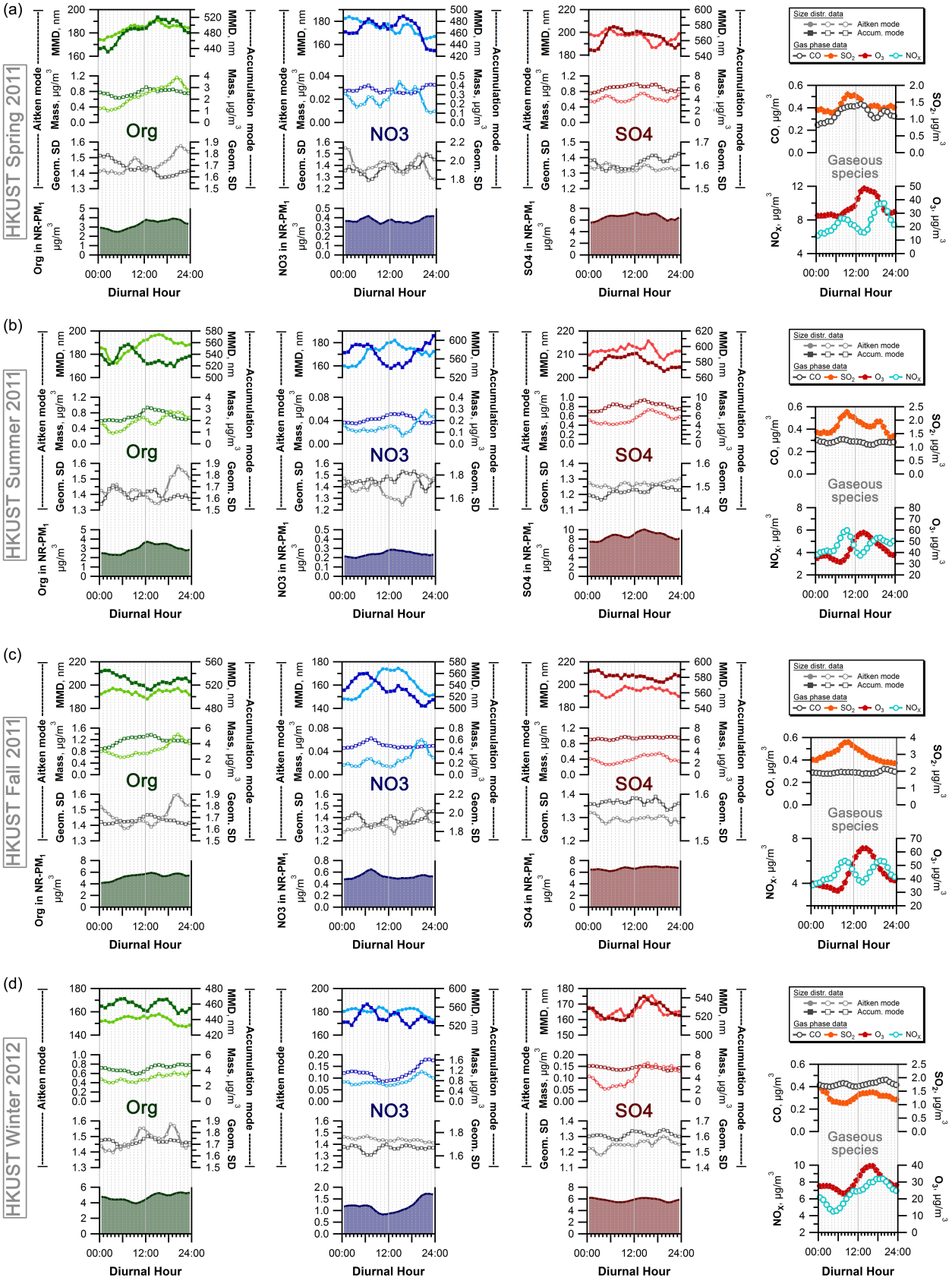
(a)
HKUST Spring 2011
(b)
HKUST Summer 2011
(c)
HKUST Fall 2011
(d)
HKUST Winter 2012
Org
NO3
SO4
Gaseous species
Size distr. data
Aitken mode
Accum. mode
Gas phase data
CO
SO2
O3
NOx
Diurnal Hour
00:00
12:00
24:00

Figure 3. Diurnal variations of mode diameter (MMD), integrated mode mass concentration and width of the Aitken mode (*lighter color*) and accumulation mode (*darker color*) from bimodal peak fits of the bin-median reconstructed size distributions at the suburban HKUST site and V-mode AMS species concentrations (line with shaded background) for organics, nitrate and sulfate (left to right) in (a) Spring 2011, (b) Summer 2011, (c) Fall 2011 and (d) Winter 2012; The right-most panel depicts the diurnal variations of relevant gas-phase pollutants (O3, CO, NOx, SO2) measured at the same site.

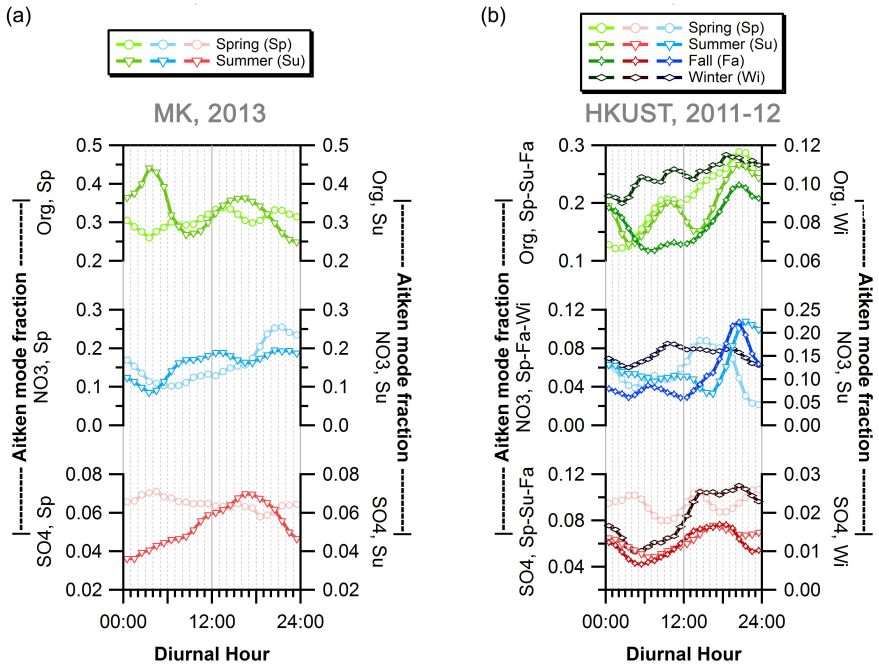

Figure 4. Diurnal variation of the fraction of Aitken mode particle mass among total submicron species mass for organics (*top*), nitrate (*middle*) and sulfate (*bottom*) at the (a) urban Mong Kong site, and (b) suburban HKUST supersite in different seasons; *based on concentrations from bin-median size distributions, seasons denoted by marker color and type of marker symbol*

3.1.2. Suburban coastal NR-PM$_1$

The suburban HKUST site as a downwind receptor of urban and regional pollution was generally dominated by sulfate and oxygenated secondary organic aerosol (SOA) components and much lower fractions of primary organic constituents, which combined typically made up less than a quarter of total organics (Li et al., 2015).

Organics

There were significant seasonal differences with larger fractions (Figure 4a) and concentrations (Figure 5c) of Aitken mode mass in total organic submicron particle mass in spring and summer compared to fall and winter, indicating greater influence of closer-ranged formation sources in the warmer season. Springtime integrated Aitken mode mass concentrations (~0.8 μg/m^3) were twice as high as those in winter (~0.4 μg/m^3). In the accumulation mode, highest particle mass loadings were observed in fall (5 μg/m^3) and lowest loadings in spring (3 μg/m^3) following the frequency pattern of continental air mass influence (Figure D12 in the Supporting Material) in each season indicating continental

transport of particulate mass or gas-phase precursors. Lowest mass concentrations in the Aitken mode typically occurred in the night hours (00:00 – 05:00) in a range of 0.3 – 0.5 μg/m^3 in spring, summer, and winter, while in fall mass loadings of 0.7 - 0.8 μg/m^3 were reached. Diurnal changes were least pronounced in winter with largely constant integrated Aitken mode particle concentrations. In the remaining seasons, varying degrees of daytime changes were apparent with a general increase around 06:00, likely owing to citybound commuter traffic from surrounding roads to the west of the sampling site at 1-2km of lateral distance. This also led to a modest increase in particle polydispersity with a discernible widening of the Aitken mode size distributions (*black solid line, lowest panels in* Figure 3). Daily maxima in spring, summer and fall were reached in the early evening (~21:00) with marked differences in absolute mass concentrations depending on the respective season, from a summer time low of 0.8 μg/m^3 to a fall season high of 1.4 μg/m^3. Mass median diameters in the Aitken mode were smaller in the night hours and displayed subtle increments during the day in the range of 10-20 nm reaching their maximum typically in the late afternoon, except for the fall season when mass median diameters displayed very little variation with time of day.

Total particle mass in the accumulation mode in spring and summer reached minima during the night hours (2 μg/m^3) and maxima (3 μg/m^3) around noon, remaining stable in the daylight hours thereafter. MMDs increased notably from 440nm at night to 510nm during the day in spring, while in summer a morning rise by ~30nm from 530nm to 560nm was obvious between 06:00 and 10:00 and coincided with the morning rush hour and the associated early morning peak of NO_x and an otherwise stable mode diameter of 530nm for the rest of the day. In fall, the increase in accumulation mode organic mass occurred much earlier, starting in the dark hours at 04:00, with a corresponding trend also evident for nitrate but absent for sulfate, indicating a common source of these organic and nitrate enriched particles. Nighttime MMDs for organics were generally larger (540nm) and decreased to a minimum of 510nm in the early afternoon accompanied by a slight widening of the distribution. In winter, mass concentrations decreased appreciably in the early morning hours and started to increase only beyond 10:00. In the colder seasons (fall, winter), a similar concentration pattern was also observed for gas-phase SO_2 which is considered as a largely regional pollutant with few distinct local sources (Yuan et al., 2013), indicating that changes in boundary layer and mixing with regional background were likely the more dominant processes in winter.

Sulfate

Aitken mode sulfate mass concentrations peaked in the afternoon from spring throughout fall with maximum concentrations reached progressively later in the afternoon (14:00 in spring; 16:00 in fall). Nominal concentrations were highest in spring and summer (0.5-0.6 μg/m^3), slightly lower in fall (0.4 μg/m^3) and reached the lowest levels in winter (0.1 μg/m^3). In addition to the afternoon peak, a conspicuous early morning peak of similar magnitude was evident in spring between 02:00 and 06:00. A greater proportion of southerly winds was evident in said time period compared to the overall seasonal wind frequency distribution (Figure D13a in the Supporting Material) and may indicate transport of sulfate from marine sources in the southern parts of Hong Kong. Diurnal variations in MMDs and GSDs were generally small and without obvious regular trends. Nominal mass median diameters were significantly lower in winter (~170nm) compared to spring and fall (~190nm) and summer (~210nm).

Trends in accumulation mode particle mass were more pronounced. In spring, a shallow concentration valley during the late evening and night hours (20:00 to 03:00) with minimum concentrations of 5 $\mu g/m^3$ was apparent, while daytime concentrations stayed largely invariant at 6 $\mu g/m^3$. The MMDs followed a similar variation with a minimum mode diameter around 550nm in the early hours of the day and slightly larger daytime MMDs around 570nm. Nominal concentrations were larger in summer with a nighttime valley concentration of 7 $\mu g/m^3$ and a well-pronounced broad day peak with a maximum of 9.5 $\mu g/m^3$ in the early afternoon (14:00-15:00). A prior additional morning peak occurred between 04:00 and 10:00 with particle mass concentrations reaching 8.5 $\mu g/m^3$ related to a consistent north-easterly morning wind pattern (Figure D13b in the Supporting Material) and likely associated with transport from north-easterly coastal regions or nighttime fisheries related maritime traffic. The diurnal trend in mass median diameter was similar to that in spring with a night minimum of 570nm and day maximum of 590nm.

In fall, accumulation mode characteristics showed no significant diurnal variability, with a largely stable integrated particle mass of 6 $\mu g/m^3$ and only subtle MMD changes (585nm at night; 575nm during the day). In winter, two concentration dips with reductions by ~0.5 $\mu g/m^3$ between 06:00 and 10:00 and between 18:00 and 22:00 were evident, while MMDs increased during the day between 10:00 and 15:00 from 520nm, peaking at a size of 540nm.

Nitrate

Nitrate particle mass in the Aitken mode was generally small from spring throughout fall amounting to 0.01 - 0.06 $\mu g/m^3$. Winter time concentrations were larger in a range of 0.06 - 0.08 $\mu g/m^3$ during the day and 0.10 - 0.12 $\mu g/m^3$ in the late evening hours. The latter evening peak centered around 21:00 was evident in most seasons (except spring) and accounted for 12-23% (0.1-0.25 $\mu g/m^3$) of total daily Aitken mode nitrate mass burden. Similar to the urban roadside location, these nighttime nitrate peaks coincided with the peak period of organic cooking aerosol concentrations (Figure D14 in the Supporting Material), which were however significantly smaller at the suburban measurement site and mainly attributed to the operation of an on-campus student canteen (Li et al., 2015). Trends in mass median diameters varied between seasons with no discernible trend in winter, a subtle decreasing trend with time of day in spring and broad daytime diameter increases in summer and fall. Solar irradiation in these two seasons was comparatively high (Figure D10b,c in the Supporting Material) indicating that photochemical nitrate production in the Aitken mode may have led to this observed growth in particle size.

Integrated particle mass concentrations in the accumulation mode only exhibited subtle variations from spring throughout fall, with essentially constant diurnal concentrations in spring, a subtle daytime peak in summer which accounted for ~ 15% of total daily accumulation mode nitrate (corresponding to 0.7 $\mu g/m^3$) and a conspicuous morning peak between 04:00 and 10:00 in fall accounting for ~ 5% of total daily accumulation mode nitrate (corresponding to 0.5 $\mu g/m^3$). Clearer seasonal differences were evident in the trends of MMDs. In spring, MMDs decreased appreciably over the late evening hours (21:00-0:00) with a concurrent widening of the size distribution (increase in GSD). In summer, accumulation mode diameters decreased during the day by ~40nm with a similar trend in accumulation mode organics. Winter time MMDs exhibited a more complex pattern with larger mode diameters in the early hours (04:00 – 10:00) and during the noon-time, and a late-afternoon dip leading to larger spread of intra-day mode diameters ranging from 510nm to 570nm.

In comparison to the urban roadside measurements, diurnal particle size characteristics and mass concentrations in the Aitken and accumulation mode were much more variable for all investigated species at the suburban HKUST site, indicating that longer time scale processes and irregular events (transport patterns, local meteorology) were probably more important in governing particle size distribution characteristics than diurnal processes.

3.2. Day-to-day size distributions

To evaluate the evolution of particle size distributions within seasons, average species-specific size distributions were generated by averaging raw distributions over 24h periods (between 0:00 and 23:59). There was clear long-term variability in both resolved Aitken and accumulation mode MMDs and integrated submode particle mass concentrations for all species (Figure D15 in the Supporting Material) and overall seasonal differences which have been briefly addressed in the discussion of the diurnal size distribution variations between seasons. Figure 5 depicts the overall average values for all daily fitted MMDs and integrated particle mass concentrations in both the Aitken and accumulation mode at the suburban HKUST and urban MK sites.

3.2.1. Seasonal trends

For the MK roadside station, particle mode diameters were generally larger in spring than in summer for all three investigated species, but with clear differences in the magnitude of changes among individual species. In the Aitken mode, organics and sulfate displayed a moderate decrease in mode diameter by 7-8% each, while nitrate saw a more significant decrease by 25% from spring to summer. In contrast, accumulation mode MMDs for organics exhibited only a subtle decrease by 5% and more substantial decreases for sulfate and nitrate by 20-22% each. Total Aitken mode particle mass decreases varied strongly: -15% for organics, -36% for sulfate and -67% for nitrate. In the accumulation mode, organics and sulfate exhibited similar relative decreases by 40-46%, while nitrate particle mass reduced drastically by 85%.

At the suburban HKUST site, Aitken mode MMDs of nitrate and organics decreased with the progression of seasons from spring to winter with highest mode diameters observed in spring and summer and appreciable decreases in winter by -9% for nitrate and -25% for organics compared to the warmer seasons. Sulfate displayed a similar winter time decrease in MMD (-15%) and an increase of similar magnitude in the summer season (+13%) compared to spring and fall. Variations in sulfate and organic accumulation mode diameters were minor between spring and fall, while wintertime MMDs were 7-12% lower. Nitrate exhibited an overall higher variability in mass median diameters in the accumulation mode in spring (larger standard deviation) and with on average 10% lower MMDs compared to other seasons. In line with the reduction in Aitken mode MMDs in winter, the integrated Aitken mode particle mass decreased as well, by -16% for organics and almost -75% for sulfate, whereas nitrate contributions remained largely stable throughout the seasons. Organic accumulation mode particle mass was significantly higher in the fall and winter season by factors of 1.6 – 2. Diurnal variations in the degree of oxygenation were least pronounced in these seasons (Li et al., 2015) suggesting that influence of transport in autumn and winter likely dominated over local formation,

thus exerting greater effects on particle mass in the larger size mode. Particulate nitrate concentrations were generally low in the accumulation mode from spring through fall, but increased sharply in winter by factors of 3 – 4. Sulfate accumulation mode mass concentrations remained more stable but saw significant summer time enhancements by ~30% likely due to photochemical activity which also led to high concentrations of Ox and a higher degree of oxygenation of organic aerosol among the four seasons (Li et al., 2015).

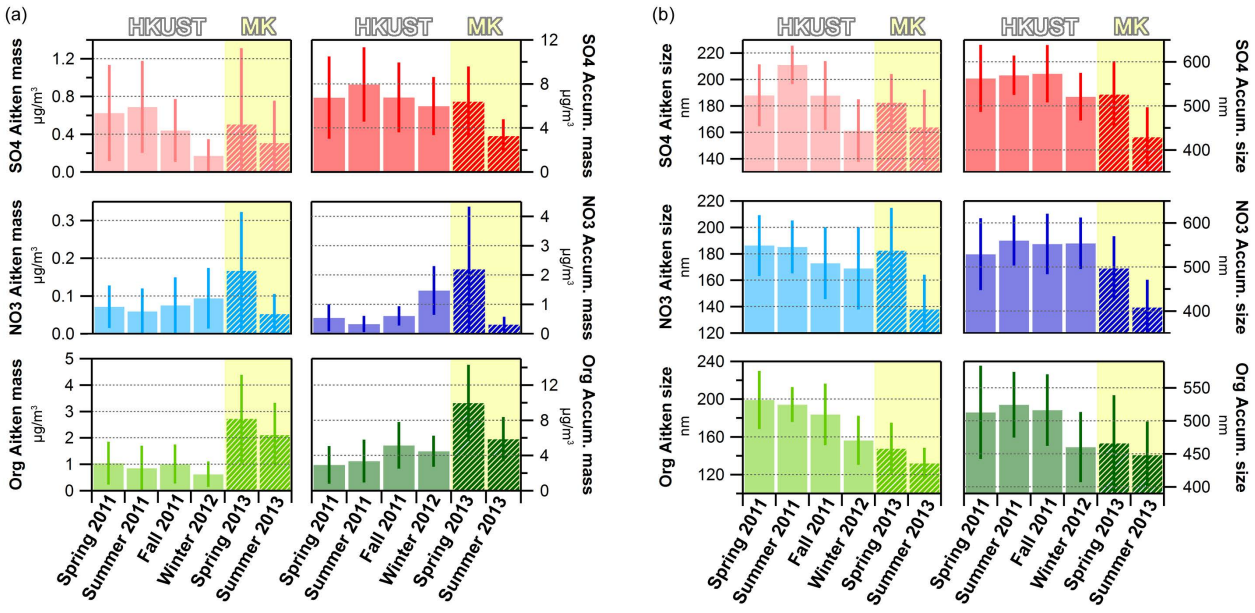

Figure 5. Average and standard deviation of daily fit values of Aitken and accumulation mode particle mass and mass median diameters at the suburban HKUST site (*solid bars*) and urban MK site (*hashed bars*). The integrated particle mass is depicted in (a), (b), (c) for the Aitken mode, and in (d), (e), (f) for the accumulation mode for sulfate, nitrate, and organics respectively. The mass median diameter is depicted in (g), (h), (i) for the Aitken mode and in (j), (k), (l) for the accumulation mode for sulfate, nitrate and organics respectively.

Large particles contribute more to particle volume and hence particle mass. Correspondingly, the total submicron concentration of a given species is typically governed by changes in the accumulation mode particle mass and accordingly observed correlation values between integrated accumulation mode particle mass and individual NR-PM_1 species mass concentrations were generally high (R_{pr}>0.90) at both measurement sites (Figure D16 in the Supporting Material). This applied to both measurement sites regardless of the season. Aitken mode trends were less akin. At the urban roadside station, neither sulfate nor nitrate particle mass in the Aitken mode notably correlated with the respective total submicron species mass concentration in spring (all R_{pr}≤0.20), whereas in summer correlations were more significant with R_{pr}=0.51 for sulfate and R_{pr}=0.80 for nitrate. This signifies that periods of greater species mass concentrations were more likely to be caused by increases in both Aitken and accumulation mode particle mass indicating that particle formation and growth affecting smaller particles was more likely to occur in the warmer season. For organics, Aitken mode particle mass and submicron species mass correlated only weakly (R_{pr} = 0.26 in spring and

520 R_{pr} = 0.38 in summer), i.e. each organic particle submode was governed by largely different dominant sources or
521 formation processes in both seasons at the roadside.
522 At the suburban background site, Aitken mode particle mass for sulfate showed little correlation with total submicron
523 sulfate concentration ($R_{pr} \leq 0.10$) apart from the spring season (R_{pr}=0.36) where more frequent wet and foggy
524 conditions may have facilitated sulfate formation in both size modes. For organics and nitrate significantly larger
525 correlation coefficients of submode particle mass to total species concentration ($0.5 \leq R_{pr} \leq 0.7$) were observed in
526 most seasons (spring, summer, winter) indicating significant influence of local or regional formation processes on
527 organic and nitrate Aitken mode particulate mass at the suburban receptor location. In the fall season, much weaker
528 correlations ($0.2 \leq R_{pr} \leq 0.4$) were likely caused by the dominance of continental air mass influence (Figure D12c in
529 the Supporting Material) and greater influence of aged accumulation mode particles on total submicron nitrate mass
530 concentrations.

531 **3.2.2. Inferred changes in mixing state**

532 Shifts in mixing state of ambient particles can be inferred from the inter-species analysis of mass median diameters.
533 Close nominal agreement (i.e. diameter ratios close to 1) infer that different species were distributed similarly across
534 the particle size range which thus most likely represents a largely internally mixed particle population, while the spread
535 of data (correlation coefficient) indicates the temporal homogeneity or divergence of resolved mode diameters. A
536 hypothetically perfectly internally mixed particle population over the whole sampling period would, therefore, yield
537 MMD ratios and Pearson's R values of 1 between species, while larger or smaller values are indicative of a greater
538 frequency of heterogeneous (i.e. more externally mixed) particle populations (Figure 6).
539 At the urban Mong Kok site, changes in accumulation mode mass median diameters for nitrate and sulfate followed
540 similar trends (R_{pr} = 0.88-0.89) and with diameter ratios close to 1 (0.94–0.95) Similarly, fitted accumulation mode
541 diameters of organic constituents predominantly followed that of sulfate in spring nominally (diameter ratio 0.88) and
542 temporally (R_{pr} = 0.80). The nominal agreement of organic and sulfate accumulation mode diameters persisted
543 (diameter ratio 1.03) overall in summer, however, there was significantly more temporal divergence (R_{pr} = 0.65)
544 indicating a greater frequency of time periods with external mixing of particle populations comprising different
545 fractions of organic constituents.
546 External mixing is more prevalent for freshly formed smaller particles which have typically undergone less
547 condensational growth, coagulation or aqueous-phase reactions. Indeed, the correlation coefficients of both nitrate
548 and organic Aitken mode MMDs with respect to sulfate were notably lower (0.50 and 0.62) indicating frequent periods
549 of particle populations with different species prevailing in different size regions within the Aitken mode.
550 Sulfate and nitrate were still more likely to occur internally mixed in the Aitken mode in spring with similar diameters
551 (nitrate to sulfate MMD ratio = 1.00), while organic Aitken mode MMDs were consistently lower, indicating greater
552 fractions of organic dominated particles towards the lower end and more inorganic dominated particles towards the
553 upper end of the fitted Aitken mode.

In summer, both nitrate and organic MMDs tended to be lower than those of sulfate (diameter ratios of 0.79 – 0.83) but similar to each other, thus implying a shift to externally mixed populations of more nitrate and organic enhanced and internally mixed smaller Aitken mode particles and sulfate dominated larger Aitken mode particles.

At the suburban HKUST site, accumulation mode MMDs of both nitrate and organics were generally quite similar to those of sulfate with diameter ratios of 0.88 – 1.06. Compared to the urban site, correlation coefficients of nitrate and sulfate were consistently lower (0.54 – 0.67) indicating a much greater frequency of time periods where sulfate and nitrate dominated particles in the accumulation exhibited significantly different particle size distributions.

In winter, organic MMDs were consistently lower than those of sulfate and nitrate indicating a greater proportion of externally mixed particle populations with organics enriched particles in the lower accumulation size range and inorganic dominated particles in the larger accumulation size range. The least variability in particle size was observed in the summer season where MMDs in both Aitken and accumulation mode displayed variations in relatively narrow ranges between 200-250nm and 500-700nm, whereas in the remaining seasons time periods with particle populations of lower MMD were more frequent, extending to MMDs as low as 100nm in the Aitken mode and 300nm in the accumulation mode.

In the Aitken mode, mass median diameters overall were quite similar across species, with diameter ratios of organic and nitrate distributions to those of sulfate in the range of 0.87 – 1.06, indicating that they generally covered a similar size range. The temporal agreement was highly variable with correlation coefficients (R_{pr}) spanning from 0.21 to 0.75 indicating that Aitken mode particle populations at the suburban site were generally more diverse and likely influenced by a greater range of particle formation and growth mechanisms compared to the urban Mong Kok site.

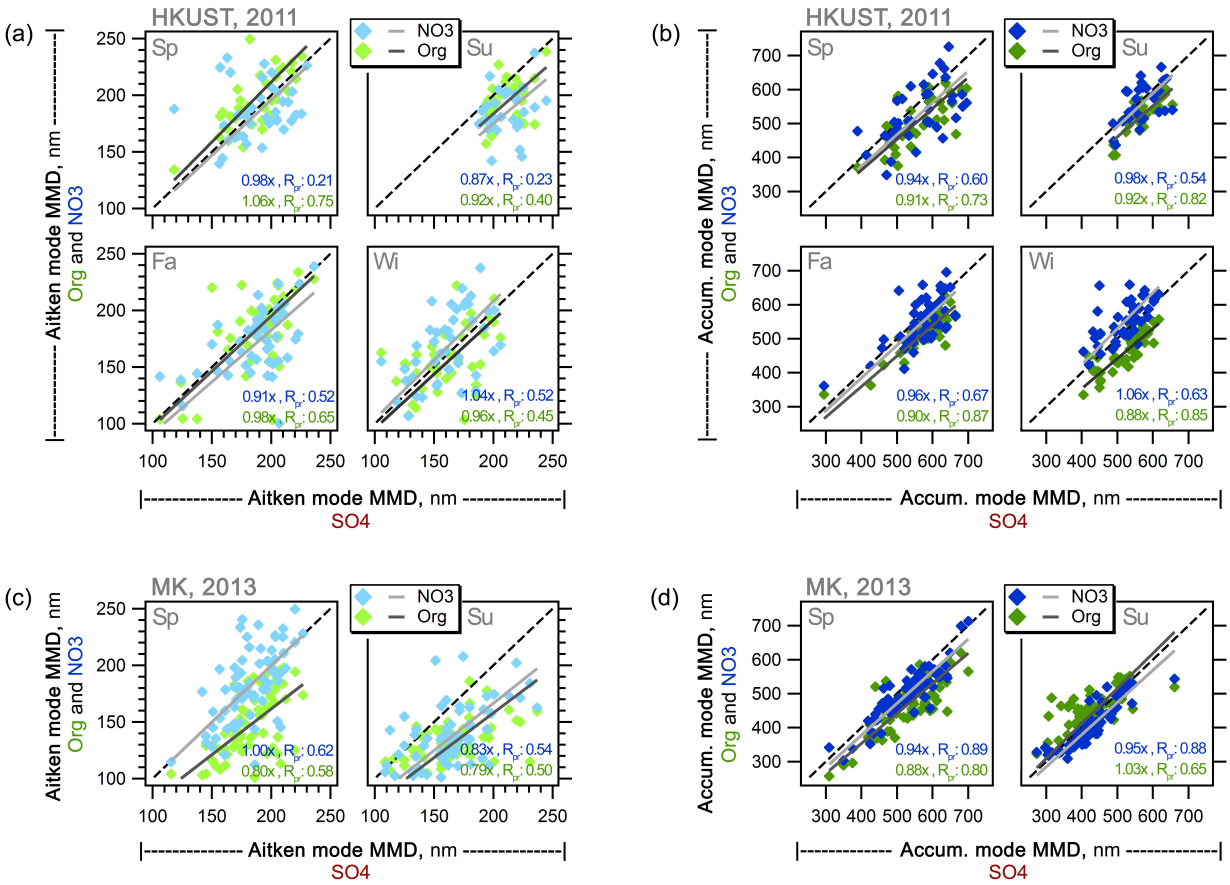

Figure 6. Scatter plots of fitted mass median diameters of organics and nitrate vs. sulfate for the (a) Aitken mode and (b) accumulation mode at the urban Mong Kok site, and (c) Aitken mode and (d) accumulation mode at the HKUST suburban site

3.3. Comparison to previous studies

Particle size distribution studies in Hong Kong are generally scarce and have focused on either size segregated filter samples (MOUDI) for general ambient measurements or electrostatic classification in particle formation and particle growth studies (Guo et al., 2012;Cheung et al., 2015) . The latter studies focus on specific and narrow time periods and lack general discussions on ambient particle size distributions.

Two ambient studies were undertaken at the suburban coastal HKUST site using size-segregated samples from a ten-stage MOUDI sampler and offline chromatographic analysis. Inorganic constituents (NH4, NO3, SO4) in fine particles (i.e. D_p<1.8 µm) were shown to follow bimodal distributions with mode diameters in the range of 0.14-0.21 µm and 0.46-0.58 µm in samples collected in the winter season, while the main mode was observed in the coarse region (4-6 µm) for all three species (Zhuang et al., 1999). A subsequent year-long observational study also reported bimodal fine particle distributions with mode diameters of 0.1-0.3 µm and 0.7–0.9 µm and 1-2 additional modes in the coarse region (Bian et al., 2014), however, the main mode in the size distributions of sulfate, ammonium, potassium and oxalate was observed in the droplet mode (0.7 – 0.9 µm) in this study. Vehicle exhaust plumes sampled on-road from a Mobile

Real-time Air Monitoring Platform (MAP) across Hong Kong's road network exhibited three distinct particle volume size distributions: a unimodal distribution with an accumulation mode at 0.2 µm and two bimodal distributions with a minor mode at 0.2 µm and the dominant mode at 0.5 or 0.7 µm (Yao et al., 2007a).

The bimodality in the fine particle range across these studies is consistent with the AMS-based results in this work. Nominally, the accumulation mode diameters from filter based studies and the chase studies are larger than those from AMS measurements where maximum mode diameters occurred at D_{va} ~ 700nm, corresponding to D_a ~ 470 (assuming D_{va} ~ D_a * density; particle density ~ 1.5 g/cm^3). Direct comparability is however limited due to fundamental differences in sizing techniques (MOUDI: atmospheric pressure; AMS: near-vacuum), sampling times (MOUDI: 24h samples, scattered time line; AMS: minute raw resolution averaged to hourly or daily, continuous time line), measurement uncertainties (MOUDI: sampling artifacts such as vapor adsorption and desorption; AMS: inlet lens transmission) and aerosol pretreatment (none for MOUDI with potential impacts on particle size in high humidity (>80%) conditions (Fang et al., 1991); AMS: removal of water prior to introduction to instrument).

4. Conclusion

A detailed analysis of AMS mass-based particle size distributions of sulfate, nitrate, and organics in submicron particulate matter measured at two contrasting locations in Hong Kong during two field campaigns has been undertaken. Deconvolution of size distributions into Aitken and accumulation submodes was accomplished by log-normal peak fitting and trends in particle size (mass median diameters), dispersity (geometric standard deviation) and overall particle mass (integrated mode area) were discussed on a diurnal time scale and on a daily basis to evaluate longer-term changes in size distribution characteristics. At the urban roadside location, clear diurnal influences of primary particle and gas-phase species were evident affecting both inorganic and organic component size distributions. Traffic and cooking contributed an estimated 0.3 – 0.9 µg/m^3 and 0.5 – 1.8 µg/m^3 of organic component particle mass in the Aitken mode, and 1.6 - 1.8 µg/m^3 and 1.0 – 2.7 µg/m^3 respectively in the accumulation mode with concentrations level varying with seasons. Notable changes in Aitken mode mass median diameters of organics were limited to the morning rush hour. Daytime particle concentration maxima of sulfate and nitrate in summer indicated substantial influence of photochemical processes, which also led to increments in mass median diameters in the accumulation mode thus inferring associated particle growth. Nocturnal nitrate formation was apparent in the accumulation mode in spring concurring with the nighttime peak of ozone at the roadside, while in the Aitken mode nitrate particle concentrations were significantly elevated during the dinner hours. Organics-related size distributions were mostly governed by intra-day changes at the urban site with very similar trends across different size distribution sets (i.e. concentration regimes), while disparities in diurnal variations among different size distribution sets were evident for nitrate and sulfate, particularly affecting the average sets, indicating stronger influence of irregular external factors which were not associated with diurnal time scale processes.

Suburban particle size distributions exhibited variable diurnal characteristics, suggesting that irregular processes such as transport and seasonal meteorological conditions were the more dominant processes influencing particle size characteristics. Aitken mode particle mass of organics was significantly larger in spring and summer indicating greater

influence of more local formation sources in the warm season. In the accumulation mode, organic particle mass concentrations were highest in fall and lowest in spring, following the frequency pattern of continental air mass influence. For sulfate, Aitken mode mass concentrations mass concentrations peaked in the afternoon from spring throughout fall with highest nominal concentrations in spring and summer and lowest levels in winter, while accumulation mode particle mass was highest in summer and fall and lowest in winter, similar to the trend observed among organic constituents.

Nitrate particle mass in the Aitken mode was generally small in most seasons (0.01 - 0.06 $\mu g/m^3$), except winter where daytime concentrations reached ~0.1 $\mu g/m^3$. In both modes, changes in mass median diameters varied temporally and in magnitude with seasons, indicating a stronger influence of specific meteorological conditions on the properties of nitrate-containing particles at the suburban site. At the urban site, periods of greater inorganic species mass concentrations were more likely to be caused by increases in both Aitken and accumulation mode particle mass in summer, indicating that particle formation and growth affecting smaller particles was more likely to occur in the warmer season. At the suburban receptor location, significant correlation of submode particle mass to total species concentration ($0.5 \leq R_{pr} \leq 0.7$) was observed for organics and nitrate in most seasons (spring, summer, winter) suggesting notable influence of local or regional formation processes on organic and nitrate Aitken mode particulate mass. Variations in particle mixing state were examined by evaluation of inter-species mass median diameter trends at both measurement sites. In the accumulation mode at the urban site, internal mixing appeared to be prevalent in spring, while greater frequency of time periods with external mixing of particle populations comprising different fractions of organic constituents was observed in summer. External mixing was predominant in the Aitken mode at the urban location in both seasons. At the suburban site, sulfate and nitrate in the accumulation mode more frequently exhibited differing particle size distributions in all seasons signifying a greater extent of external mixing. In winter, external mixing of more organics enriched particles in the lower accumulation size range was evident.

Acknowledgements

This work was supported by the Environmental Conservation Fund of Hong Kong (project number ECWW09EG04). Chak K. Chan gratefully acknowledges the startup fund of the City University of Hong Kong.

References

Abbatt, J. P. D., Broekhuizen, K., and Pradeep Kumar, P.: Cloud condensation nucleus activity of internally mixed ammonium sulfate/organic acid aerosol particles, Atmospheric Environment, 39, 4767-4778, 10.1016/j.atmosenv.2005.04.029, 2005.

Ahlquist, N. C., and Charlson, R. J.: A New Instrument for Evaluating the Visual Quality of Air, Journal of the Air Pollution Control Association, 17, 467-469, 10.1080/00022470.1967.10469006, 1967.

Aiken, A. C., Salcedo, D., Cubison, M. J., Huffman, J. A., DeCarlo, P. F., Ulbrich, I. M., Docherty, K. S., Sueper, D., Kimmel, J. R., Worsnop, D. R., Trimborn, A., Northway, M., Stone, E. A., Schauer,

J. J., Volkamer, R. M., Fortner, E., de Foy, B., Wang, J., Laskin, A., Shutthanandan, V., Zheng, J., Zhang, R., Gaffney, J., Marley, N. A., Paredes-Miranda, G., Arnott, W. P., Molina, L. T., Sosa, G., and Jimenez, J. L.: Mexico City aerosol analysis during MILAGRO using high resolution aerosol mass spectrometry at the urban supersite (T0) - Part 1: Fine particle composition and organic source apportionment, Atmospheric Chemistry and Physics, 9, 6633-6653, 2009.

Bahreini, R., Dunlea, E. J., Matthew, B. M., Simons, C., Docherty, K. S., DeCarlo, P. F., Jimenez, J. L., Brock, C. A., and Middlebrook, A. M.: Design and Operation of a Pressure-Controlled Inlet for Airborne Sampling with an Aerodynamic Aerosol Lens, Aerosol Science and Technology, 42, 465-471, 10.1080/02786820802178514, 2008.

Bian, Q., Huang, X. H. H., and Yu, J. Z.: One-year observations of size distribution characteristics of major aerosol constituents at a coastal receptor site in Hong Kong – Part 1: Inorganic ions and oxalate, Atmos. Chem. Phys., 14, 9013-9027, 10.5194/acp-14-9013-2014, 2014.

Bohren, C. F., and Huffman, D. R.: Absorption and scattering of light by small particles, in: Absorption and Scattering of Light by Small Particles, Wiley-VCH Verlag GmbH, 1-11, 1983.

Canagaratna, M. R., Jayne, J. T., Jimenez, J. L., Allan, J. D., Alfarra, M. R., Zhang, Q., Onasch, T. B., Drewnick, F., Coe, H., Middlebrook, A., Delia, A., Williams, L. R., Trimborn, A. M., Northway, M. J., DeCarlo, P. F., Kolb, C. E., Davidovits, P., and Worsnop, D. R.: Chemical and microphysical characterization of ambient aerosols with the aerodyne aerosol mass spectrometer, Mass Spectrometry Reviews, 26, 185-222, 10.1002/mas.20115, 2007.

Charlson, R. J., Langner, J., Rodhe, H., Leovy, C. B., and Warren, S. G.: Perturbation of the northern hemisphere radiative balance by backscattering from anthropogenic sulfate aerosols*, Tellus B, 43, 152-163, 10.1034/j.1600-0889.1991.t01-1-00013.x, 1991.

Cheung, K., Ling, Z. H., Wang, D. W., Wang, Y., Guo, H., Lee, B., Li, Y. J., and Chan, C. K.: Characterization and source identification of sub-micron particles at the HKUST Supersite in Hong Kong, Science of The Total Environment, 527–528, 287-296, http://dx.doi.org/10.1016/j.scitotenv.2015.04.087, 2015.

Crippa, M., DeCarlo, P. F., Slowik, J. G., Mohr, C., Heringa, M. F., Chirico, R., Poulain, L., Freutel, F., Sciare, J., Cozic, J., Di Marco, C. F., Elsasser, M., Nicolas, J. B., Marchand, N., Abidi, E., Wiedensohler, A., Drewnick, F., Schneider, J., Borrmann, S., Nemitz, E., Zimmermann, R., Jaffrezo, J. L., Prévôt, A. S. H., and Baltensperger, U.: Wintertime aerosol chemical composition and source apportionment of the organic fraction in the metropolitan area of Paris, Atmos. Chem. Phys., 13, 961-981, 10.5194/acp-13-961-2013, 2013.

Davidson, C. I., Phalen, R. F., and Solomon, P. A.: Airborne Particulate Matter and Human Health: A Review, Aerosol Science and Technology, 39, 737-749, 10.1080/02786820500191348, 2005.

693 DeCarlo, P. F., Slowik, J. G., Worsnop, D. R., Davidovits, P., and Jimenez, J. L.: Particle morphology
694 and density characterization by combined mobility and aerodynamic diameter measurements. Part
695 1: Theory, Aerosol Science and Technology, 38, 1185-1205, 10.1080/027868290903907, 2004.
696 Docherty, K. S., Aiken, A. C., Huffman, J. A., Ulbrich, I. M., DeCarlo, P. F., Sueper, D., Worsnop, D. R.,
697 Snyder, D. C., Peltier, R. E., Weber, R. J., Grover, B. D., Eatough, D. J., Williams, B. J.,
698 Goldstein, A. H., Ziemann, P. J., and Jimenez, J. L.: The 2005 Study of Organic Aerosols at
699 Riverside (SOAR-1): instrumental intercomparisons and fine particle composition, Atmospheric
700 Chemistry and Physics, 11, 12387-12420, 10.5194/acp-11-12387-2011, 2011.
701 Drewnick, F., Hings, S. S., DeCarlo, P., Jayne, J. T., Gonin, M., Fuhrer, K., Weimer, S., Jimenez, J. L.,
702 Demerjian, K. L., Borrmann, S., and Worsnop, D. R.: A new time-of-flight aerosol mass
703 spectrometer (TOF-AMS) - Instrument description and first field deployment, Aerosol Science
704 and Technology, 39, 637-658, 10.1080/02786820500182040, 2005.
705 Elser, M., Huang, R. J., Wolf, R., Slowik, J. G., Wang, Q., Canonaco, F., Li, G., Bozzetti, C.,
706 Daellenbach, K. R., Huang, Y., Zhang, R., Li, Z., Cao, J., Baltensperger, U., El-Haddad, I., and
707 Prévôt, A. S. H.: New insights into PM2.5 chemical composition and sources in two major cities
708 in China during extreme haze events using aerosol mass spectrometry, Atmos. Chem. Phys., 16,
709 3207-3225, 10.5194/acp-16-3207-2016, 2016.
710 Farmer, D. K., Matsunaga, A., Docherty, K. S., Surratt, J. D., Seinfeld, J. H., Ziemann, P. J., and Jimenez,
711 J. L.: Response of an aerosol mass spectrometer to organonitrates and organosulfates and
712 implications for atmospheric chemistry, Proceedings of the National Academy of Sciences of the
713 United States of America, 107, 6670-6675, 10.1073/pnas.0912340107, 2010.
714 Gill, P. E., Murray, W., and Wright, M. H.: The Levenberg-Marquardt method, in: Practical optimization,
715 Academic Press, London, 1981.
716 Griffith, S. M., Huang, X. H. H., Louie, P. K. K., and Yu, J. Z.: Characterizing the thermodynamic and
717 chemical composition factors controlling PM2.5 nitrate: Insights gained from two years of online
718 measurements in Hong Kong, Atmospheric Environment, 122, 864-875,
719 http://dx.doi.org/10.1016/j.atmosenv.2015.02.009, 2015.
720 Guo, H., Wang, D. W., Cheung, K., Ling, Z. H., Chan, C. K., and Yao, X. H.: Observation of aerosol size
721 distribution and new particle formation at a mountain site in subtropical Hong Kong, Atmos.
722 Chem. Phys., 12, 9923-9939, 10.5194/acp-12-9923-2012, 2012.
723 Huang, X. F., He, L. Y., Hu, M., Canagaratna, M. R., Sun, Y., Zhang, Q., Zhu, T., Xue, L., Zeng, L. W.,
724 Liu, X. G., Zhang, Y. H., Jayne, J. T., Ng, N. L., and Worsnop, D. R.: Highly time-resolved
725 chemical characterization of atmospheric submicron particles during 2008 Beijing Olympic

Games using an Aerodyne High-Resolution Aerosol Mass Spectrometer, Atmospheric Chemistry and Physics, 10, 8933-8945, 10.5194/acp-10-8933-2010, 2010.

Huang, X. F., He, L. Y., Hu, M., Canagaratna, M. R., Kroll, J. H., Ng, N. L., Zhang, Y. H., Lin, Y., Xue, L., Sun, T. L., Liu, X. G., Shao, M., Jayne, J. T., and Worsnop, D. R.: Characterization of submicron aerosols at a rural site in Pearl River Delta of China using an Aerodyne High-Resolution Aerosol Mass Spectrometer, Atmospheric Chemistry and Physics, 11, 1865-1877, 10.5194/acp-11-1865-2011, 2011.

Huang, X. H. H., Bian., Q. J., Ng, W. M., Louie, P. K. K., and Yu, J. Z.: Characterization of PM2.5 Major Components and Source Investigation in Suburban Hong Kong: A One Year Monitoring Study, Aerosol and Air Quality Research 14, 237-250, 2014.

Jayne, J. T., Leard, D. C., Zhang, X. F., Davidovits, P., Smith, K. A., Kolb, C. E., and Worsnop, D. R.: Development of an aerosol mass spectrometer for size and composition analysis of submicron particles, Aerosol Science and Technology, 33, 49-70, 2000.

Jimenez, J. L., Jayne, J. T., Shi, Q., Kolb, C. E., Worsnop, D. R., Yourshaw, I., Seinfeld, J. H., Flagan, R. C., Zhang, X., Smith, K. A., Morris, J. W., and Davidovits, P.: Ambient aerosol sampling using the Aerodyne Aerosol Mass Spectrometer, J. Geophys. Res., 108, 8425, 10.1029/2001jd001213, 2003.

John, W.: Size Distribution Characteristics of Aerosols, in: Aerosol Measurement, John Wiley & Sons, Inc., 41-54, 2011.

Kerminen, V. M., Paramonov, M., Anttila, T., Riipinen, I., Fountoukis, C., Korhonen, H., Asmi, E., Laakso, L., Lihavainen, H., Swietlicki, E., Svenningsson, B., Asmi, A., Pandis, S. N., Kulmala, M., and Petäjä, T.: Cloud condensation nuclei production associated with atmospheric nucleation: a synthesis based on existing literature and new results, Atmos. Chem. Phys., 12, 12037-12059, 10.5194/acp-12-12037-2012, 2012.

Köhler, H.: The nucleus in and the growth of hygroscopic droplets, Transactions of the Faraday Society, 32, 1152-1161, 10.1039/tf9363201152, 1936.

Lee, B. P., Li, Y. J., Yu, J. Z., Louie, P. K. K., and Chan, C. K.: Physical and chemical characterization of ambient aerosol by HR-ToF-AMS at a suburban site in Hong Kong during springtime 2011, Journal of Geophysical Research: Atmospheres, 118, 8625-8639, 10.1002/jgrd.50658, 2013.

Lee, B. P., Li, Y. J., Yu, J. Z., Louie, P. K. K., and Chan, C. K.: Characteristics of submicron particulate matter at the urban roadside in downtown Hong Kong—Overview of 4 months of continuous high-resolution aerosol mass spectrometer measurements, Journal of Geophysical Research: Atmospheres, 120, 7040-7058, 10.1002/2015JD023311, 2015.

759 Li, Y. J., Lee, B. Y. L., Yu, J. Z., Ng, N. L., and Chan, C. K.: Evaluating the degree of oxygenation of
760 organic aerosol during foggy and hazy days in Hong Kong using high-resolution time-of-flight
761 aerosol mass spectrometry (HR-ToF-AMS), Atmos. Chem. Phys., 13, 8739-8753, 10.5194/acp-
762 13-8739-2013, 2013.
763 Li, Y. J., Lee, B. P., Su, L., Fung, J. C. H., and Chan, C. K.: Seasonal characteristics of fine particulate
764 matter (PM) based on high resolution time-of-flight aerosol mass spectrometric (HR-ToF-AMS)
765 measurements at the HKUST Supersite in Hong Kong, Atmos. Chem. Phys., 15, 37-53,
766 doi:10.5194/acp-15-37-2015, 2015.
767 Liu, P. S. K., Deng, R., Smith, K. A., Williams, L. R., Jayne, J. T., Canagaratna, M. R., Moore, K.,
768 Onasch, T. B., Worsnop, D. R., and Deshler, T.: Transmission efficiency of an aerodynamic
769 focusing lens system: Comparison of model calculations and laboratory measurements for the
770 Aerodyne Aerosol Mass Spectrometer, Aerosol Science and Technology, 41, 721-733,
771 10.1080/02786820701422278, 2007.
772 Man, H., Zhu, Y., Ji, F., Yao, X., Lau, N. T., Li, Y., Lee, B. P., and Chan, C. K.: Comparison of Daytime
773 and Nighttime New Particle Growth at the HKUST Supersite in Hong Kong, Environmental
774 Science & Technology, 49, 7170-7178, 10.1021/acs.est.5b02143, 2015.
775 Meng, J. W., Yeung, M. C., Li, Y. J., Lee, B. Y. L., and Chan, C. K.: Size-resolved cloud condensation
776 nuclei (CCN) activity and closure analysis at the HKUST Supersite in Hong Kong, Atmos. Chem.
777 Phys., 14, 10267-10282, 10.5194/acp-14-10267-2014, 2014.
778 Mohr, C., DeCarlo, P. F., Heringa, M. F., Chirico, R., Slowik, J. G., Richter, R., Reche, C., Alastuey, A.,
779 Querol, X., Seco, R., Peñuelas, J., Jiménez, J. L., Crippa, M., Zimmermann, R., Baltensperger,
780 U., and Prévôt, A. S. H.: Identification and quantification of organic aerosol from cooking and
781 other sources in Barcelona using aerosol mass spectrometer data, Atmos. Chem. Phys., 12, 1649-
782 1665, 10.5194/acp-12-1649-2012, 2012.
783 Rupakheti, M., Leaitch, W. R., Lohmann, U., Hayden, K., Brickell, P., Lu, G., Li, S. M., Toom-Sauntry,
784 D., Bottenheim, J. W., Brook, J. R., Vet, R., Jayne, J. T., and Worsnop, D. R.: An intensive study
785 of the size and composition of submicron atmospheric aerosols at a rural site in Ontario, Canada,
786 Aerosol Science and Technology, 39, 722-736, 10.1080/02786820500182420, 2005.
787 Saarikoski, S., Carbone, S., Decesari, S., Giulianelli, L., Angelini, F., Canagaratna, M., Ng, N. L.,
788 Trimborn, A., Facchini, M. C., Fuzzi, S., Hillamo, R., and Worsnop, D.: Chemical
789 characterization of springtime submicrometer aerosol in Po Valley, Italy, Atmos. Chem. Phys.,
790 12, 8401-8421, 10.5194/acp-12-8401-2012, 2012.
791 Salcedo, D., Onasch, T. B., Dzepina, K., Canagaratna, M. R., Zhang, Q., Huffman, J. A., DeCarlo, P. F.,
792 Jayne, J. T., Mortimer, P., Worsnop, D. R., Kolb, C. E., Johnson, K. S., Zuberi, B., Marr, L. C.,

Volkamer, R., Molina, L. T., Molina, M. J., Cardenas, B., Bernabe, R. M., Marquez, C., Gaffney, J. S., Marley, N. A., Laskin, A., Shutthanandan, V., Xie, Y., Brune, W., Lesher, R., Shirley, T., and Jimenez, J. L.: Characterization of ambient aerosols in Mexico City during the MCMA-2003 campaign with Aerosol Mass Spectrometry: results from the CENICA Supersite, Atmospheric Chemistry and Physics, 6, 925-946, 2006.

Schwartz, S. E.: The whitehouse effect—Shortwave radiative forcing of climate by anthropogenic aerosols: an overview, Journal of Aerosol Science, 27, 359-382, http://dx.doi.org/10.1016/0021-8502(95)00533-1, 1996.

Setyan, A., Zhang, Q., Merkel, M., Knighton, W. B., Sun, Y., Song, C., Shilling, J. E., Onasch, T. B., Herndon, S. C., Worsnop, D. R., Fast, J. D., Zaveri, R. A., Berg, L. K., Wiedensohler, A., Flowers, B. A., Dubey, M. K., and Subramanian, R.: Characterization of submicron particles influenced by mixed biogenic and anthropogenic emissions using high-resolution aerosol mass spectrometry: results from CARES, Atmos. Chem. Phys., 12, 8131-8156, 10.5194/acp-12-8131-2012, 2012.

Slowik, J. G., Stainken, K., Davidovits, P., Williams, L. R., Jayne, J. T., Kolb, C. E., Worsnop, D. R., Rudich, Y., DeCarlo, P. F., and Jimenez, J. L.: Particle morphology and density characterization by combined mobility and aerodynamic diameter measurements. Part 2: Application to combustion-generated soot aerosols as a function of fuel equivalence ratio, Aerosol Science and Technology, 38, 1206-1222, 10.1080/027868290903916, 2004.

Sun, C., Lee, B. P., Huang, D., Jie Li, Y., Schurman, M. I., Louie, P. K. K., Luk, C., and Chan, C. K.: Continuous measurements at the urban roadside in an Asian megacity by Aerosol Chemical Speciation Monitor (ACSM): particulate matter characteristics during fall and winter seasons in Hong Kong, Atmos. Chem. Phys., 16, 1713-1728, 10.5194/acp-16-1713-2016, 2016.

Sun, Y., Zhang, Q., Macdonald, A. M., Hayden, K., Li, S. M., Liggio, J., Liu, P. S. K., Anlauf, K. G., Leaitch, W. R., Steffen, A., Cubison, M., Worsnop, D. R., van Donkelaar, A., and Martin, R. V.: Size-resolved aerosol chemistry on Whistler Mountain, Canada with a high-resolution aerosol mass spectrometer during INTEX-B, Atmos. Chem. Phys., 9, 3095-3111, 10.5194/acp-9-3095-2009, 2009.

Sun, Y. L., Zhang, Q., Schwab, J. J., Demerjian, K. L., Chen, W. N., Bae, M. S., Hung, H. M., Hogrefe, O., Frank, B., Rattigan, O. V., and Lin, Y. C.: Characterization of the sources and processes of organic and inorganic aerosols in New York city with a high-resolution time-of-flight aerosol mass spectrometer, Atmospheric Chemistry and Physics, 11, 1581-1602, 10.5194/acp-11-1581-2011, 2011.

826 Takegawa, N., Miyakawa, T., Watanabe, M., Kondo, Y., Miyazaki, Y., Han, S., Zhao, Y., van Pinxteren,
827 D., Bruggemann, E., Gnauk, T., Herrmann, H., Xiao, R., Deng, Z., Hu, M., Zhu, T., and Zhang,
828 Y.: Performance of an Aerodyne Aerosol Mass Spectrometer (AMS) during Intensive Campaigns
829 in China in the Summer of 2006, Aerosol Science and Technology, 43, 189-204,
830 10.1080/02786820802582251, 2009.
831 Ulbrich, I. M., Canagaratna, M. R., Cubison, M. J., Zhang, Q., Ng, N. L., Aiken, A. C., and Jimenez, J.
832 L.: Three-dimensional factorization of size-resolved organic aerosol mass spectra from Mexico
833 City, Atmos. Meas. Tech., 5, 195-224, 10.5194/amt-5-195-2012, 2012.
834 Westervelt, D. M., Pierce, J. R., Riipinen, I., Trivitayanurak, W., Hamed, A., Kulmala, M., Laaksonen,
835 A., Decesari, S., and Adams, P. J.: Formation and growth of nucleated particles into cloud
836 condensation nuclei: model–measurement comparison, Atmos. Chem. Phys., 13, 7645-7663,
837 10.5194/acp-13-7645-2013, 2013.
838 Williams, L. R., Gonzalez, L. A., Peck, J., Trimborn, D., McInnis, J., Farrar, M. R., Moore, K. D., Jayne,
839 J. T., Robinson, W. A., Lewis, D. K., Onasch, T. B., Canagaratna, M. R., Trimborn, A., Timko,
840 M. T., Magoon, G., Deng, R., Tang, D., de la Rosa Blanco, E., Prévôt, A. S. H., Smith, K. A., and
841 Worsnop, D. R.: Characterization of an aerodynamic lens for transmitting particles greater than 1
842 micrometer in diameter into the Aerodyne aerosol mass spectrometer, Atmos. Meas. Tech., 6,
843 3271-3280, 10.5194/amt-6-3271-2013, 2013.
844 Yao, X., Lau, N. T., Chan, C. K., and Fang, M.: Size distributions and condensation growth of submicron
845 particles in on-road vehicle plumes in Hong Kong, Atmospheric Environment, 41, 3328-3338,
846 10.1016/j.atmosenv.2006.12.044, 2007a.
847 Yao, X., Ling, T. Y., Fang, M., and Chan, C. K.: Size dependence of in situ pH in submicron atmospheric
848 particles in Hong Kong, Atmospheric Environment, 41, 382-393,
849 10.1016/j.atmosenv.2006.07.037, 2007b.
850 Yuan, Z., Yadav, V., Turner, J. R., Louie, P. K. K., and Lau, A. K. H.: Long-term trends of ambient
851 particulate matter emission source contributions and the accountability of control strategies in
852 Hong Kong over 1998–2008, Atmospheric Environment, 76, 21-31,
853 http://dx.doi.org/10.1016/j.atmosenv.2012.09.026, 2013.
854 Zhang, J. K., Sun, Y., Liu, Z. R., Ji, D. S., Hu, B., Liu, Q., and Wang, Y. S.: Characterization of
855 submicron aerosols during a month of serious pollution in Beijing, 2013, Atmos. Chem. Phys.,
856 14, 2887-2903, 10.5194/acp-14-2887-2014, 2014.
857 Zhang, Q., Stanier, C. O., Canagaratna, M. R., Jayne, J. T., Worsnop, D. R., Pandis, S. N., and Jimenez, J.
858 L.: Insights into the chemistry of new particle formation and growth events in Pittsburgh based on

aerosol mass spectrometry, Environmental Science & Technology, 38, 4797-4809, 10.1021/es035417u, 2004.

Zhang, Q., Canagaratna, M. R., Jayne, J. T., Worsnop, D. R., and Jimenez, J. L.: Time- and size-resolved chemical composition of submicron particles in Pittsburgh: Implications for aerosol sources and processes, Journal of Geophysical Research-Atmospheres, 110, D07s09 Artn d07s09, 2005.

Zheng, M., Kester, D. R., Wang, F., Shi, X., and Guo, Z.: Size distribution of organic and inorganic species in Hong Kong aerosols during the wet and dry seasons, J. Geophys. Res., 113, D16303, 10.1029/2007jd009494, 2008.

Zhuang, H., Chan, C. K., Fang, M., and Wexler, A. S.: Size distributions of particulate sulfate, nitrate, and ammonium at a coastal site in Hong Kong, Atmospheric Environment, 33, 843-853, 10.1016/s1352-2310(98)00305-7, 1999.

Supporting Material

Diurnal and day-to-day characteristics of ambient particle mass size distributions from HR-ToF-AMS measurements at an urban site and a suburban site in Hong Kong

Berto P. Lee[1], Hao Wang[2], and Chak K. Chan[1,2*]

[1]School of Energy and Environment, City University of Hong Kong, Hong Kong, China

[2]Division of Environment, Hong Kong University of Science and Technology, Hong Kong, China

Correspondence to: Chak K. Chan (chak.k.chan@cityu.edu.hk)

A. Particle size characterization by HR-AMS

The working principle of the AMS has been described extensively in the literature (Canagaratna et al., 2007;DeCarlo et al., 2006;Drewnick et al., 2005;Jimenez et al., 2003;Jimenez et al., 2007). The particle size acquisition mode (*PToF mode*) relies on aerodynamic sizing as the measurement of particle flight time between two fixed points in space in near vacuum conditions. The incident particle beam passes a rotating double-slit disk, which permits pulses of particles to enter the flight chamber. The chopper operates at a fixed frequency (~150 Hz) and has a duty cycle of 2-4% depending on individual instruments. Recent updates to the instrument design include a different chopper design (ePToF – efficient particle time-of-flight) with a higher particle throughput rate. Data in this study originate from instruments of the older conventional PToF design and is also the basis for following discussion.

The acceleration of a particle into the vacuum interior of the AMS is a function of its size (Jimenez et al., 2003) and thus particles of different size in the pulse ensemble travel at different velocities which are determined from particle flight times over a fixed flight path (i.e. the length of the chamber). Ions arriving at the detector are counted as a function of time between two subsequent particle packages passing through the particle chopper slit. Averaging over several chopper cycles yields a distribution of ions with respect to particle size and enables the measurement of mass concentrations of specific ions as a function of particle size, or of specific bulk species (Organics, SO4, NO3, NH4, Chl) by employing the fragmentation table as in the unit mass resolution acquisition mode (*V-mode*).

Primary logged data in PToF mode is the particle flight time from which velocity is directly inferred due to the fixed flight path length. Velocity can be related to particle diameter by calibration with a set of particles of known size. AMS sizing takes place in near vacuum conditions with particles subject to the free molecular flow regime rather than the transition regime, and consequently AMS size distributions are reported in terms of vacuum-aerodynamic diameter. The relationship between electrical mobility (D_m) and vacuum-aerodynamic diameter (D_{va}) is given by (Jayne et al., 2000):

$$D_{va} = D_m \times \delta_p \times S \qquad \text{Eq. A1}$$

where δ_p is the particle density and S a particle shape factor for non-spherical particles or those with internal voids. S has been experimentally determined for nitrate (S=0.8). For most other particles, where information on the shape factor are unknown, particles are assumed spherical (S=1). DeCarlo et al. provide a more fundamental discussion of the relationships of different particle diameters and their relation to particle density (DeCarlo et al., 2004;Slowik et al., 2004). Particle size calibrations for the AMS instrument in this study were carried out pre- and post-campaign with sets of monodisperse polystyrene latex particles (PSL, Duke Scientific, CA) in the range of 80nm to 800nm (at least 8 individual particle sizes per calibration). To compensate for the slow evaporation of PSL, the vaporizer temperature was temporarily increased to 800°C from its default value of 600°C for the duration of the calibration. As PSL ion flight traces (m/z 104) are typically broad, the particle flight time was chosen as the leading edge rather than apex of the signal trace, with an addition of half a chopper width time (*0.5*duty cycle/chopper frequency*) to account for chopper broadening. D_{va} in nm and particle velocity v in m/s calculated from the fixed chamber length and measured flight times are related empirically by the following equation (Jayne et al., 2000):

$$v = v_l + \frac{v_g - v_l}{1 + \left(\frac{D_{va}}{D^*}\right)^b} \qquad \text{Eq. A2}$$

where v_l is the gas velocity inside the aerodynamic lens, v_g the velocity of the gas as it leaves the lens, D_{va} the vacuum aerodynamic diameter calculated from the PSL particle diameter and the PSL density of 1.05 g/cm^3 and a shape factor of 1. D* and b are empirical parameters without concrete physical meaning. As per calibration only particle velocity v and vacuum aerodynamic diameter D_{va} are known. The remaining parameters are determined by a non-linear curve fit of v against D_{va} using the relationship describe by Equation A2.

B. Treatment of PToF data

Standard AMS data treatment procedures were employed for the integration of the ion signals in SQUIRREL for unit-mass resolution data (*V-mode and PToF mode*) and PIKA for high resolution data (*W-mode*).

While in V- and W-mode, ions signals from particle constituents are inferred from the difference of blocked (gas-phase ion signals) and unblocked (sum of gas-phase and particle-phase ion signals) particle beam mass spectra, the baseline in the PToF mode for each m/z in the acquisition range is established by averaging of the ion signal in two defined time regions (DC markers) at the very beginning and very end of the chopper cycle. These correspond to velocities of particles beyond the upper and lower transmission capability of the instrument and can therefore represent background ion contributions (Allan et al., 2003).

In m/z channels where gas-phase species may interfere with the first DC marker region (e.g. m/z 15 or m/z 44), only the second DC marker is used for the PToF baseline. In this work, DC markers for all m/z ratios in the range of 12 – 150 were checked individually to determine the most appropriate selection of DC markers for each m/z channel. Mass

concentrations per PToF mode run are calculated by application of the quantification principles of the unit-mass resolution mode (*V-mode*) with additional corrections for the chopper frequency and slit width to account for the lower number of particles passing into the flight chamber. As the chopping of the particle beam lowers overall sensitivity, the integrated particle mass concentration for each PToF run was normalized to the V-mode concentration of the same time step. To remove any remaining background biases, ambient size distributions in this study were background-corrected by subtraction of the size distributions acquired during particle-free time periods (ambient air sampled through HEPA-filter bypass).

For the evaluation of longer term trends in size distributions, the original AMS mass size distributions at 10min resolution were averaged to 24h distributions (from 00:00 to 23:59 each day) to evaluate progressive change in particle size distributions ("day-to-day") beyond diurnal influences. Regular reoccurring trends, i.e. diurnal variations, were in turn examined by grouping size distributions by their hour time stamp and reconstructing representative size distributions from the average, median, 25^{th} and 75^{th} percentile of each size bin for each hour of the day.

Lognormal peaks were fitted to each 24h and hour-of-day AMS mass size distribution respectively employing the *Multipeak Fit V2* algorithm in *Igor Pro (Wavemetrics)* using a simple vertical offset as the baseline and initial guesses on peak position, height, and width based on visual inspection of the raw size distribution. The multipeak fitting tool employs the Levenberg-Marquardt algorithm (Gill et al., 1981) as a non-linear least squares fit and iteratively adjusts the initial fit parameter guesses until a convergent solution with minimized residuals is achieved. In sporadic cases, the fitted solution led to excessive deviations from the initial guesses with greatly shifted peak locations and large fluctuations in peak width. In such cases, results from the peak fits of immediately adjacent size distributions (i.e. previous and next distributions in the sequence) were evaluated and used to adjust the fitting process by fixing either the location (*primary*) or the width of the peak (*secondary*) to the average value of the two adjacent fitted distributions.

For the diurnal size distributions, measurement data from time periods with large differences in species concentration levels were pooled together. The averaging of mass (or volume) based size distribution involves different uncertainties for each size bin due to the cubic relationship between particle mass (or volume) and particle diameter and the corresponding improvement in signal-to-noise ratio with increasing particle size. To establish reliable diurnal trends we adopt an approach similar to the analysis of conventional species concentration diurnal trends by evaluating size distributions reconstructed from the average, median, 25^{th} and 75^{th} percentile of each size bin. Similar diurnal trends in the fitting parameters across these different size distributions would confirm that changes were indeed recurrent daily while divergent trends would indicate that irregular processes (e.g. episodic events) were more significant in determining size distribution characteristics. Since episodic pollution events and clean periods (e.g. prolonged precipitation) were not removed from the dataset, the quantitative analysis focuses on trends observed in the median dataset to minimize skewing effects of high and low concentration periods.

Uncertainties can arise from the peak fitting process itself. While the bimodality of the size distributions was obvious in most cases (i.e. a main mode with a shoulder towards smaller particle sizes, e.g. Figure D1), accumulation mode particle mass can occasionally dominate the mass size distribution and diminish the Aitken mode. To achieve confidence in the appropriateness of the bimodal fitting we evaluated both unimodal and bimodal peak fits whenever the Aitken to accumulation mode peak ratio was <10% and we depict a representative example below (Figure D2a.

b). The distribution of the fit residuals (Figure D2c, d) was examined and cumulative probability distributions of the fit residuals compared by the Kolmogorov-Smirnov test (Figure D2e) to assess whether fit residuals were significantly different at 95% confidence level (CL). It is evident that the bimodal fit performs better at resolving the raw size distribution in the smaller size region and overall yields a more normal residual distribution. The Kolmogorov-Smirnov test confirms that the residual distributions are statistically different ($D>D_{critical}$ at 95% CL). We tested all borderline cases using the outlined procedure. In this study, bimodal fits yielded unanimously better results in all cases for both diurnal and day-to-day size distributions and all investigated species, i.e. the Aitken mode always remained clearly distinguishable from the accumulation mode.

While the peak fitting algorithm yields a unique individual solution with a set of parameters for which resulting residuals (*difference of fitted and original distribution*) are minimized, the surrounding solution space provides a potentially infinite number of similar solutions with slightly larger residuals. The standard deviations of the fit parameters can provide an estimate of the variability of the peak parameters between the final fit solution and the surrounding solution space. We evaluated the uncertainty in peak area (i.e. integrated mode particle mass) which represents the combined uncertainty of the peak position, width and height (which altogether directly determine the peak area) for all fitted size distributions in this work.

Figure D3 depicts the standard deviation of resolved peak area (i.e. integrated mode particle mass concentration) nominally and relative to the peak area for the diurnal size distributions of NO3 at the urban Mong Kok site in summer 2013 and Tables C1-C2 summarize the values of percent standard deviations for all species at both measurement sites respectively. The median datasets, which were used for quantitative discussion for the diurnal size distribution analysis, exhibited particle mass uncertainties of 14-48% in the Aitken mode and 1-12% in the accumulation mode at the suburban HKUST site, and 7-44% in the Aitken mode and 1-6% in the accumulation mode at the urban MK site. Figure D4 depicts the 75^{th} percentile-bin diurnal variation of NO3 (which displayed the largest uncertainties in Figure D3) with the corresponding peak area variability, and shows that the interpretation of the diurnal variation would remain largely unaffected from the incurred uncertainties.

For the day-to-day 24h size distributions a corresponding analysis was undertaken, with Figure D5 depicting the size distributions of NO3 at the HKUST site for all covered seasons exemplarily, and Table C3 summarizes the values of percent standard deviations for all species at both measurement sites respectively. Peak fit uncertainties typically increase with decreasing integrated peak area and can exceed the values of the peak area in the Aitken mode in a small number of cases (e.g. Figure D5c,e – ratios >1). Quantification of the Aitken mode may not be possible at high levels of confidence in these isolated cases. They were retained in the dataset due to their low frequency of occurrence and to enable a complete discussion over the full concentration range without biasing towards larger concentration (i.e. fitted peak areas) values.

C. Additional Tables

Table C1. Percentiles of relative standard deviation (*rows; corresponding to the box-whiskers plot in Figure D3e,f*) in percent from lognormal peak fits (bimodal deconvolution) for the resolved Aitken mode (a) and accumulation mode (b) particle concentration for diurnal size distributions at the HKUST supersite (2011/12), *columns* describe the data set, i.e. reconstructed size distributions from the 25th percentile, median, 75th percentile and mean of the size bins
Sp=Spring, Su=Summer, Fa=Fall, Wi=Winter

(a)

Aitken mode		25th PC Distr.				Median Distr.				75th PC Distr.				Mean Distr.				Range
% SD		Sp	Su	Fa	Wi	Sp	Su	Fa	Wi	Sp	Su	Fa	Wi	Sp	Su	Fa	Wi	
NO3 (UST)	PC-90	67	76	39	85	76	44	54	55	80	75	56	39	36	77	44	42	36-85
	PC-75	52	42	28	57	66	32	39	40	61	59	44	29	22	38	35	34	22-66
	PC-50	**36**	**33**	**22**	**46**	**44**	**26**	**31**	**22**	**40**	**43**	**34**	**23**	**18**	**28**	**24**	**30**	**18-46**
	PC-25	29	25	16	28	26	14	24	18	25	29	22	17	14	19	20	25	14-29
	PC-10	21	20	15	24	19	12	19	15	17	19	17	10	13	13	15	21	10-24
SO4 (UST)	PC-90	38	38	42	74	19	36	39	43	22	40	40	42	19	36	37	81	19-81
	PC-75	35	33	38	55	18	28	33	32	18	30	35	64	17	30	30	66	17-66
	PC-50	**28**	**30**	**33**	**32**	**16**	**26**	**27**	**25**	**14**	**24**	**27**	**27**	**14**	**24**	**26**	**48**	**14-48**
	PC-25	21	25	26	24	13	21	22	21	11	18	24	22	12	21	23	40	11-40
	PC-10	17	23	24	19	11	20	20	13	10	14	20	19	10	19	22	35	10-35
Org (UST)	PC-90	52	23	41	44	42	28	32	27	47	48	45	53	46	29	24	32	23-53
	PC-75	41	18	26	28	30	22	27	22	26	39	35	44	36	23	21	25	18-44
	PC-50	**26**	**14**	**17**	**21**	**19**	**18**	**21**	**17**	**20**	**32**	**26**	**35**	**23**	**18**	**19**	**21**	**14-35**
	PC-25	16	11	13	18	17	16	19	15	18	28	20	29	18	14	16	17	11-29
	PC-10	9	9	10	11	14	9	15	12	15	20	17	21	17	11	14	16	9-21

(b)

Accum. mode		25th PC Distr.				Median Distr.				75th PC Distr.				Mean Distr.				Range
% SD		Sp	Su	Fa	Wi	Sp	Su	Fa	Wi	Sp	Su	Fa	Wi	Sp	Su	Fa	Wi	
NO3 (UST)	PC-90	8	5	8	4	7	5	6	3	4	9	6	3	3	4	5	1	1-9
	PC-75	6	4	7	3	3	4	5	2	4	7	5	2	2	3	5	1	1-7
	PC-50	**4**	**3**	**5**	**2**	**3**	**3**	**5**	**2**	**3**	**4**	**5**	**2**	**2**	**3**	**4**	**1**	**1-5**
	PC-25	3	3	4	2	2	3	4	1	3	3	4	2	2	2	4	1	1-4
	PC-10	2	2	4	1	2	2	4	1	2	2	3	1	2	2	3	1	1-4
SO4 (UST)	PC-90	2	3	3	5	2	2	2	3	3	2	3	4	2	2	2	2	2-5
	PC-75	2	2	2	2	2	2	2	2	2	2	2	3	1	2	2	2	1-3
	PC-50	**2**	**2**	**2**	**1**	**2**	**2**	**2**	**2**	**2**	**2**	**2**	**2**	**1**	**2**	**2**	**1**	**1-2**
	PC-25	2	2	2	1	1	2	2	1	1	2	2	2	1	2	2	1	1-2
	PC-10	1	2	1	1	1	2	2	1	1	1	2	1	1	2	2	1	1-2
Org (UST)	PC-90	29	12	16	9	18	8	9	5	10	6	7	3	18	7	5	5	3-29
	PC-75	18	9	11	7	10	5	5	3	6	4	5	2	11	5	4	3	2-18
	PC-50	**12**	**7**	**5**	**5**	**6**	**4**	**4**	**3**	**4**	**3**	**4**	**2**	**7**	**3**	**3**	**3**	**2-12**
	PC-25	7	4	3	3	5	3	3	2	3	2	3	2	5	2	2	2	2-7
	PC-10	4	4	1	2	4	2	2	1	2	2	2	1	2	1	2	2	1-4

Table C2. Percentiles of relative standard deviation (*rows; corresponding to the box-whiskers plot in Figure D3e,f*) in percent from lognormal peak fits (bimodal deconvolution) for the resolved Aitken mode (a) and accumulation mode (b) particle concentration for diurnal size distributions at the urban MK site (2013), *columns* describe the data set, i.e. reconstructed size distributions from the 25th percentile, median, 75th percentile and mean of the size bins
Sp=Spring, Su=Summer

(a)

Aitken mode % SD		25th PC Distr. Sp	25th PC Distr. Su	Median Distr. Sp	Median Distr. Su	75th PC Distr. Sp	75th PC Distr. Su	Mean Distr. Sp	Mean Distr. Su	Range
NO3 (MK)	PC-90	38	46	40	34	40	41	22	26	22-46
	PC-75	27	34	26	28	34	35	20	16	16-35
	PC-50	**15**	**24**	**23**	**21**	**25**	**28**	**18**	**14**	**14-28**
	PC-25	9	20	19	17	18	22	15	12	9-22
	PC-10	6	19	16	14	15	20	13	11	6-20
SO4 (MK)	PC-90	63	46	35	38	24	31	23	21	21-63
	PC-75	50	36	30	36	21	28	21	20	20-50
	PC-50	**44**	**33**	**28**	**24**	**20**	**23**	**19**	**18**	**18-44**
	PC-25	37	27	24	21	17	20	15	17	15-37
	PC-10	33	25	21	19	15	18	15	16	15-33
Org (MK)	PC-90	22	12	22	19	30	21	15	14	12-30
	PC-75	16	10	12	12	18	11	12	8	8-18
	PC-50	**10**	**8**	**10**	**9**	**10**	**9**	**8**	**7**	**7-10**
	PC-25	8	7	8	7	7	8	6	6	6-8
	PC-10	7	6	7	6	6	6	5	5	5-7

(b)

Accum. mode % SD		25th PC Distr. Sp	25th PC Distr. Su	Median Distr. Sp	Median Distr. Su	75th PC Distr. Sp	75th PC Distr. Su	Mean Distr. Sp	Mean Distr. Su	Range
NO3 (MK)	PC-90	9	9	6	7	3	5	2	5	2-9
	PC-75	6	8	4	5	3	4	2	4	2-8
	PC-50	**4**	**6**	**3**	**4**	**2**	**3**	**2**	**3**	**2-6**
	PC-25	2	5	2	4	2	3	1	3	1-5
	PC-10	2	4	1	3	1	3	1	2	1-4
SO4 (MK)	PC-90	4	3	2	3	2	5	2	3	2-5
	PC-75	3	2	2	3	2	4	2	2	2-4
	PC-50	**3**	**2**	**2**	**2**	**1**	**4**	**2**	**2**	**1-4**
	PC-25	2	2	2	2	1	3	1	2	1-3
	PC-10	2	2	1	2	1	3	1	2	1-3
Org (MK)	PC-90	9	8	8	7	9	5	6	6	5-9
	PC-75	6	7	5	5	5	4	5	4	4-7
	PC-50	**5**	**5**	**4**	**4**	**3**	**4**	**3**	**4**	**3-5**
	PC-25	4	4	3	3	3	3	3	3	3-4
	PC-10	2	3	3	3	5	2	2	2	2-3

Table C3. Percentiles of percent standard deviation (*rows; corresponding to the box-whiskers plot in Figure D5e,f*) from lognormal peak fits (bimodal deconvolution) for the resolved Aitken mode and accumulation mode for 24h day-to-day size distributions at the suburban HKUST site (a) and the urban MK site (b) for all investigated species, *columns* describe the uncertainties in terms of quartiles of resolved peak area, where Q1 refers to the lowest 25% and Q4 the highest 25% of resolved peak area (see also Figure D4)

(a)

HKUST '11/12 % SD		NO3					SO4					Org				
		Q1	Q2	Q3	Q4	Range	Q1	Q2	Q3	Q4	Range	Q1	Q2	Q3	Q4	Range
Aitken mode	PC-90	95	64	50	27	27-95	97	78	49	30	30-97	62	37	28	26	26-62
	PC-75	58	47	37	24	24-58	91	57	36	20	20-91	41	24	21	22	21-41
	PC-50	**47**	**35**	**25**	**17**	**17-47**	**60**	**39**	**29**	**16**	**16-60**	**30**	**17**	**14**	**17**	**14-30**
	PC-25	30	25	20	13	13-30	32	26	21	13	13-32	25	14	10	12	10-25
	PC-10	20	16	15	8	8-20	24	18	13	11	11-24	16	11	6	7	6-16
Accum. mode	PC-90	31	9	7	4	4-31	4	3	3	3	3-4	18	11	9	7	7-18
	PC-75	13	6	5	3	3-13	3	3	3	2	2-3	9	7	6	5	5-9
	PC-50	**8**	**4**	**3**	**2**	**2-8**	**2**	**2**	**2**	**2**	**~2**	**6**	**4**	**5**	**3**	**3-6**
	PC-25	3	3	2	2	2-3	2	2	2	2	~2	4	3	3	2	2-4
	PC-10	1	2	2	1	1-2	2	2	2	1	1-2	3	2	2	2	2-3

(b)

MK '13 % SD		NO3					SO4					Org				
		Q1	Q2	Q3	Q4	Range	Q1	Q2	Q3	Q4	Range	Q1	Q2	Q3	Q4	Range
Aitken mode	PC-90	62	52	47	30	30-62	94	50	29	24	24-94	23	17	13	16	13-23
	PC-75	41	42	30	25	25-42	47	35	22	16	16-47	16	14	11	12	11-16
	PC-50	**28**	**34**	**21**	**18**	**18-34**	**33**	**24**	**17**	**12**	**12-33**	**11**	**10**	**6**	**8**	**6-11**
	PC-25	21	22	19	12	12-22	26	17	13	9	9-26	8	7	5	6	5-8
	PC-10	6	10	13	8	6-13	19	14	10	5	5-19	6	5	3	3	3-6
Accum. mode	PC-90	22	21	6	6	6-22	7	6	6	4	4-7	13	8	9	8	8-13
	PC-75	17	10	5	3	3-17	4	4	4	2	2-4	8	7	6	4	4-8
	PC-50	**10**	**6**	**4**	**2**	**2-10**	**3**	**2**	**2**	**1**	**1-3**	**6**	**5**	**4**	**2**	**2-6**
	PC-25	6	3	2	2	2-6	2	2	1	1	1-2	4	4	3	2	2-4
	PC-10	3	1	2	1	1-3	1	1	1	1	~1	2	3	2	1	1-3

Table C4. Median organic subcomponent concentrations in NR-PM_1 prior to and during meal hours at the urban MK site and their fractional contribution to total change in Organics in NR-PM_1 (Lee et al., 2015)

Mass conc. μg m^{-3}	Spring				Summer			
	SOA	COA	HOA	Total Org	SOA	COA	HOA	Total Org
Pre-lunch 09:00 – 11:00	3.9	3.0	3.9	10.9	1.6	2.6	2.3	6.5
Lunch 12:00 – 14:00	4.6	7.0	4.0	15.8	1.8	4.0	2.1	8.0
Contribution to ΔTotal Org	+16.3%	+81.4%	+2.3%	---	+18.3%	+94.1%	-8.6%	---
Pre-dinner 15:00 – 17:00	4.4	4.0	3.8	12.1	1.7	3.3	2.3	7.3
Dinner 19:00 – 21:00	4.6	9.2	4.1	17.9	1.6	6.3	2.3	10.1
Contribution to ΔTotal Org	+4.7%	+89.6%	+5.7%	---	-4.4%	+106.3%	-1.9%	---

Table C5. Ratio of 10^{th} and 90^{th} percentile mass concentration to median mass concentration of submicron (NR-PM_1) species at the urban MK site (Lee et al., 2015)

Percentile ratio	Spring			Summer		
	Org	SO4	NO3	Org	SO4	NO3
10^{th} / 50^{th}	0.5	0.3	0.3	0.4	0.3	0.5
90^{th} / 50^{th}	2.1	1.7	2.8	2.3	1.8	2.2

D. Additional Figures

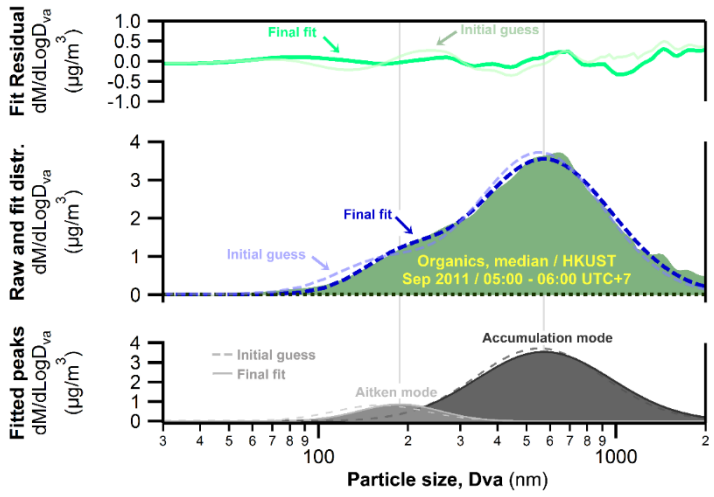

Figure D1. Example of a log-normal peak fit *(Multipeak Fit V2, Igor Pro, Wavemetrics, Levenberg-Marquardt algorithm)* of an AMS organics size distribution

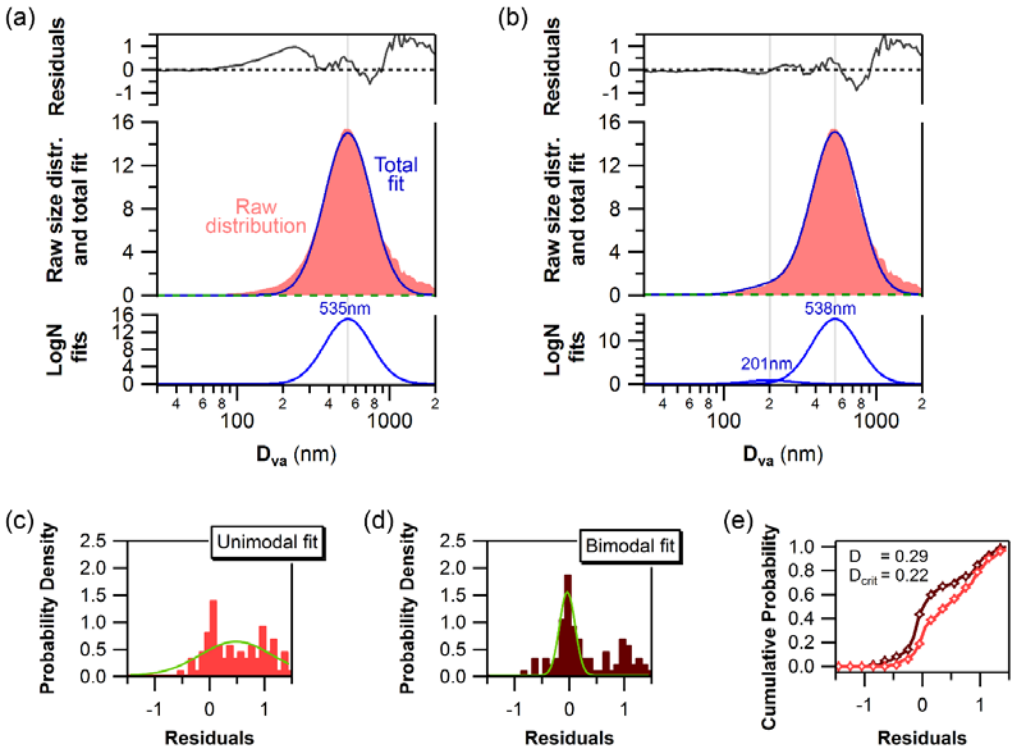

Figure D2. 24h average size distribution of sulfate (12/12/2011, suburban HKUST site) with (a) unimodal and (b) bimodal logN peak fitting applied; histograms of residuals from the unimodal (c) and bimodal (d) distributions with Gaussian fit (green); and cumulative probability density functions of uni- and bimodal fit residuals (e) with Kolmogorov-Smirnov D metric values at 95% confidence level

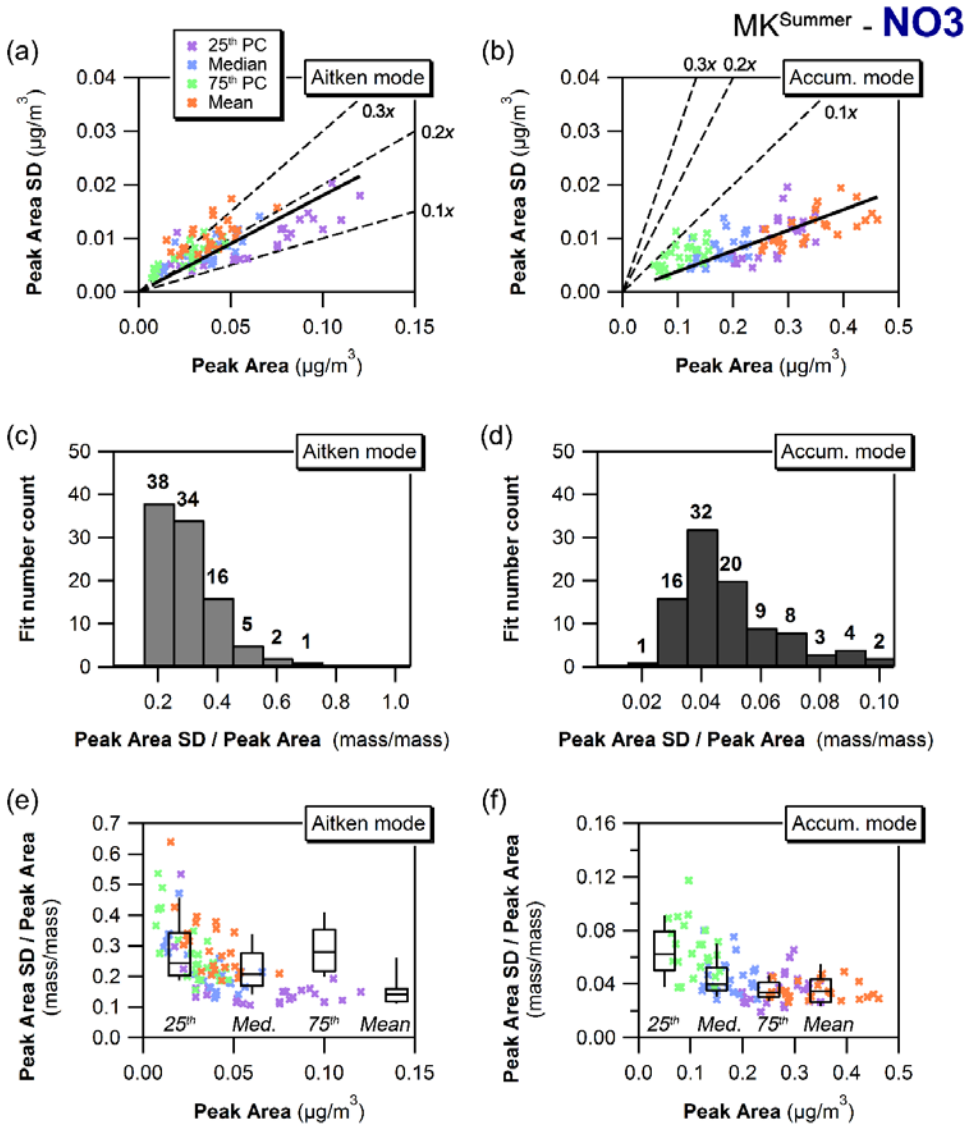

Figure D3. Standard deviation of peak area as a function of mode peak area (a,b), histogram of relative standard deviation i.e. the ratio of standard deviation to mode peak area (c,d) where the last bin also contains all values beyond the last bin range, and relative standard deviation as a function of mode peak area (e,f) for the fitted Aitken and accumulation mode with binned box-whiskers plot (25^{th} to 75^{th} PC box with horizontal median line and 10^{th} to 90^{th} PC whiskers where bins refer to quartiles of peak area from lowest Q1 to highest Q4); data for diurnal size distributions of NO3 at the urban Mong Kok site in summer 2013.

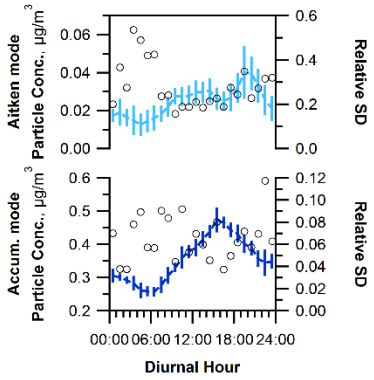

Figure D4. Plot of 75th percentile-bin diurnal variation with peak area fit variability and relative standard deviation (corresponding to green data and second to last box in Figure D3e,f)

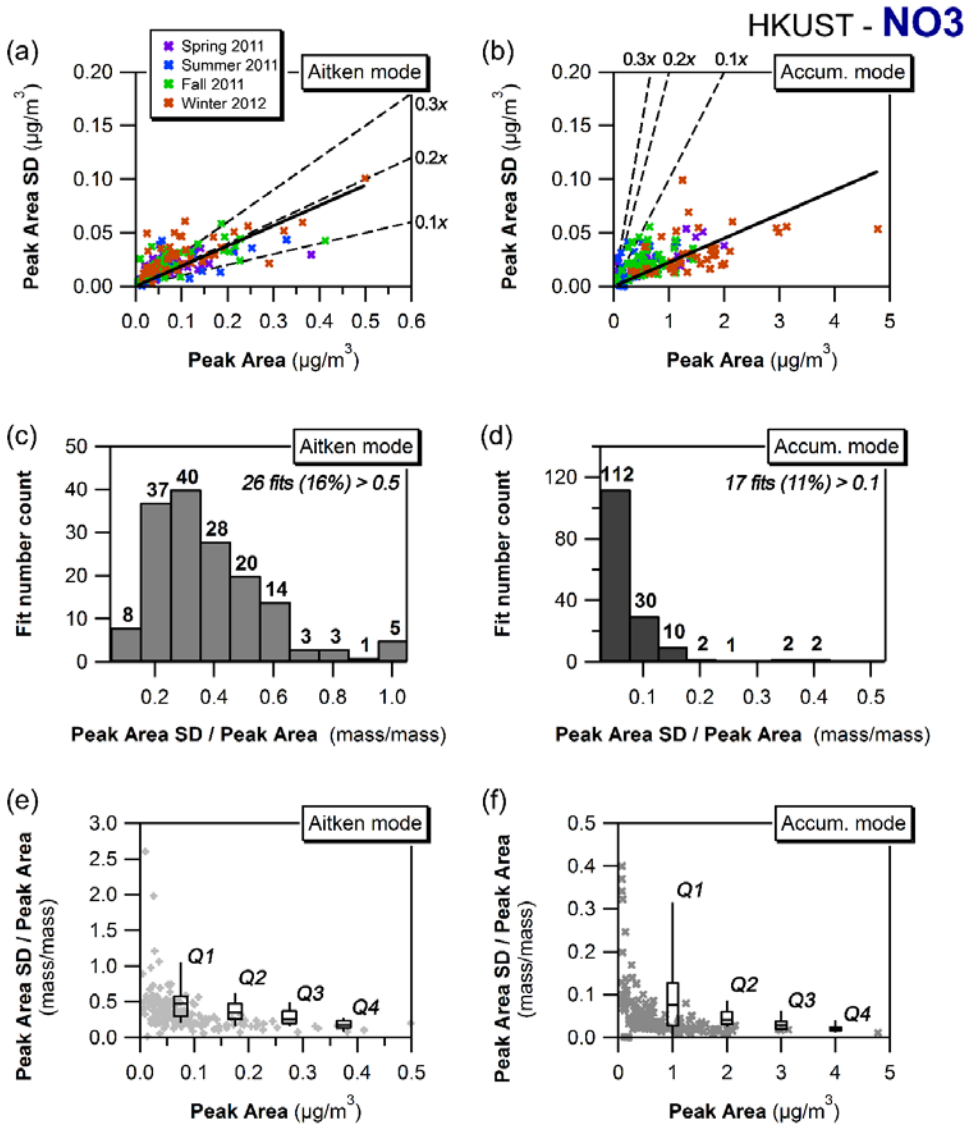

Figure D5. Standard deviation of peak area as a function of mode peak area (a,b), histogram of relative standard deviation i.e. the ratio of standard deviation to mode peak area (c,d) where the last bin also contains all values beyond the last bin range, and relative standard deviation as a function of mode peak area (e,f) for the fitted Aitken and accumulation mode with binned box-whiskers plot (25th to 75th PC box with horizontal median line and 10th to 90th PC whiskers where bins refer to quartiles of peak area from lowest Q1 to highest Q4); data for day-to-day size distributions of NO3 at the HKUST site including all seasons.

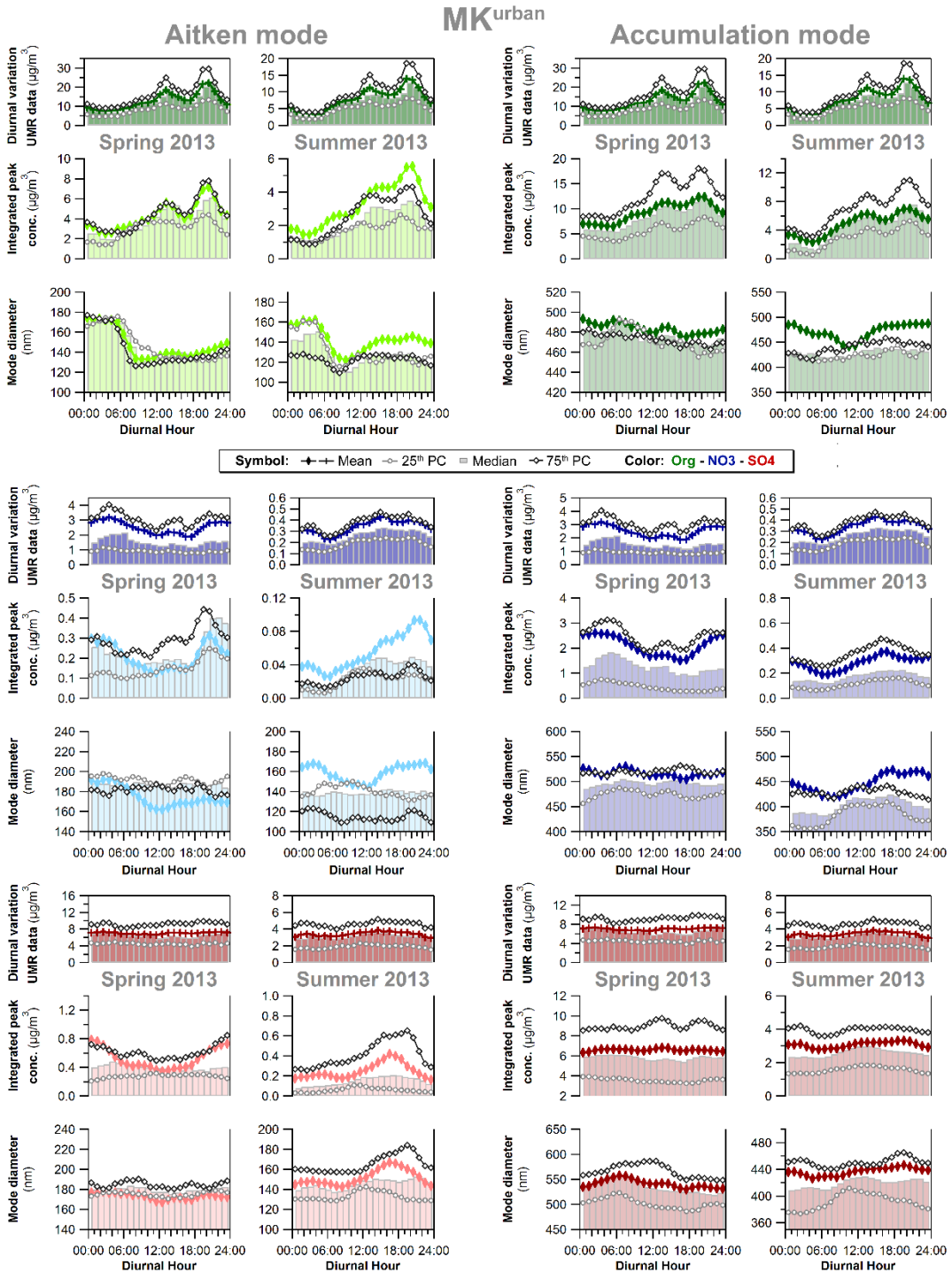

Figure D6. Mode diameter (mass median diameter - MMD), integrated particle mass concentration and width (geometric standard deviation - GSD) of the Aitken mode and accumulation mode from bimodal diurnal peak fits of organic, nitrate and sulfate size distributions at the Mong Kok urban site in spring 2013 and summer 2013; the top panel depicts the diurnal variations of total measured submicron organic, nitrate and sulfate concentrations (AMS V-mode data)

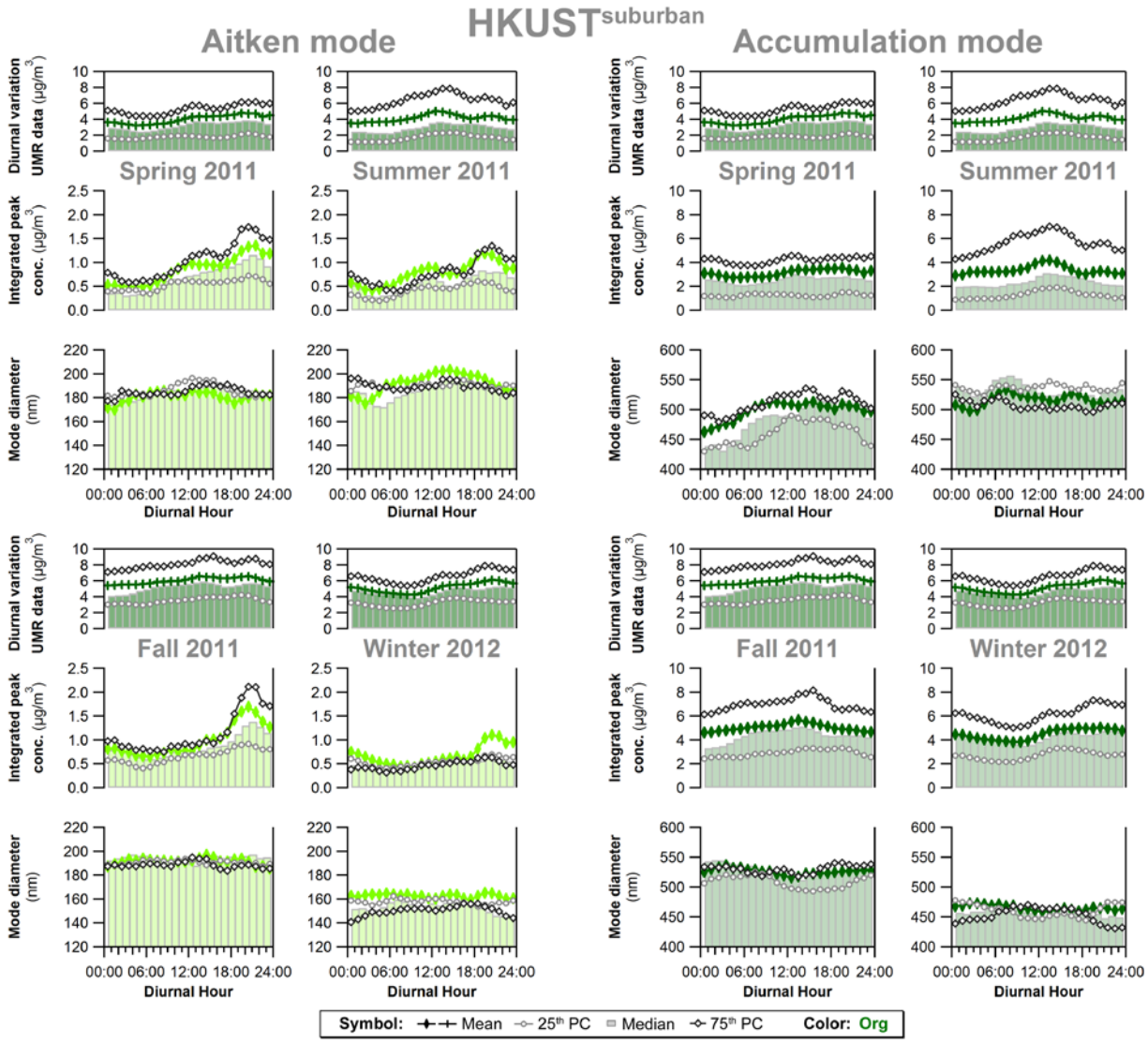

Figure D7. Mode diameter (mass median diameter - MMD), integrated particle mass concentration and width (geometric standard deviation - GSD) of the Aitken mode and accumulation mode from bimodal diurnal peak fits of organic size distributions at the suburban HKUST site in four seasons (May 2011- Feb 2012); the top panel depicts the diurnal variations of total measured submicron organic concentrations (AMS V-mode data)

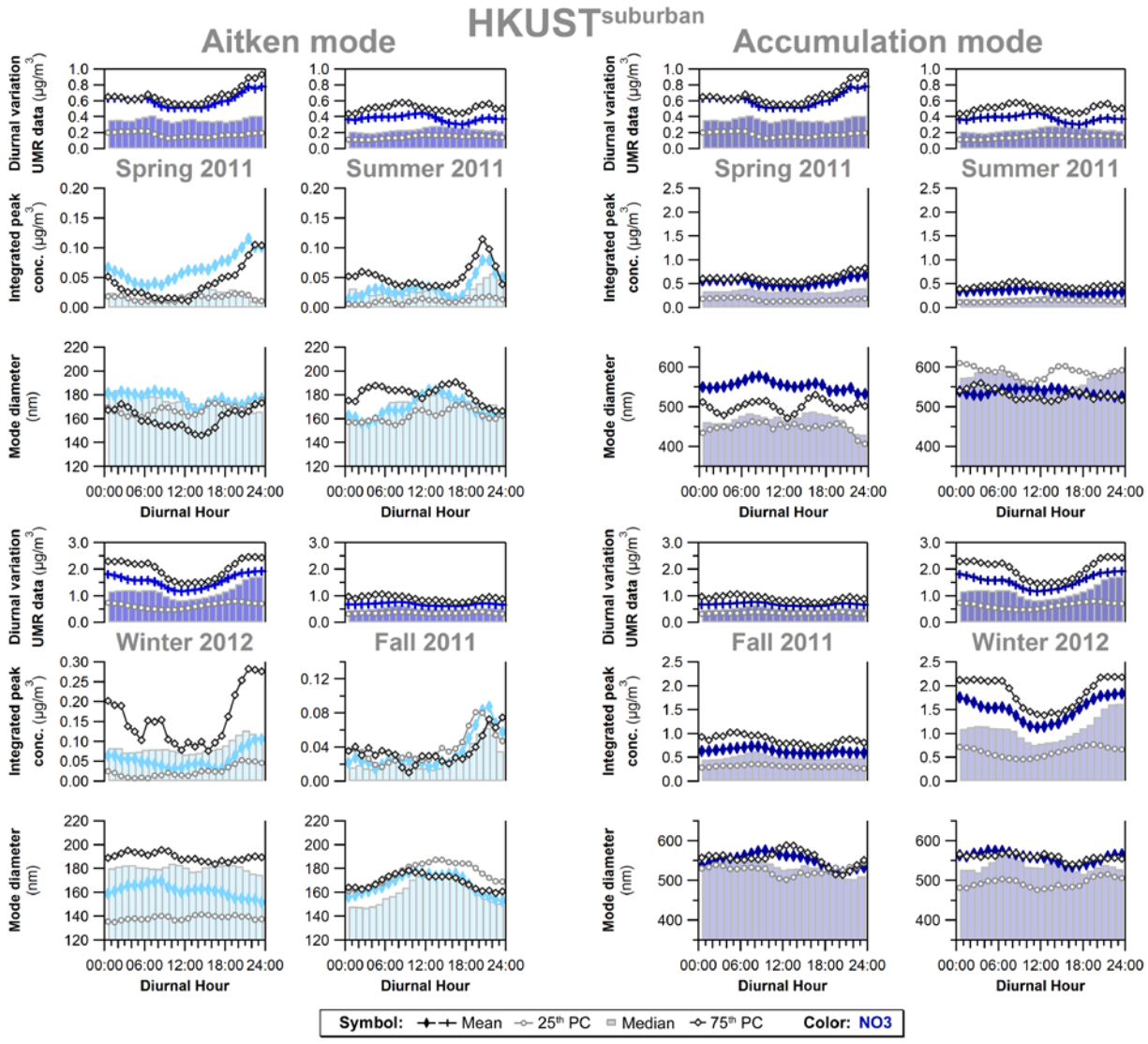

Figure D8. Mode diameter (mass median diameter - MMD), integrated particle mass concentration and width (geometric standard deviation - GSD) of the Aitken mode and accumulation mode from bimodal diurnal peak fits of nitrate size distributions at the suburban HKUST site in four seasons (May 2011- Feb 2012); the top panel depicts the diurnal variations of total measured submicron nitrate concentrations (AMS V-mode data)

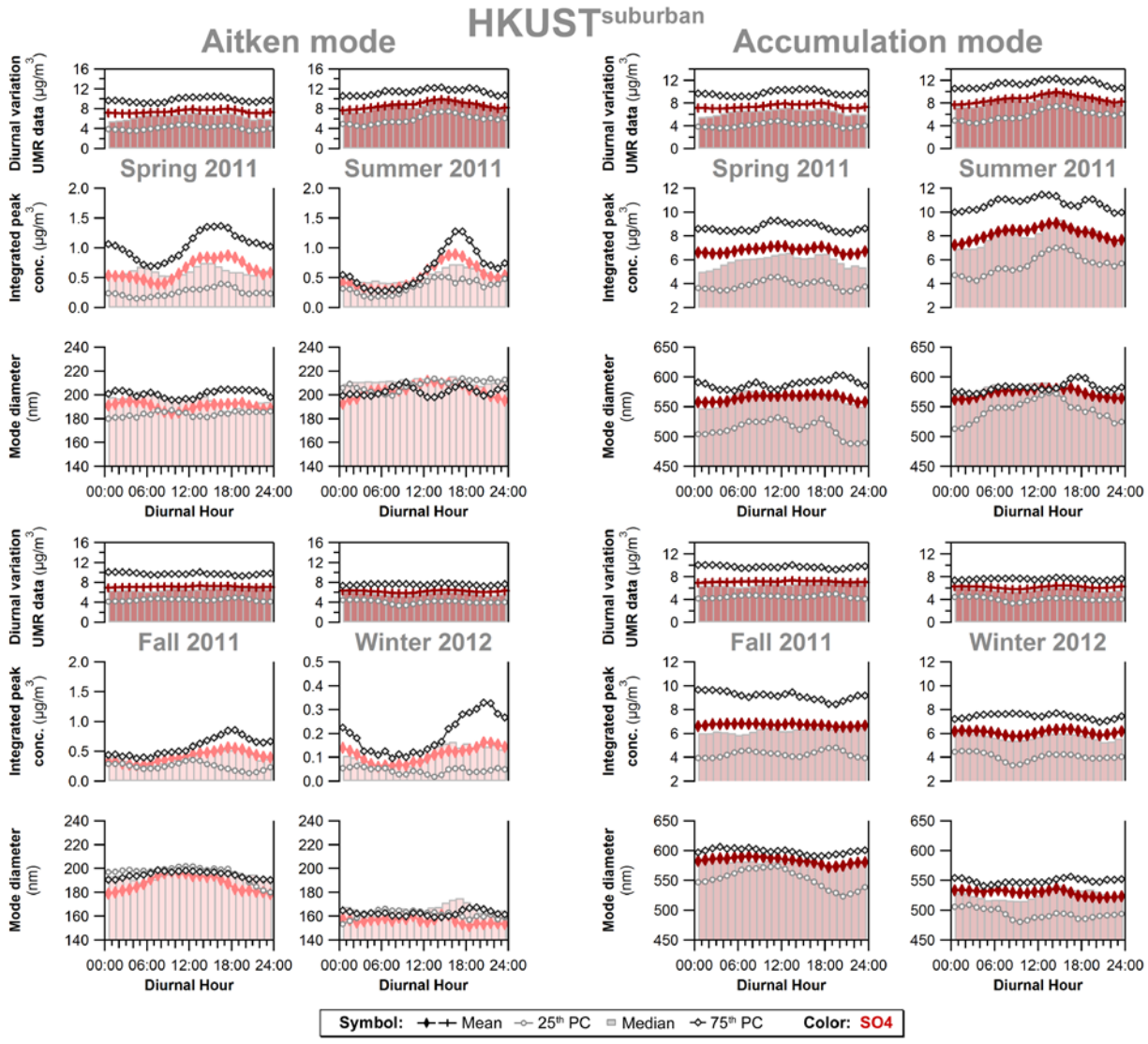

Figure D9. Mode diameter (mass median diameter - MMD), integrated particle mass concentration and width (geometric standard deviation - GSD) of the Aitken mode and accumulation mode from bimodal diurnal peak fits of sulfate size distributions at the suburban HKUST site in four seasons (May 2011- Feb 2012); the top panel depicts the diurnal variations of total measured submicron sulfate concentrations (AMS V-mode data)

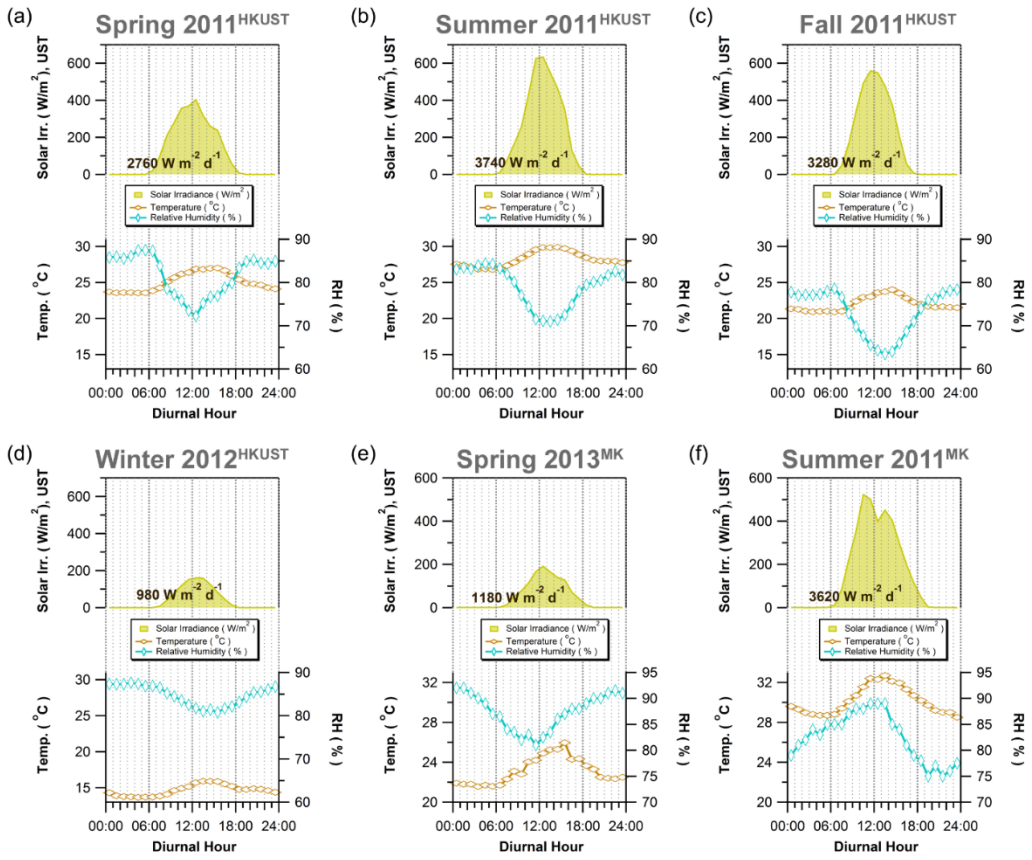

Figure D10. Diurnal variation of temperature (*orange*), RH (*blue*) and solar irradiance (*yellow*) in four seasons in 2011-2012 as well as spring and summer 2013; temperature and RH measurements from the HKUST supersite for the four seasons in 2011-2012, and from the Mong Kok urban site for spring and summer 2013; solar irradiance data always from the HKUST supersite.

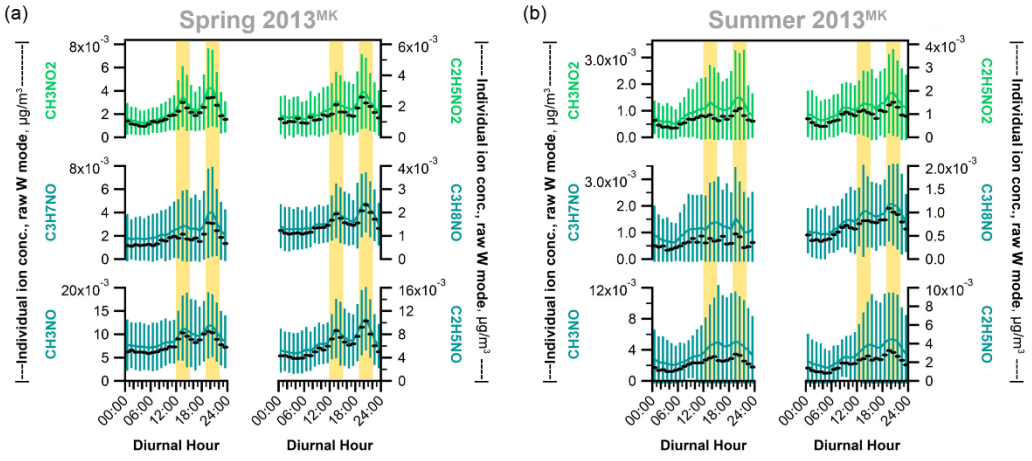

Figure D11. Diurnal variation of fitted $C_xH_yN_zO$ and $C_xH_yN_zO_2$ ions (*raw W-mode mass concentrations*) at the urban Mong Kok site in 2013 in spring (a) and summer (b), meal hours highlighted in yellow

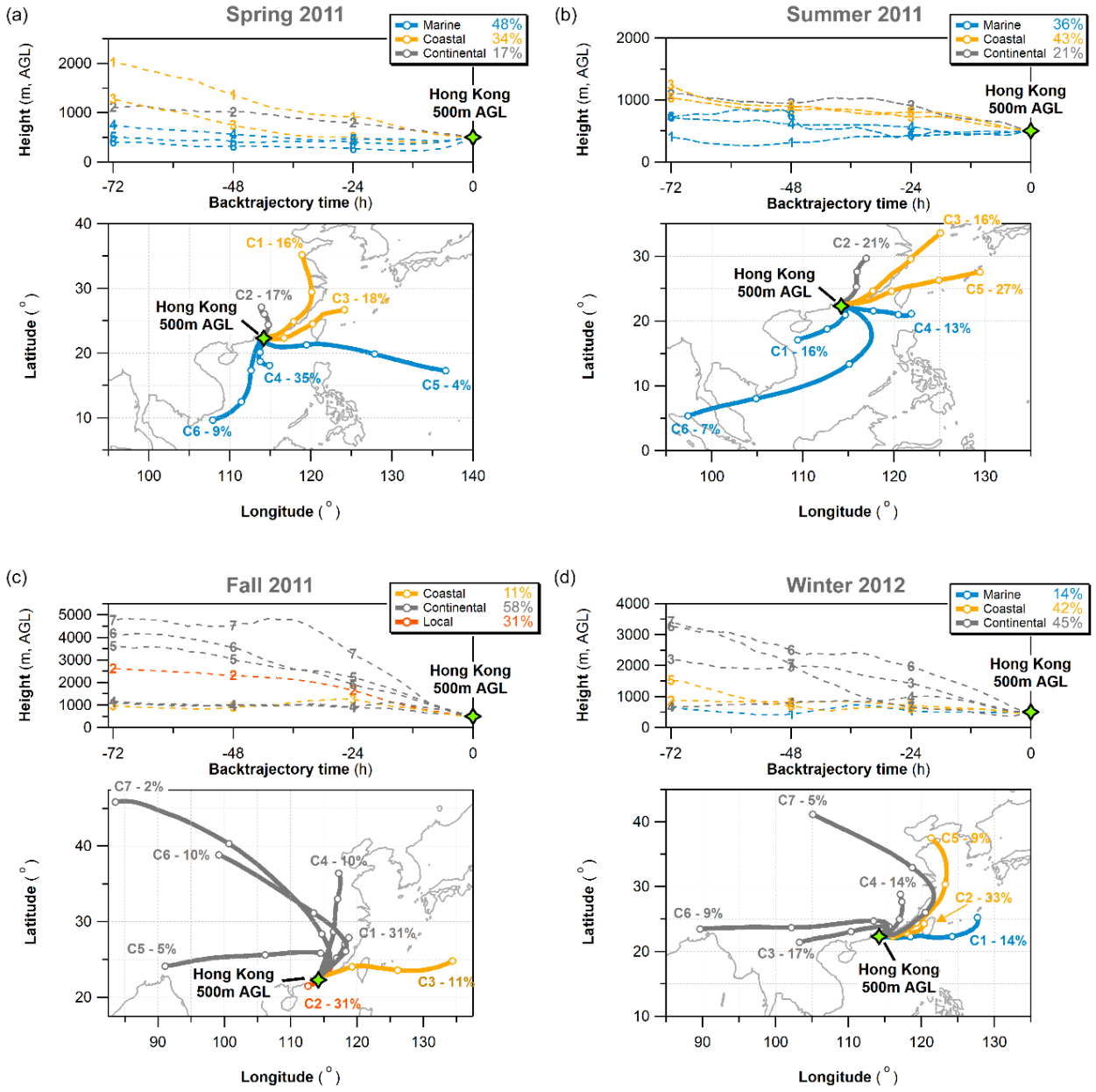

Figure D12. Means of clustered back trajectories (HYSPLIT4, 72h back trajectories) in each sampling season at the suburban HKUST site in (a) spring, (b) summer, (c) fall and (d) winter 2011-2012

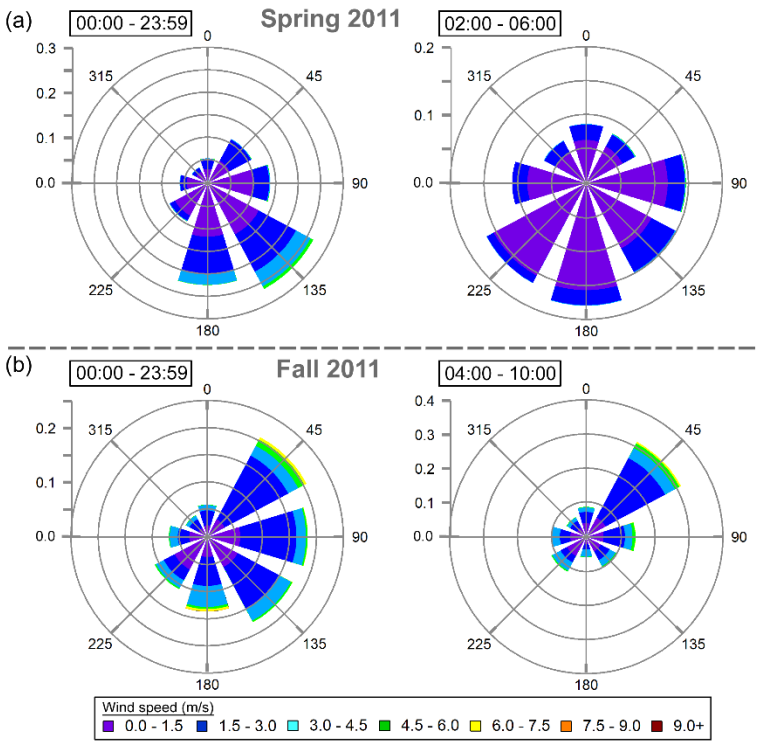

Figure D13. Wind rose plots for observed surface wind frequency at the suburban HKUST site in spring 2011 (2011-05) for the whole sampling period and the nighttime period between 02:00 and 06:00 (a) and in summer 2011 (2011-09) for the whole sampling period and the morning period between 04:00 and 10:00

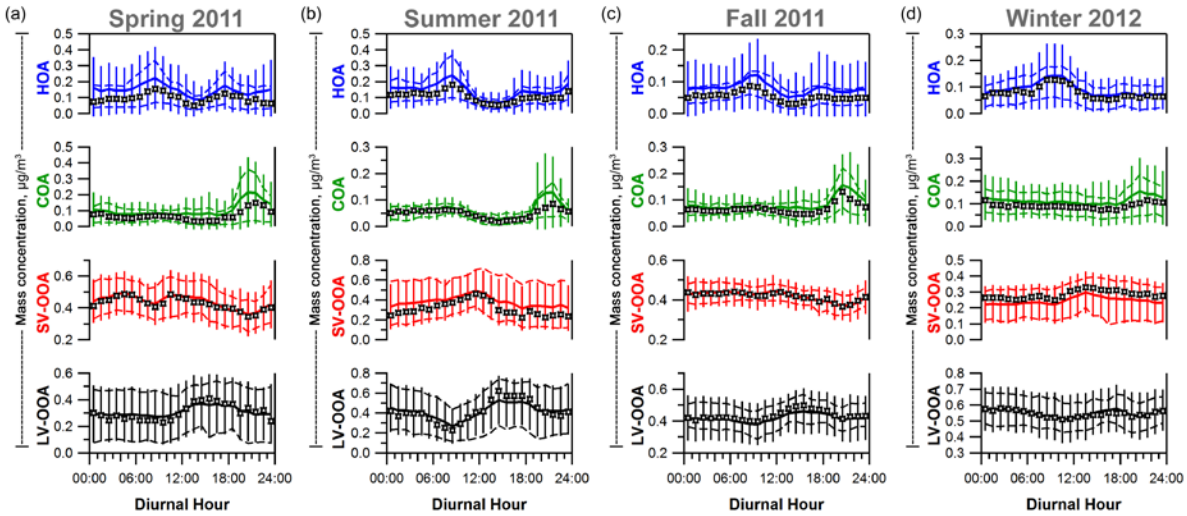

Figure D14. Diurnal variation of PMF-resolved organic aerosol factors at the suburban HKUST site in (a) spring, (b) summer, (c) fall and (d) winter 2011-2012, mean as colored solid line with standard deviations, median as open markers, 25th and 75th percentiles as hashed colored lines, for details see Li et al. (Li et al., 2015).

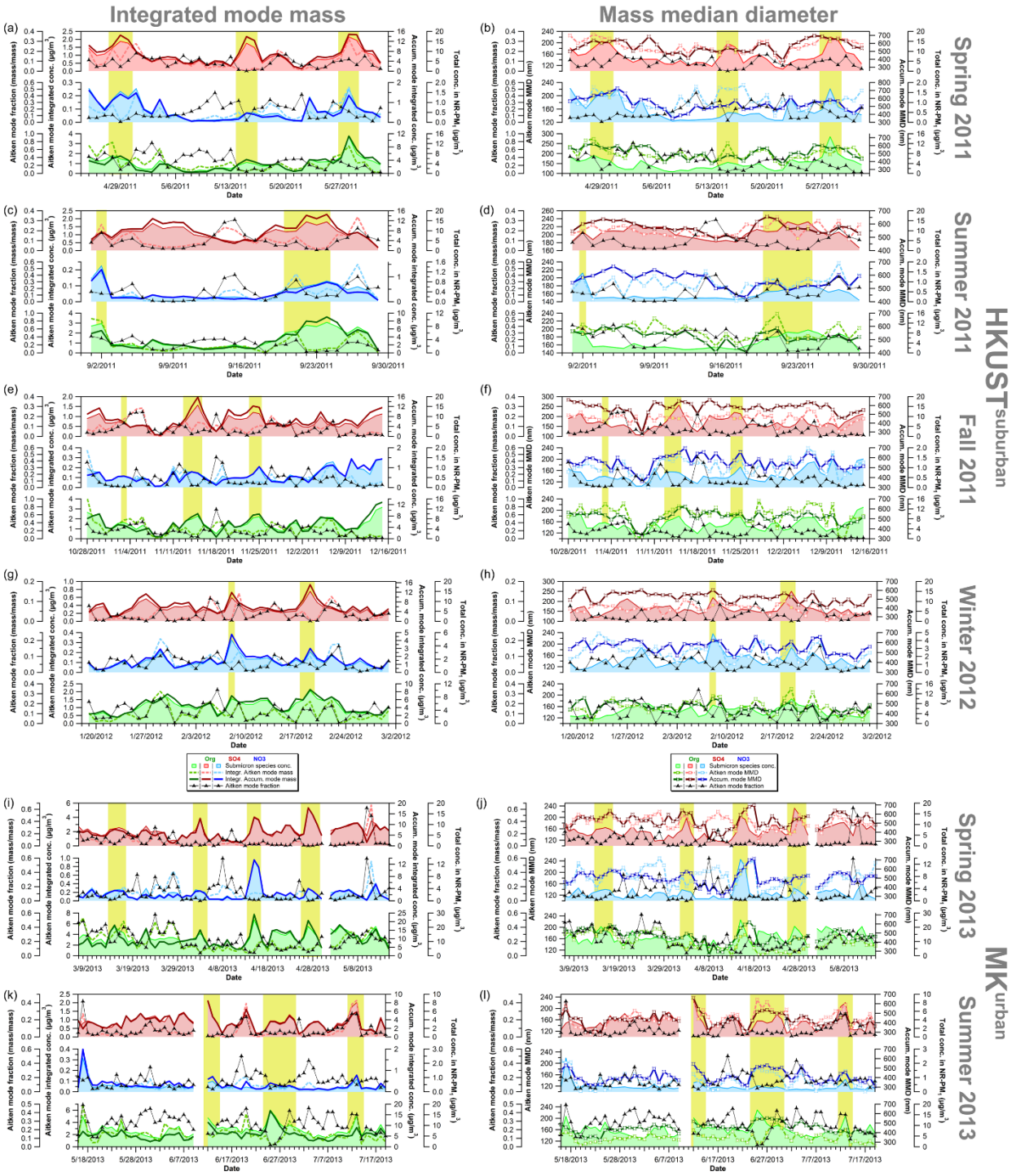

Figure D15. Time series of integrated particle mass concentrations (left-hand panels) and mass median diameters (right-hand panels) of Aitken and accumulation modes at the suburban HKUST supersite in four seasons in 2011-2012 (a-h) and the urban Mong Kok site in 2013 (i-l), total species mass concentrations are based on V-mode measurements.

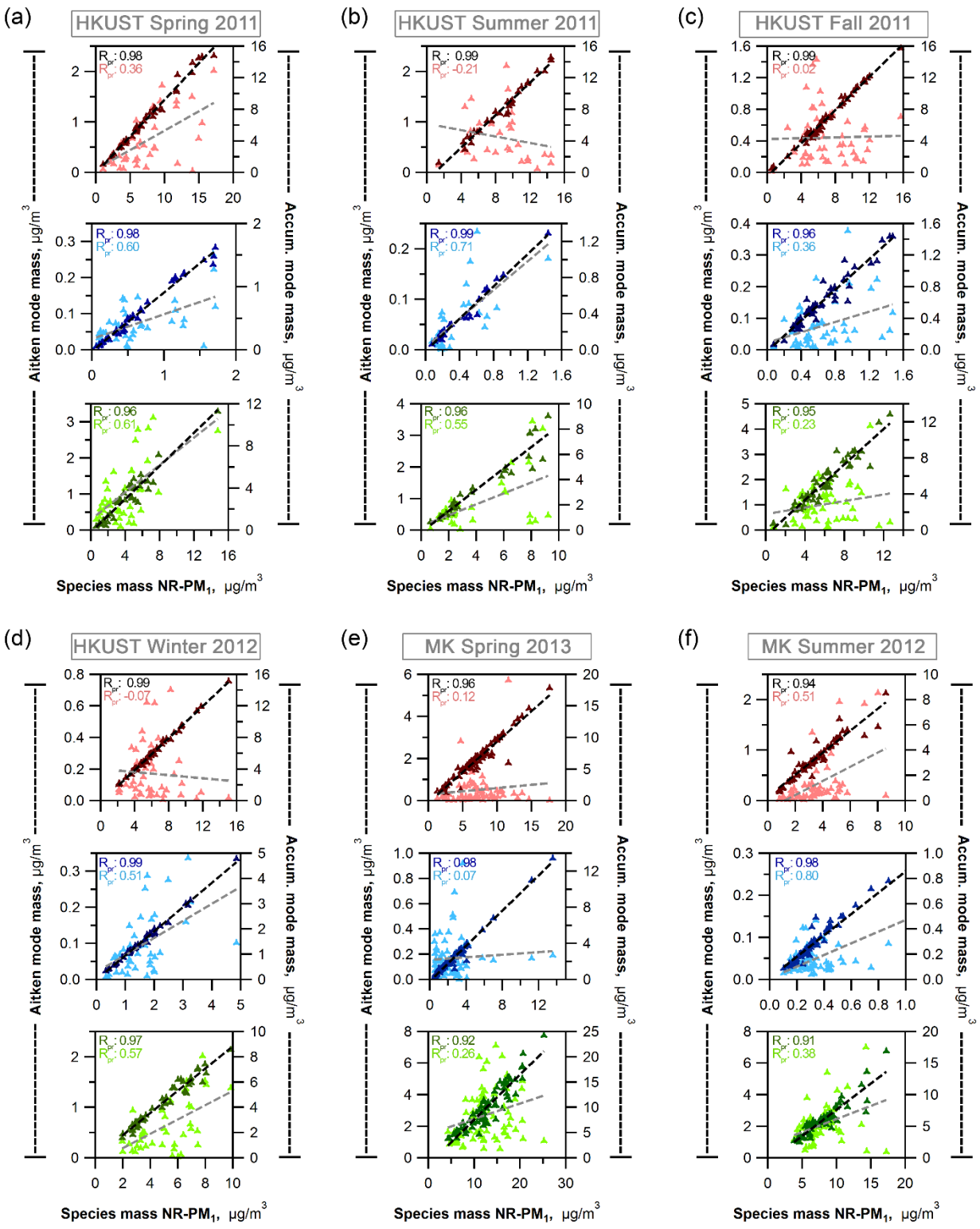

Figure D16. Scatter plot of Aitken and accumulation mode mass concentrations and total species concentrations in NR-PM$_1$ (V-mode at the HKUST supersite (a-d) and the Mong Kok urban site (e-f)

References

Allan, J. D., Jimenez, J. L., Williams, P. I., Alfarra, M. R., Bower, K. N., Jayne, J. T., Coe, H., and Worsnop, D. R.: Quantitative sampling using an Aerodyne aerosol mass spectrometer - 1. Techniques of data interpretation and error analysis, Journal of Geophysical Research-Atmospheres, 108, 4090 10.1029/2002jd002358, 2003.

Canagaratna, M. R., Jayne, J. T., Jimenez, J. L., Allan, J. D., Alfarra, M. R., Zhang, Q., Onasch, T. B., Drewnick, F., Coe, H., Middlebrook, A., Delia, A., Williams, L. R., Trimborn, A. M., Northway, M. J., DeCarlo, P. F., Kolb, C. E., Davidovits, P., and Worsnop, D. R.: Chemical and microphysical characterization of ambient aerosols with the aerodyne aerosol mass spectrometer, Mass Spectrometry Reviews, 26, 185-222, 10.1002/mas.20115, 2007.

DeCarlo, P. F., Slowik, J. G., Worsnop, D. R., Davidovits, P., and Jimenez, J. L.: Particle morphology and density characterization by combined mobility and aerodynamic diameter measurements. Part 1: Theory, Aerosol Science and Technology, 38, 1185-1205, 10.1080/027868290903907, 2004.

DeCarlo, P. F., Kimmel, J. R., Trimborn, A., Northway, M. J., Jayne, J. T., Aiken, A. C., Gonin, M., Fuhrer, K., Horvath, T., Docherty, K. S., Worsnop, D. R., and Jimenez, J. L.: Field-deployable, high-resolution, time-of-flight aerosol mass spectrometer, Analytical Chemistry, 78, 8281-8289, 10.1021/ac061249n, 2006.

Drewnick, F., Hings, S. S., DeCarlo, P., Jayne, J. T., Gonin, M., Fuhrer, K., Weimer, S., Jimenez, J. L., Demerjian, K. L., Borrmann, S., and Worsnop, D. R.: A new time-of-flight aerosol mass spectrometer (TOF-AMS) - Instrument description and first field deployment, Aerosol Science and Technology, 39, 637-658, 10.1080/02786820500182040, 2005.

Gill, P. E., Murray, W., and Wright, M. H.: The Levenberg-Marquardt method, in: Practical optimization, Academic Press, London, 1981.

Jayne, J. T., Leard, D. C., Zhang, X. F., Davidovits, P., Smith, K. A., Kolb, C. E., and Worsnop, D. R.: Development of an aerosol mass spectrometer for size and composition analysis of submicron particles, Aerosol Science and Technology, 33, 49-70, 2000.

Jimenez, J. L., Jayne, J. T., Shi, Q., Kolb, C. E., Worsnop, D. R., Yourshaw, I., Seinfeld, J. H., Flagan, R. C., Zhang, X., Smith, K. A., Morris, J. W., and Davidovits, P.: Ambient aerosol sampling using the Aerodyne Aerosol Mass Spectrometer, J. Geophys. Res., 108, 8425, 10.1029/2001jd001213, 2003.

Jimenez, J. L., Decarlo, P., Kimmel, J. R., Huffman, J. A., Ulbrich, I., Dunlea, E., Trimborn, A., Northway, M. J., Jayne, J. T., Aiken, A. C., Gonin, M., Fuhrer, K., Horvath, T., Docherty, K. S., and Worsnop, D. R.: Development and application of a high-resolution time-of-flight aerosol mass spectrometer, Abstracts of Papers of the American Chemical Society, 233, 590-590, 2007.

Lee, B. P., Li, Y. J., Yu, J. Z., Louie, P. K. K., and Chan, C. K.: Characteristics of submicron particulate matter at the urban roadside in downtown Hong Kong—Overview of 4 months of continuous high-resolution aerosol mass spectrometer measurements, Journal of Geophysical Research: Atmospheres, 120, 7040-7058, 10.1002/2015JD023311, 2015.

Li, Y. J., Lee, B. P., Su, L., Fung, J. C. H., and Chan, C. K.: Seasonal characteristics of fine particulate matter (PM) based on high resolution time-of-flight aerosol mass spectrometric (HR-ToF-AMS) measurements at the HKUST Supersite in Hong Kong, Atmos. Chem. Phys., 15, 37-53, doi:10.5194/acp-15-37-2015, 2015.

Slowik, J. G., Stainken, K., Davidovits, P., Williams, L. R., Jayne, J. T., Kolb, C. E., Worsnop, D. R., Rudich, Y., DeCarlo, P. F., and Jimenez, J. L.: Particle morphology and density characterization by combined mobility and aerodynamic diameter measurements. Part 2: Application to combustion-generated soot aerosols as a function of fuel equivalence ratio, Aerosol Science and Technology, 38, 1206-1222, 10.1080/027868290903916, 2004.